AN ABSTRACT OF THE DISSERTATION OF

Brent Searle Matteson for the degree of Doctor of Philosophy in Chemistry presented on May 27, 2010.

Title: The Chemistry of Acetohydroxamic Acid Related to Nuclear Fuel Reprocessing

Abstract approved: _____

Alena Paulenova

Used Nuclear Fuel (UNF) contains transuranic (TRU) elements and numerous fission products as a result of the uranium fission process and neutron activation that occur in commercial light water power reactors. Recent environmental and nuclear proliferation concerns have spawned the development of advanced reprocessing techniques to close the nuclear fuel cycle. By separating specific elemental groups, sustainable fuel sources can be created while minimizing the need for long-term geologic storage of high-level radioactive waste and reducing nuclear proliferation risk by avoiding the isolation of Pu. To facilitate in the separation of specific elements, acetohydroxamic acid (AHA) is proposed to effectively partition Np and Pu from U. AHA forms hydrophilic acetohydroxamate complexes with Pu^{4+} and Np^{4+} and reduces NpO_2^{2+} to its inextractable NpO_2^{+} oxidation state. This study contributes fundamental knowledge of AHA chemistry in relation to reprocessing techniques including its reactivity towards several elements present in UNF.

The thermodynamic, kinetic, and extraction features of the chemistry of AHA with various metals were investigated. The complexation of Zr^{4+}, UO_2^{2+}, and Fe^{3+} with AHA was analyzed by UV-Vis spectroscopy. It was determined that the conditional stability constants of Zr·AHA complexes are four orders of magnitude greater than for uranyl·AHA complexes, indicating that AHA is a promising complexant to separate tetravalent metals from hexavalent uranium. The reduction kinetics of NpO_2^{2+} to NpO_2^{+} by AHA was monitored using near infrared spectroscopy with stopped-flow and standard

1cm cuvette apparatus. Results showed that AHA can be used to rapidly reduce NpO_2^{2+} to NpO_2^{+}. Lastly, the effect of AHA on the distribution of selected metals and between nitric acid and 1.1 $mol \cdot L^{-1}$ tri-*n*-butyl phosphate in *n*-dodecane was studied. AHA was found to significantly decrease the extraction of tetravalent metals without affecting the extraction of uranium, which remained in the organic phase.

The Chemistry of Acetohydroxamic Acid Related to Nuclear Fuel Reprocessing

by
Brent Searle Matteson

A DISSERTATION
submitted to
Oregon State University

in partial fulfillment of
the requirements for the
degree of
Doctor of Philosophy

Presented May 27, 2010
Commencement June 2011

Doctor of Philosophy dissertation of Brent Searle Matteson presented on May 27, 2010.

APPROVED:

Major Professor, representing Chemistry

Chair of the Department of Chemistry

Dean of the Graduate School

I understand that my dissertation will become part of the permanent collection of Oregon State University libraries. My signature below authorizes release of my dissertation to any reader upon request.

Brent Searle Matteson, Author

ACKNOWLEDGEMENTS

I would like to express my gratitude to my advisor Dr. Alena Paulenova, who provided years of direction and insight during my graduate career.

I thank all past and current members of the radiochemistry laboratory group at Oregon State University. The thoughtful discussions and fun times in lab will always be remembered.

I have been fortunate to develop great friendships with many people of Oregon. I thank you all for the good times and great adventures.

I thank my girlfriend, Pamela Archer, for her caring support that was vital for my success as a graduate student.

Lastly, I would like to thank my father Michael, mother Carol, and brother Wade for their invaluable support. Without their guidance, the completion of my degree would not have been possible.

CONTRIBUTION OF AUTHORS

Dr. Peter Tkac assisted with the interpretation of the complexation data. Martin Precek provided a numerical modeling program for neptunium reduction analysis. Dr. Peter Sprunger created a program to align the SQUAD input files. Lin Kong provided the uranium spectroscopy experiments.

TABLE OF CONTENTS

Page

TABLE OF CONTENTS (continued)

TABLE OF CONTENTS (continued)

Page

LIST OF FIGURES

LIST OF FIGURES (continued)

Figure Page

LIST OF TABLES

LIST OF ACRONYMS

AAIII	2,7-Bis(2-arsonophenylazo)-1,8-dihydroxynaphthalene-3,6-disulfonic Acid
AHA	Acetohydroxamic Acid
amu	Atomic Mass Unit
AMUSE	Argonne Model for Universal Solvent Extraction
An	Actinoid
ANL	Argonne National Laboratory
BHA	Benzohydroxamic Acid
CCD	Chlorinated Cobalt Dicarbollide
CMPO	Octyl(phenyl)-N,N-diisobutylcarboylmethyl-phosphine Oxide
CR	Count Rate
DOE	Department of Energy
DTPA	Diethylenetriamine Pentaacetic Acid
FHA	Formohydroxamic Acid
FP	Fission Product
FPEX	Fission Product Extraction
FS-13	Phenyltrifluoromethyl Sulfone
H_2MBP	Monobutyl Phosphoric Acid
HDBP	Dibutyl Phosphoric Acid
HDEHP	Di-(2-ethylhexyl)phosphoric Acid
HPGe	High Purity Germanium Detector
HLW	High-Level Waste
I	Ionic Strength
ICP-AES	Inductively Coupled Plasma Atomic Emission Spectroscopy
INL	Idaho National Laboratory
LHS	Left Hand Side
Ln	Lanthanoid
LSC	Liquid Scintillation Counting
MOX	Mixed Oxide
NaI	Sodium Iodide Detector
NPEX	Neptunium Plutonium Extraction
ORNL	Oak Ridge National Laboratory
PEG	Polyethylene Glycol

LIST OF ACRONYMS (continued)

ppm	Parts-Per-Million
PUREX	Plutonium Uranium Extraction
RK4	Runge-Kutta Fourth Order
SHE	Standard Hydrogen Electrode
SIT	Specific Ion Interaction Theory
SQUAD	Stability Quotients from Absorption Data
SRP	Standard Reduction Potential
TALSPEAK	Trivalent Actinide Lanthanide Separations by Phosphorus-Reagent Extraction from Aqueous Komplexes
TBP	Tri-*n*-butyl Phosphate
TRU	Transuranic
TRUEX	Transuranium Extraction
TTA	Thenoyltrifluroracetone
UNF	Used Nuclear Fuel
UREX	Uranium Extraction
UREX+	Uranium Extraction (Suite of Extraction Processes)

LIST OF SYMBOLS

A	Pre-Exponential Factor
A_i	Activity of Species *i*
C_i	Molar Concentration of Species *i*
D	Distribution Ratio
E	Cell Potential (Specific Conditions)
E^o	Cell Potential (Standard Conditions)
E_A	Activation Energy
F	Faraday's Constant
ΔG	Gibbs Energy (Specific Conditions)
ΔG^o	Gibbs Energy (Standard Conditions)
ΔH	Enthalpy of Reaction
K_{mn}	Equilibrium Constant
m_i	Molal Concentration of Species *i*
NIR	Near-Infrared
R	Gas Constant
ΔS	Entropy of Reaction
$t_{1/2}$	Half Life
UV	Ultraviolet
v/v	Volume Percentage
Vis	Visible
z	Ionic Charge
α	Alpha Decay
α	Order of Reaction
β	Stability Constant
β'	Conditional Stability Constant
β^-	Negatron Decay
γ	Gamma Radiation
γ_i	Activity Coefficient
ε	DeBye-Hückel Interaction Coefficient
μ	Ionic Strength
$\bar{\nu}$	Antineutrino

DEDICATION

For my parents:

Michael Searle Matteson

and

Carol Joan Matteson

The Chemistry of Acetohydroxamic Acid Related to Nuclear Fuel Reprocessing

1 INTRODUCTION

1.1 Overview of Project

The need to reprocess used nuclear fuel (UNF) from high-level radioactive waste (HLW) has resulted in extraordinary advances in industrial solvent extraction. Starting in the early 1950's, the plutonium uranium extraction (PUREX) process has been adopted by several countries to recovery uranium and plutonium that exist in UNF from commercial power reactors. The United States, however, has not reprocessed its UNF for over thirty years and stores its approximate 60,000 metric tons of UNF (as of the year 2010) in temporary storage [1]. These interim storage sites are located throughout the country, including Department of Energy (DOE) facilities, such as the Hanford site in Washington, and on location at commercial power plants. In order to manage our country's UNF, long-term geologic storage facilities have been proposed for waste storage for an indefinite period of time. Yucca Mountain, located in Nevada, was licensed by the US Nuclear Regulatory Commission to contain 70,000 metric tons of commercial UNF [2]. The site has been given significant consideration as the United States' permanent storage location of its UNF, even though Yucca Mountain would be nearly at its current licensed capacity if all of the US's UNF were to be placed at the site [1]. Due to environmental, economical, and political concerns, Yucca Mountain has not been utilized to date. On March 23, 2010 the US DOE filed a motion with the Nuclear Regulatory Commission to withdraw the license application for the Yucca Mountain high-level nuclear waste repository [2]. Therefore, the United States does not currently have a definitive plan to store or reprocess its UNF.

1.2 Motivation

As a result of the uncertainty of the final destination of the United States' UNF, radioactive waste from commercial power reactors remains a continual and unresolved problem. Therefore, advanced reprocessing schemes are being developed to effectively

separate radioisotopes to reduce both the cost and environmental impact of future reprocessing by minimizing the volume and heat generation of materials required for long-term geologic storage. Due to the ubiquity of the PUREX process, a tremendous breadth of information is known about the extraction of U and Pu by tri-*n*-butyl phosphate (TBP) from acidic media [3-6]. However, much less is known about the chemistry and extraction of minor actinoids (An), lanthanoids (Ln), and fission products that also exist in UNF, and a better understanding of the role of these elements in advanced reprocessing must be determined. For example, ^{237}Np is produced in significant quantities as a result of neutron irradiation of ^{235}U in fuel rods in nuclear reactors and is also produced from the radioactive decay of ^{241}Am, another minor An produced in reactors. When the fuel rods are removed and dissolved in nitric acid for reprocessing in PUREX, neptunium exists in multiple oxidation states and can be distributed in several product streams [3]. A lab-scale demonstration of uranium extraction (UREX+) [4], a suite of advanced reprocessing schemes being developed at Argonne National Laboratory (ANL), successfully extracted uranium and technetium from TRU elements and fission products. Acetohydroxamic acid (AHA) is a reductant/complexant that was added to a segment of UREX+ called uranium extraction (UREX) to facilitate the control of Pu and Np. However, in the process for recovering Pu(IV) and Np(IV) from the fission products and Am and Cm, only 71% of Np remained in the tetravalent oxidation state. A significant portion as Np(V) was not extracted when desired. All neptunium was ultimately recovered in a later process stream by reducing neptunium using hydrogen peroxide and sodium nitrite to Np(IV) for extraction and was then stripped with AHA. Therefore, a better understanding of neptunium chemistry is needed to effectively control its destination in UREX+.

In order to partition Pu and Np from hexavalent uranium by solvent extraction in the UREX process, AHA must reduce Pu and Np to inextractable oxidation states and/or form hydrophilic complexes with these two elements. In addition, AHA must have a minimal effect on the extraction of UO_2^{2+}. Previous literature [5-8] indicates that AHA does not significantly decrease the extraction of U in UREX process conditions. However, little is discussed as to why UO_2^{2+} is insignificantly affected by AHA.

Therefore, additional work is needed to better understand the interaction between UO_2^{2+} and AHA.

Zirconium is produced as a fission product of U during irradiation in commercial power reactors in a greater quantity than Np [5]. Also, Zr, in the form of zircaloy, is used for cladding of fuel rods in nuclear reactors because it possesses a very low thermal neutron cross section and is resistant to corrosion. During de-cladding and dissolution of UNF, additional Zr can be combined with the dissolved UNF, albeit nonradioactive Zr [6]. Therefore, Zr exists in a significant quantity in dissolved UNF and its reactivity must be considered in advanced reprocessing schemes since it has similar chemical properties as tetravalent actinides and also reacts with the AHA that would be added for the control of the extraction of U, Pu, and Np.

AHA has great promise for use in the UREX solvent extraction process to effectively separate Pu and Np from U. By removing certain elements from the UNF waste the volume, radiotoxicity, and heat load of radioactive waste stored in a geologic repository would be significantly reduced. However, the chemistry of AHA and its effect on various elements in UNF must be better understood. The knowledge gained on the laboratory scale can be used for process flowsheet modeling of the UREX+ extraction process and ultimately implemented on an industrial scale to close the nuclear fuel cycle.

1.3 Objectives

Prior to the reprocessing of UNF by the UREX+ process, the role of AHA and how it affects the chemistry of various metal ions must be fully understood. The objectives of this research are to determine how AHA affects the extraction, complexation, and reduction of various metals, such as U, Np, and Zr in UNF reprocessing conditions. The effect of AHA on the extraction of these metals by TBP from acidic media has been studied. The complexation of U, Zr, and Fe with AHA has been studied at various acidic conditions. Stability constants of the complexes were calculated using computational modeling programs. The kinetics of reduction of hexavalent Np by AHA has been

monitored at various temperatures, concentration ratios, and acidities using near-infrared spectroscopy and a stopped-flow apparatus.

1.4 Overview of Document

The work presented in this dissertation was collected at the Oregon State University Laboratory of Transuranic Elements. The dissertation is written in a manuscript format to facilitate submission of its main chapters to scholarly journals for publication and is organized into 8 chapters followed by a bibliography and appendices. The introduction and discussion sections of the manuscripts include information that is also discussed in the general review of the dissertation.

Chapter 1 introduces high-level waste processing and the role of AHA in the advanced reprocessing of UNF, along with motivation for the research. **Chapter 2** provides an extensive review of prior literature, which includes the chemistry of UNF elements in several separation processes, as well as AHA's effect on the extraction, reduction, and complexation of metals in UNF. **Chapter 3** entitled "Complexation Chemistry of Zirconium(IV), Uranium(VI), and Iron(III) with Acetohydroxamic Acid" and **Chapter 5** "A Study of the Kinetics of the Reduction of Neptunium(VI) by Acetohydroxamic Acid in Perchloric Acid" are the manuscripts that have been accepted for publication. They are provided in this dissertation without changes, except for their citations which can be found in the bibliography. These two manuscripts focus on the chemistry of AHA with selected metals in perchlorate medium. Additional experiments were performed to study the chemistry of AHA in nitric acid, which is the typical aqueous phase medium for UNF reprocessing. The results of AHA complexation with Zr in nitric acid are presented and discussed in **Chapter 4**. The reduction of Np(VI) with AHA in nitric acid are reported in **Chapter 6**, which includes details of the spectroscopic experiments and the rate constants calculated for this system. **Chapter 7** includes the experimental details, results, and discussion of the extraction of various metals by TBP from acidic media. **Chapter 8** provides a summary of key results and major conclusions common to the entire dissertation, followed by a bibliography of the entire document in **Chapter 9**. Lastly, the appendices (**Chapters 10** through **12**) provide supporting information for the author's work presented in this dissertation.

2 REVIEW OF LITERATURE

2.1 Chemistry of Metals under Separation Process Conditions

2.1.1 Actinoids

2.1.1.1 Uranium

Uranium has the highest atomic number of all naturally occurring elements and was named after the planet Uranus, which was thought to be the furthest planet from the sun in our solar system at the time of uranium's discovery in 1789 [7, 8]. Like all other An elements, none of its isotopes are stable and decay over time. U exists in nature primarily as ^{238}U (99.3%) with a half-life ($t_{1/2}$) of 4.5 billion years, ^{235}U to a much lesser extent (0.7%) with a $t_{1/2}$ of 0.7 billion years, and ^{234}U in minute amounts (0.006%) with a $t_{1/2}$ of 245,500 years [9]. Two naturally occurring decay chains result from the decay of uranium. The actinium series begins with ^{235}U and after numerous alpha (α) and negatron (β^-) radioactive decays, ^{207}Pb is the resulting stable element. The radium series is initiated when ^{238}U α decays to ^{234}Th, and results in ^{206}Pb after several additional α and β^- decays. Both of these decay series result in the formation of radioactive radon gas, which is responsible for the majority of most human's exposure to ionizing radiation and contributes to adverse health effects, such as lung cancer [10].

Uranium is the fuel source for the United States' nuclear power reactors for the generation of electricity, which consists of enriched uranium dioxide, with 3-5% enrichment of ^{235}U and the remaining as ^{238}U. The fuel is enriched by isotope separation, such as gaseous diffusion or gas centrifugation [11]. ^{235}U is a fissile material and will undergo nuclear fission upon activation by a neutron. Americium-beryllium or plutonium-beryllium devices are often used as a thermal neutron source to initiate the fission of ^{235}U; however, once the fission process commences, it becomes a self-sustaining reaction that is moderated by the addition or removal of neutron absorbing

control rods. As a result of the fission process neutrons, a tremendous amount of energy is released. An example reaction is described by Equation 2.1.

$$ {}^{1}_{0}n + {}^{235}_{92}U \xrightarrow{fission} {}^{89}_{36}Kr + {}^{144}_{56}Ba + 3\,{}^{1}_{0}n + \gamma + 193MeV \qquad 2.1 $$

The reaction described by Equation 2.1 is one of many reactions that result from the activation and fission of ^{235}U. The number of neutrons produced typically varies from two to three, which can then activate additional ^{235}U, sustaining the chain reaction. The amount of energy released from the reaction is 193MeV/fission on average, and includes the kinetic energy of the fission products (FP) and neutrons, as well as energy from the prompt emission of gamma radiation (γ) [12]. The fission products tend to not be of equal mass, but rather two atoms with an atomic mass unit (amu) of about 90 to 100 amu and 130 to 140 amu. This results in the formation of many radioisotopes, such as lanthanoids, transition metals, and gaseous products. Some fission products act as neutron poisons and by absorbing neutrons, they decrease the efficiency of the fission process of uranium in nuclear fuel rods. As a result, the fuel rods must be replaced after four to five years.

When the fuel rods are removed from reactors, the UNF still contains mostly ^{238}U (96%) and some ^{235}U (<1%). For reprocessing, the UNF is dissolved in moderately concentrated nitric acid where the uranium exists primarily as the hexavalent oxidation state (uranyl, UO_2^{2+}). Uranium remains as UO_2^{2+} throughout reprocessing since it is the most stable oxidation state in acidic solutions, as indicated by the Latimer diagram shown in Figure 2.1 (adapted from [13]). The standard reduction potentials (SRPs) of UO_2^{2+}/UO_2^{+} and UO_2^{2+}/U^{4+} are relatively small positive values and an indication that UO_2^{2+} is a weak oxidizing agent and therefore not easily reduced. On the other hand, the standard oxidization potential of U^{4+}/UO_2^{2+} is -0.27V versus a standard hydrogen electrode (SHE) and indicates that U^{4+} is a strong reducing agent. U^{4+} has been used to reduce plutonium and neptunium in reprocessing of UNF [14, 15].

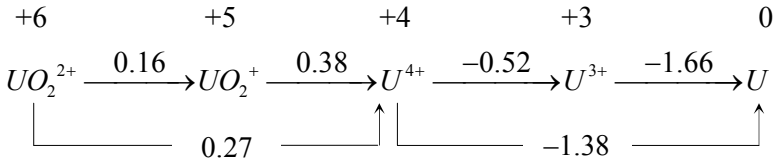

Figure 2.1: Latimer diagram of U SRPs versus SHE in acidic solution.

Hydrolysis and polymerization of metals is described by Equation 2.2, where the formation constant K_{mn} is defined by Equation 2.3. Uranyl hydrolyzes and polymerizes above pH 2 [16]. At an ionic strength (μ) of 1 mol·L^{-1}, temperature of 298K, and uranyl concentration of 0.1 mol·L^{-1} the $(UO_2)_2(OH)_2^{2+}$ dimer begins to form. At a pH above 4, the $(UO_2)_3(OH)_5^{+}$ trimer is the dominant species [16]. However, when UNF is dissolved in 3-4 mol·L^{-1} HNO_3, uranium exists as UO_2^{2+} or as a uranyl nitrate complex so hydrolysis and polymerization is not of significant concern. Other actinoids with higher atomic numbers, such as plutonium, tend to hydrolyze more readily because of differences in their ionic radii.

$$mM_{(aq)}^{z+} + nH_2O_{(l)} \rightleftharpoons [M_m(OH)_n]_{(aq)}^{(z\cdot m-n)+} + nH_{(aq)}^{+} \qquad 2.2$$

$$K_{mn} = \frac{[M_m(OH)_n][H^+]^n}{[M]^m} \qquad 2.3$$

Uranyl nitrate is readily extracted by tri-*n*-butyl phosphate (TBP, Figure 2.2) from typical reprocessing conditions consisting of a 3-4 mol·L^{-1} HNO_3 aqueous phase and TBP dissolved to 30% (1.1 mol·L^{-1}) by volume (v/v) in a hydrocarbon diluent, such as *n*-dodecane or odorless kerosene [17].

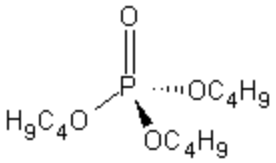

Figure 2.2: Structure of TBP.

The mechanism of the extraction of UO_2^{2+} by TBP is described by Equation 2.4. Uranyl is extracted as a neutral solvate, as the metal charge is compensated by the coordination of two nitrate ions. The extraction of uranyl is enhanced with increasing nitrate concentration, driving the equilibrium of Equation 2.4 to the right by mass action. Additional information on the extraction of U can be found in sections 2.2.1 and 7.3.1.

$$UO_{2\,(aq)}^{2+} + 2NO_{3\,(aq)}^{-} + 2TBP_{(org)} \rightleftharpoons UO_2(NO_3)_2 \cdot 2TBP_{(org)} \qquad 2.4$$

2.1.1.2 Plutonium

Plutonium was first synthesized by Seaborg and coworkers in 1940 [18] and has received tremendous attention ever since for peaceful uses, such as nuclear power and thermoelectric batteries, and also for use in nuclear weapons. To continue to the trend of naming elements with high atomic numbers for the planets in our solar system, plutonium was named after Pluto, which was thought to be ninth planet in our solar system at the time of Pu's discovery [19]. Today Pluto is considered a dwarf planet, but plutonium continues to bear its name. Pu does not exist in nature and is produced as a byproduct in commercial nuclear power plants, one reaction described by Equation 2.5, and is generated in cyclotrons and breeder reactors [20].

$${}_0^1n + {}_{92}^{238}U \rightarrow {}_{92}^{239}U \xrightarrow{23.5\ \text{min}} \beta^- + \overline{\nu} + {}_{93}^{239}Np \xrightarrow{2.4\ \text{days}} {}_{94}^{239}Pu + \beta^- + \overline{\nu} \qquad 2.5$$

Plutonium is produced as several isotopes, including ^{238}Pu ($t_{1/2}$ 87.5 years) and ^{239}Pu ($t_{1/2}$ 24,100 years) [9]. ^{238}Pu emits a large amount of thermal energy with little penetrating radiation, making it a good source for thermoelectric generators to heat electronic devices in spacecrafts. It was also used to power artificial pacemakers for human hearts during the past half century; however, ^{238}Pu has been replaced by lithium-iodine batteries in recent years [21]. ^{239}Pu is a fissile isotope and is the primary component in nuclear weapons. Upon absorption of a neutron, plutonium can undergo spontaneous fission and release a tremendous amount of energy (199MeV/fission on average) from the kinetic energy of prompt neutrons, fission products, and prompt γ emission. One such reaction is described by Equation 2.6 [12].

$${}_0^1n + {}_{94}^{239}Pu \xrightarrow{fission} {}_{41}^{101}Nb + {}_{53}^{135}I + 4\,{}_0^1n + 199MeV \qquad 2.6$$

Plutonium has several properties that are unique compared to other actinoids and most elements. Under atmospheric pressure, solid Pu metal has six allotropes which vary in both crystal structure and density, with the simple monoclinic and face-centered cubic densities differing by more than 25% at constant pressure [22]. An increase in density can facilitate in ^{239}Pu achieving criticality, whether it be intentional or not. Also, the change in allotropic forms makes the machining of plutonium difficult. When dissolved in acidic media, Pu can exist as several stable oxidation states, ranging from trivalent (Pu^{3+}) to hexavalent (PuO_2^{2+}) [23]. On the other hand, thorium and uranium are most stable a single oxidation state as the tetra- and hexavalent oxidation states, respectively. The similarity of the SRPs (approximately 1 volt versus SHE) of the plutonium oxidation states ranging from Pu^{3+} to PuO_2^{2+} causes this equilibrium, as shown in its Latimer diagram (Figure 2.3, adapted from [13]).

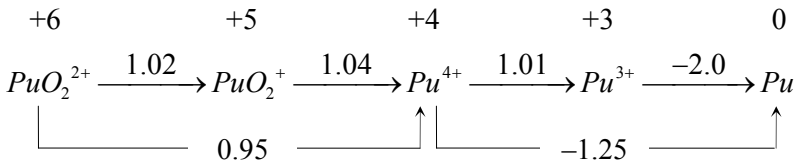

Figure 2.3: Latimer diagram of Pu SRPs versus SHE in acidic solution.

In dissolved UNF, Pu exists primarily in the tetravalent (Pu^{4+}) and PuO_2^{2+} oxidation states. Both forms are readily extracted by TBP (Equations 2.7 and 2.8) during the initial co-extraction with U and separated from most fission products and the trivalent actinides and lanthanides.

$$Pu^{4+}_{(aq)} + 4NO_{3\,(aq)}^{-} + 2TBP_{(org)} \rightleftharpoons Pu(NO_3)_4 \cdot 2TBP_{(org)} \qquad 2.7$$

$$PuO_2^{2+}{}_{(aq)} + 2NO_3^{-}{}_{(aq)} + 2TBP_{(org)} \rightleftharpoons PuO_2(NO_3)_2 \cdot 2TBP_{(org)} \qquad 2.8$$

To separate Pu from U, a reducing agent is added to reduce Pu to Pu^{3+} to strip it back to a fresh aqueous phase. In the past ferrous iron, as ferrous sulfamate, has been used to reduce Pu to its poorly extracted trivalent oxidation state. With an oxidation potential of -0.771 V versus SHE for Fe^{2+}/Fe^{3+} [13], ferrous iron is thermodynamically capable of reducing Pu in a high oxidation state to Pu^{3+}. The Gibbs free energy and Nernst

Equations can be combined to show that the free energy of a reduction-oxidation reaction is directly proportional to the cell potential of the reaction (Equation 2.9), where ΔG is the free energy of reaction under specific and standard-state conditions (ΔG^o), n is the number of moles of electrons transferred in the reaction, F is Faraday's constant (96485 $C \cdot mol^{-1}$), and E is the cell potential under specific and standard-state conditions (E^o). So with a large positive Pu reduction potential of approximately 1 V and a smaller negative oxidation potential for Fe^{2+}/Fe^{3+}, E is positive so ΔG becomes negative and is an indication that the reaction would be spontaneous.

$$\Delta G = -nFE \quad \text{or} \quad \Delta G^o = -nFE^o \qquad 2.9$$

More recently, U(IV) has been used instead of ferrous iron to reduce high valency plutonium to Pu^{3+}. With an oxidation potential of -0.27 V versus SHE for U^{4+}/UO_2^{2+}, tetravalent uranium can also be used to reduce Pu. By adding U instead of Fe, nothing extraneous is added to the product stream. Any uranium that was oxidized to UO_2^{2+} by the reduction of Pu or unreacted U^{4+} can be separated from the reduced Pu^{3+} by re-extraction of U by TBP.

Plutonium is susceptible to disproportionation in acidic solutions and undergoes several reactions which result in an equilibrium of its oxidation states and is highly dependent on the acid concentration. Pu^{4+} disproportionates at low acidity, forming Pu^{3+} and pentavalent PuO_2^{+} (Equation 2.10). PuO_2^{+} can then react with Pu^{4+} to form Pu^{3+} and PuO_2^{2+} (Equation 2.11), which readily occurs since it is simply an electron transfer from PuO_2^{+} to Pu^{4+} and the di-oxygen bonds are neither created nor destroyed. Pentavalent Pu also disproportionates at low PuO_2^{+} concentrations (beginning at 10^{-8} $mol \cdot L^{-1}$) to Pu^{4+} and PuO_2^{2+} (Equation 2.12) [24]. These reactions contribute to the insignificant concentration of PuO_2^{+} in aqueous feed solutions in UNF reprocessing. When Pu^{4+} is initially diluted in 0.5 $mol \cdot L^{-1}$ hydrochloric acid , the oxidation state equilibrium distribution is 26.3%, 62.7%, 0.5%, and 10.5% for Pu^{3+}, Pu^{4+}, PuO_2^{+}, and PuO_2^{2+}, respectively [25]. At higher acidity, the contribution of PuO_2^{+} is even less. Only at extremely low Pu concentrations ($\sim 10^{-12}$ $mol \cdot L^{-1}$) and higher pH (5 though 9) does the pentavalent oxidation state exist in

significant amounts, such as in ocean and fresh waters, where PuO_2^+ exists in majority compared to the other oxidation states [20].

$$2Pu^{4+}_{(aq)} + 2H_2O_{(l)} \rightleftharpoons Pu^{3+}_{(aq)} + PuO^{+}_{2\,(aq)} + 4H^{+}_{(aq)} \quad 2.10$$

$$PuO^{+}_{2\,(aq)} + Pu^{4+}_{(aq)} \rightleftharpoons PuO^{2+}_{2\,(aq)} + Pu^{3+}_{(aq)} \quad 2.11$$

$$2PuO^{+}_{2\,(aq)} + 4H^{+}_{(aq)} \rightleftharpoons Pu^{4+}_{(aq)} + PuO^{2+}_{2\,(aq)} + 2H_2O_{(l)} \quad 2.12$$

The atomic and ionic radii of the actinoids decrease with increasing atomic number as a result of the subsequent filling of the 5f subshell (Figure 2.4, [23, 26]).

Th^{4+}	U^{4+}	Np^{4+}	Pu^{4+}
97.2	91.8	90.3	88.7

Figure 2.4: Effective ionic radii of tetravalent actinoids, in picometers.

This trend has been described as the An contraction [20]. Accordingly, the charge densities of the An ions increase with increasing atomic number. The probability of formation of complexes and hydrolysis increases with atomic number as well. In general, this pattern can be seen by comparing the hydrolysis formation constants and distribution ratios of the tetravalent actinoids. $Th(OH)^{3+}$ has a much lower hydrolysis formation constant $\log_{10}K_{11}^{o} = -3.3 \pm 0.1$ [27] than $Pu(OH)^{3+}$, whose formation constant $\log_{10}K_{11}^{o} = -0.78 \pm 0.60$ [28], where K_{mn} is described by Equation 2.3. Therefore, plutonium hydrolyzes and polymerizes more readily than most other actinoids, even in high acidity. In particular, the polymerization of plutonium can result in its inextractability. The formation of plutonium precipitates and polymerized species is of concern in UNF reprocessing and should be avoided.

2.1.1.3 Thorium

Thorium is an An element found in the earth's rocks and soil. ^{232}Th is the only thorium isotope that occurs in nature in any significance, has a $t_{1/2}$ of 14 billion years, and decays to ^{228}Rn [9]. Other isotopes, such as $^{228,231,234}Th$, exist in equilibrium concentrations in

naturally-occurring radioactive decay chains. One such decay chain is the thorium series, where ^{232}Th is the initial radioisotope and after a series of α and β^- decays, ^{208}Pb results as the stable end product. Thorium has been given considerable attention as a nuclear fuel source throughout the past several decades [29]. Although ^{232}Th itself is not fissile, and thus will not undergo nuclear fission, it is fertile so it does absorb neutrons and decays, resulting in the formation of ^{233}U (Equation 2.13).

$$ {}^{1}_{0}n + {}^{232}_{90}Th \rightarrow {}^{233}_{90}Th \xrightarrow[\beta^-]{\text{22 minutes}} {}^{233}_{91}Pa \xrightarrow[\beta^-]{\text{27 days}} {}^{233}_{92}U \qquad 2.13 $$

^{233}U can be bred for fuel to generate electricity in nuclear reactors. The use of thorium as a fuel source, instead of ^{235}U, had its advantages because thorium can be used in its natural isotopic state and does not have to be enriched. Also, thorium is more abundant in nature than uranium and is potentially a more sustainable fuel source. However, in the United States ^{235}U, and not ^{233}U bred from ^{232}Th, remains as the radioisotope of choice for commercial power reactor fuel.

UNF is the result of the fission process of ^{235}U that occurs in United States' commercial power reactors. Thorium exists in insignificant quantities in UNF as the result of alpha decay of various isotopes of uranium. Therefore, the role of thorium in UNF reprocessing is not of great importance. However, thorium exists exclusively in the tetravalent oxidation state (Th^{4+}) and can be used as a chemical analogue for other tetravalent actinoids, such as plutonium and neptunium. Thorium readily hydrolyzes and polymerizes in pH solutions above pH > 3 [30], but exists as the unhydrolyzed Th^{4+} cation in the strongly acidic solutions.

Thorium is extracted by TBP from acidic media [17] (Equation 2.14) as a neutral solvate. The metal charge is compensated by the coordination of four nitrate ions [31]. The extraction of Th is less than other actinoids because of its larger ionic radius (Figure 2.4).

$$ Th^{4+}_{(aq)} + 4NO^{-}_{3\,(aq)} + 2TBP_{(org)} \rightleftharpoons Th(NO_3)_4 \cdot 2TBP_{(org)} \qquad 2.14 $$

2.1.2 Minor Actinoids

2.1.2.1 Neptunium

Neptunium is the first transuranic (TRU) element on the periodic table and was synthesized by the neutron activation of uranium in a cyclotron and published in 1940 [32, 33]. With an atomic number of 93 and the next element heavier than uranium, neptunium was named after the planet Neptune, which is the next planet beyond Uranus [8]. Natural Np no longer exists on earth in any significance. A neptunium radioactive decay chain was present on earth with ^{237}Np decaying and ultimately resulting in the formation of stable ^{209}Bi. However, ^{237}Np has a $t_{1/2}$ of 2.14 million years and is too short to still exist as a primordial element. Today, Np is typically produced as a byproduct in nuclear reactors as the result of neutron activation and β^- decay of ^{237}U (Equation 2.15).

$$\begin{matrix} {}^{235}_{92}U(n,\gamma)\,{}^{236}_{92}U(n,\gamma) \\ \searrow \\ {}^{238}_{92}U(n,2n) \end{matrix} \quad {}^{237}_{92}U \xrightarrow{6.7\ \mathrm{d}} {}^{237}_{93}Np + {}^{0}_{-1}\beta^- + \bar{\nu} \qquad 2.15$$

In moderately concentrated HNO_3, neptunium exists primarily in the pentavalent (NpO_2^+) and hexavalent (NpO_2^{2+}) oxidation states, and in the tetravalent (Np^{4+}) oxidation state to a lesser extent. Unlike most other actinoid elements, Np's pentavalent oxidation state is stable. Katz and Seaborg [34] describe neptunium as having, "a place of honor among the most interesting of the elements" because the NpO_2^+ ion, "is practically unique in the Periodic Table". NpO_2^+ is of significant concern due to its significant mobility in the environment and absorption by humans compared to other actinoids [35]. The trivalent (Np^{3+}) oxidation state only exists in an anaerobic environment and the heptavalent oxidation state (NpO_5^{3-}) is unstable in strongly acidic solutions. These two oxidation states are non-existent in UNF dissolved in HNO_3 and not of concern [36]. The Latimer diagram for neptunium in acidic solutions is shown in Figure 2.5 (adapted from [13]).

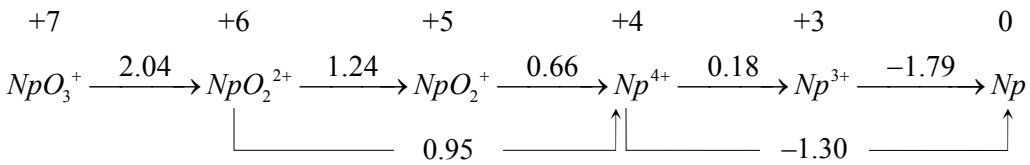

Figure 2.5: Latimer diagram of Np SRPs versus SHE in acidic solution.

All three states (Np^{4+}, NpO_2^+, NpO_2^{2+}) are in equilibrium with their relative proportions determined by the acidity, complexation agents, and redox potentials (Equation 2.16). In low acidity (< 2.0 mol·L^{-1}), NpO_2^+ is the dominate species. However, NpO_2^+ slowly disproportionates above 2.0 mol·L^{-1} HNO_3 to the tetra- and hexavalent states, and is nonexistent above 8.0 mol·L^{-1} HNO_3 [37]. This disproportionation reaction is of particular importance in reprocessing because the neptunium oxidation states are greatly dependent on the acidity of the aqueous phase.

$$2NpO_{2\,(aq)}^{+} + 4H_{(aq)}^{+} \rightleftharpoons Np_{(aq)}^{4+} + NpO_{2\,(aq)}^{2+} + 2H_2O_{(l)} \qquad 2.16$$

To further complicate the oxidation states of neptunium, NpO_2^+ is oxidized by nitric acid when a catalytic amount (10^{-5} to 10^{-3} mol·L^{-1}) of nitrous acid is present (Equation 2.17) [38].

$$2NpO_{2\,(aq)}^{+} + NO_{3\,(aq)}^{-} + 3H_{(aq)}^{+} \rightleftharpoons 2NpO_{2\,(aq)}^{2+} + HNO_{2(aq)} + H_2O_{(l)} \qquad 2.17$$

HNO_2 is formed during fuel dissolution from the radiolysis of nitric acid, and was also added in catalytic amounts to the fuel stream at the US Hanford reprocessing plant to oxidize neptunium to NpO_2^{2+} [39]. Oxidation is favored at high nitric acid and low nitrous acid concentrations. However, if higher concentrations of nitrous acid are present NpO_2^{2+} will reduce to NpO_2^+, so HNO_2 must be maintained in catalytic amounts if neptunium is to be kept in the readily extractable hexavalent oxidation state. When UNF is dissolved in nitric acid, Np^{4+} exists in a lesser concentration than either NpO_2^+ or NpO_2^{2+}. As indicated by its Latimer diagram (Figure 2.5), the NpO_2^{2+}/Np^{4+} and NpO_2^+/Np^{4+} reduction potentials are significantly lower than the NpO_2^{2+}/NpO_2^+ reduction potential. These lower potentials occur because the dioxo bond would need to be ruptured in order to reduce neptunium to the tetravalent oxidation state. Therefore, neither NpO_2^{2+}

nor NpO_2^+ are easily reduced to Np^{4+} (except for the disproportionation of NpO_2^+) (Equation 2.16), which explains why Np^{4+} is less concentrated in aqueous reprocessing.

Under acidic conditions, pentavalent neptunium essentially remains in the aqueous phase, whereas neptunium in the tetra- and hexavalent oxidation states is extracted into TBP/dodecane solutions as adducts of neutral nitrate complexes with TBP.

$$Np^{4+}_{(aq)} + 4NO_{3\,(aq)}^{-} + 2TBP_{(org)} \rightleftharpoons Np(NO_3)_4 \cdot 2TBP_{(org)} \qquad 2.18$$

$$NpO_2^{2+}{}_{(aq)} + 2NO_3^{-}{}_{(aq)} + 2TBP_{(org)} \rightleftharpoons NpO_2(NO_3)_2 \cdot 2TBP_{(org)} \qquad 2.19$$

From Equations 2.18 and 2.19, it can be expected that the extraction of both Np^{4+} and NpO_2^{2+} is enhanced as the nitric acid concentration is increased. However, a maximum distribution occurs at 5 mol·L^{-1} HNO_3 and 8 mol·L^{-1} HNO_3 for NpO_2^{2+} and Np^{4+}, respectively [37]. This is caused by the extraction of HNO_3 by the basic phosphoryl group of tri-butyl phosphate. At high nitric acid concentrations, increased amount of HNO_3 extracted by TBP reduces the amount of free TBP available for extracting neptunium. In order to enhance the extraction of neptunium without increasing the acidity of the aqueous phase, salting-out agents can be used. By adding non-extractable nitrates, such as $LiNO_3$ or $Al(NO_3)_3$, the equilibrium of Equations 2.18 and 2.19 shifts to the right and aids in a more complete extraction of neptunium. In addition, a salting-out agent has a strong affinity for water and becomes hydrated in aqueous solutions. This effect is as if neptunium is dissolved in a smaller quantity of water; thus, the relative concentration of the neptunium increases which also facilitates with its extraction [40].

Neptunium is more susceptible to hydrolysis than either Th or U because of its smaller radius and larger effective cationic charge. Np^{4+} begins to hydrolyze (Equation 2.2) in solutions with a pH $\geq$ 1. NpO_2^{2+}, with an effective charge less than Np^{4+} (Figure 2.6, [20]) hydrolyzes at a higher pH of 3 [16]. As the NpO_2^{2+} concentration increases with decreasing pH, insoluble neptunium polymerized species begin to form [41]. The formation of any actinoid precipitate should be avoided to minimize reprocessing complexity.

An^{4+}	AnO_2^{2+}	An^{3+}	AnO_2^{+}
4.0	3.3	3.0	2.2

Figure 2.6: Effective cationic charges of actinoids.

2.1.2.2 Americium and Curium

Americium and Curium with atomic numbers 95 and 96, respectively, are TRU elements that lie beyond Pu on the periodic table and are not found in nature. Am was first synthesized by Glenn T. Seaborg in 1944 by successive neutron capture reactions of ^{239}Pu and was named after the Americas (Equation 2.20) [42]. Cm was synthesized by Seaborg shortly thereafter at the University of Berkeley by bombarding ^{239}Pu with helium ions in a cyclotron (Equation 2.21) [42]. Curium was named in honor of Marie and Pierre Curie, two early chemists/physicists who studied radioactive elements and discovered polonium and radium.

$$2\,{}_{0}^{1}n + {}_{94}^{239}Pu \rightarrow {}_{94}^{241}Pu \xrightarrow[\beta^-]{14.35\ \text{a}} {}_{95}^{241}Am \qquad 2.20$$

$${}_{2}^{4}He + {}_{94}^{239}Pu \rightarrow {}_{96}^{242}Cm + {}_{0}^{1}n \qquad 2.21$$

Both Am and Cm are created in UNF as the result of sequential neutron activations and decays of U, Pu, and Am itself. The isotopes of interest are ^{241}Am ($t_{1/2}$ = 433 years), ^{234}Am ($t_{1/2}$ = 7400 years), ^{243}Cm ($t_{1/2}$ = 29 years) and ^{244}Cm ($t_{1/2}$ = 18 years) [43]. All of these radioisotopes are alpha emitters and contribute significantly to the heat and radiotoxicity of UNF. Therefore, considerable research has been done on these two elements to separate them from the uranium waste stream and isolate Am and Cm from other elements in solvent extraction reprocessing. Both exist exclusively in the trivalent oxidation state (Am^{3+} and Cm^{3+}) in acidic solutions, as indicated by their Latimer diagrams (Figure 2.7, adapted from [13]). AmO_2^{+}/Am^{3+}, Am^{4+}/Am^{3+}, and Cm^{4+}/Cm^{3+} reduction potentials are large positive values, indicating that the higher valency cations are good oxidizing agents and will themselves be reduced to their trivalent oxidation states. Also, the reduction potentials to their zero oxidation states are negative potentials,

so Am^{3+} and Cm^{3+} are poor oxidizing agents and are not easily reduced. Therefore, both Am and Cm are thermodynamically most stable in their respective trivalent oxidation states.

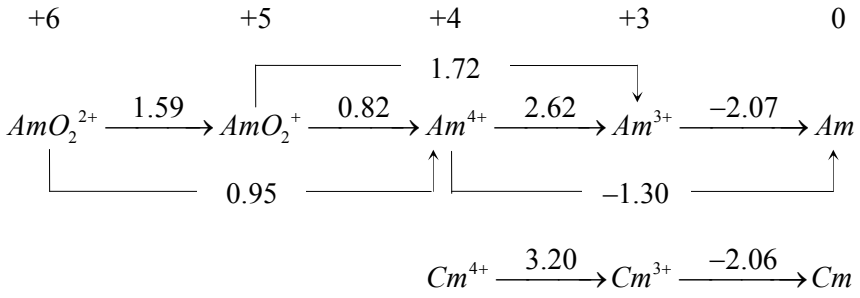

Figure 2.7: Latimer diagrams of Am and Cm SRPs versus SHE in acidic solution.

Trivalent metals are not well extracted by TBP in typical UNF reprocessing conditions. M^{3+} cations have a lower effective cationic charge than either M^{4+} or MO_2^{2+} cations (Figure 2.6), so the coordination of nitrate ions to trivalent metals is not as strong as the nitrate coordination to tetra- or hexavalent metals. Also, an additional TBP molecule is required for the extraction of trivalent metals compared to M^{4+} or MO_2^{2+} cations. Therefore, Am^{3+} and Cm^{3+} mostly remain in the aqueous phase and can be separated from UO_2^{2+} and Pu^{4+}. However, due to the heat load and radiotoxicity contribution by Am and Cm in UNF, there is a need to separate Am and Cm from the shorter lived fission products, such as the trivalent lanthanides. Advanced reprocessing schemes have been developed to separate Am and Cm from trivalent lanthanides based on their differences of ionic radii. A review of one of these processes is described in section 2.2.2.5. Once Am and Cm are separated, they can be irradiated with fast neutrons from a nuclear reactor. These activated Am and Cm isotopes then undergo fission to various radioactive fission products with shorter half-lives. Nonradioactive fission products are also produced. The goal of the transmutation is to convert Am and Cm to nonradioactive and shorter lived elements to significantly decrease the long term radiotoxicity of UNF [43].

2.1.3 Fission Products

2.1.3.1 Zirconium

Zirconium is produced in significant quantities as ^{95}Zr, and ^{93}Zr to a less extent, in nuclear fuel as the result of the fission process of uranium. In fact, zirconium is the third most abundant fission product by mass during the first ten years after the removal of commercial power reactor fuel rods [44]. ^{95}Zr can be produced directly from the fission of ^{235}U, as well as from the decay of ^{95}Y ($t_{1/2}$ 10.3 minutes), which is another fission product of ^{235}U. With a long half-life of 1.5 million years and low concentration, ^{93}Zr does not significantly contribute to the activity of UNF [44]. On the other hand, ^{95}Zr has a short $t_{1/2}$ of 64 days, emits two energetic γ *ra*ys at 724 and 757 keV, and β^- decays to ^{95}Nb [9]. ^{95}Nb also has an energetic gamma ray at 766 keV when it β^- decays to stable ^{95}Mo. During initial dissolution of UNF, ^{95}Zr and ^{95}Nb contribute a large fraction of the total γ activity of the aqueous feed [45] and their β decays are shown below (Equation 2.22).

$$^{95}_{40}Zr \xrightarrow{64\text{ days}} {}^{0}_{-1}\beta + \bar{\nu} + {}^{95}_{41}Nb \xrightarrow{35\text{ days}} {}^{95}_{42}Mo + {}^{0}_{-1}\beta + \bar{\nu} \qquad 2.22$$

Zirconium is also an important metal in the nuclear industry and is used for the cladding of nuclear fuel rods because of its low neutron cross section and alloys are resistance to corrosion. During the decladding of the fuel nonradioactive zirconium, ^{90,91,92,94,96}Zr, can be dissolved with the fuel and present in UNF reprocessing aqueous feed solutions [6].

Between ^{95}Zr produced as a fission product of uranium and nonradioactive Zr from the decladding of fuel, zirconium exists in the aqueous feed of dissolved UNF in significant quantities. Of all the fission products produced from irradiated nuclear fuel, ^{95}Zr along with its daughter ^{95}Nb and ruthenium, are considered the "most troublesome" elements in terms of reprocessing [6, 44] because of the Zr oxidation state, strong tendency to hydrolyze and polymerize in acidic solutions, and challenging extraction equilibrium. Zirconium exists exclusively in the tetravalent oxidation state in aqueous solutions, as indicated by its brief Latimer diagram (Figure 2.8, adapted from [13]). As a result,

zirconium has similar chemical properties as the tetravalent actinoids, such as Pu^{4+} and Np^{4+}, and follows them in waste streams in solvent extraction.

$$\begin{array}{cc} +4 & 0 \\ Zr^{4+} & \xrightarrow{-1.55} Zr \end{array}$$

Figure 2.8: Latimer diagram of Zr SRPs versus SHE in acidic solution.

Zirconium will hydrolyze and polymerize in aqueous feed solutions, with nitrate anions competing for coordination sites with both water and hydroxide anions on the Zr^{4+} cation, which forms complexes with the general formula [39]:

$$[Zr(OH)_x(NO_3)_y(H_2O)_z]^{4-x-y}_{(aq)} \qquad x+y \le 4 \qquad 2.23$$

Previous studies performed in perchloric acid, a non-complexing strong acid, postulated that trimeric ($Zr_3(OH)_4^{8+}$ or $Zr_3(OH)_5^{7+}$) and tetrameric ($Zr_4(OH)_8^{8+}$) species begin to form at approximately 5×10^{-4} mol·L^{-1} zirconium solutions in 1 mol·L^{-1} $HClO_4$ [46]. More recently, Ekberg et al. [47] determined that the monomeric hydrolyzed species $Zr(OH)^{3+}$, $Zr(OH)_2^{2+}$, $Zr(OH)_3^{+}$, and $Zr(OH)_4$ and polymeric species $Zr_2(OH)_6^{2+}$, $Zr_3(OH)_4^{8+}$, and $Zr_4(OH)_8^{8+}$ exist in acidic solutions, and the solubility of Zr^{4+} in solution is dependent on acid strength and metal concentration. Uncomplexed Zr^{4+} is the dominant species only in high $HClO_4$ solutions ($\geq$ 1 mol·L^{-1}) and very low concentrations of zirconium ($\leq 10^{-5}$ mol·L^{-1}). A typical HNO_3 aqueous feed solution contains approximately 0.1 mol·L^{-1} Zr; however, the zirconium concentration is highly dependent on the type of fuel, its burnup time, and the cooling time of the fuel rods prior to dissolution. Nonetheless, the high concentration of zirconium results in significant hydrolyzed and polymerized species that exist in the HNO_3 feed solution.

Metal cations must coordinate with nitrate ions in the aqueous phase prior to being extracted by TBP. These metal·nitrate complexes also compete for free TBP with the extraction of HNO_3 itself. At high acid concentrations, nitric acid is very well extracted by TBP. This results in a distribution maximum of the metal at high HNO_3

concentrations, which occurs at approximately 6-8 mol·L^{-1} HNO_3 for Pu^{4+} and Np^{4+}. On the other hand, the extraction of zirconium continuously increases as the equilibrium concentration of HNO_3 in the aqueous phase increases [48]. Numerous studies have attempted to determine the extraction mechanism(s) of Zr by TBP. An early study found that only the disolvate species was formed by the extraction of Zr (Equation 2.24) [44]. However, a later and more comprehensive study of the thermodynamic analysis of experimental distribution data determined that two additional Zr species (Equations 2.26 and 2.25) were extracted by TBP, as well as the unhydrolyzed species (Equation 2.24) [49, 50]. Solovkin [49, 50] determined that the two hydrated species are extracted at lower HNO_3 concentrations, whereas the unhydrolyzed tetranitrate complex dominates at higher acid concentrations (6 mol·L^{-1} HNO_3). He did not determine that any monosolvate species, $Zr(NO_3)_4$·TBP, was formed or extracted. Prior studies found that this species was the dominate complex for TBP concentrations ≤ 0.3 mol·L^{-1} [53, 55, 56].

$$Zr^{4+}{}_{(aq)} + 4NO_{3\,(aq)}^{-} + 2TBP_{(org)} \rightleftharpoons Zr(NO_3)_4 \cdot 2TBP_{(org)} \qquad 2.24$$

$$Zr(OH)^{3+}{}_{(aq)} + 3NO_3{}^{-}{}_{(aq)} + 2TBP_{(org)} \rightleftharpoons Zr(OH)(NO_3)_3 \cdot 2TBP_{(org)} \qquad 2.25$$

$$Zr(OH)_2{}^{2+}{}_{(aq)} + 2NO_3{}^{-}{}_{(aq)} + 2TBP_{(org)} \rightleftharpoons Zr(OH)_2(NO_3)_2 \cdot 2TBP_{(org)} \qquad 2.26$$

One hypothesis that better describes zirconium's unusual extraction equilibrium considers other solvated species that greatly enhance the extraction of Zr [51]. TBP is relatively unstable with respect to ionizing radiation and decomposes into several degradation products. When TBP interacts with highly energetic γ rays from radioisotopes such as ^{95}Zr and ^{95}Nb, TBP can degrade to dibutyl phosphoric acid (HDBP) or monobutyl phosphoric acid (H_2MBP). Both TBP and HDBP extract Zr into the organic phase and the solvates can be stripped back to the aqueous phase. In typical dissolved UNF, the HDBP:H_2MBP concentration ratio is on the order of 10:1, so HDBP has a greater influence on the amount of zirconium extracted (Equation 2.27). $Zr(MBP)_2$ complexes that exist in the organic phase are not strippable using dilute nitric acid, meaning that all zirconium that coordinates with MBP in the organic phase is completely retained and cannot be back extracted to the aqueous phase [51]. This results from the

fact that H_2MBP is an acidic extractant, so a low hydrogen-ion concentration enhances the extraction of $Zr(MBP)_2$, as described by Equation 2.28.

$$Zr^{4+}_{(aq)} + 4HDBP_{(org)} \rightleftharpoons Zr(DBP)^{4+}_{(org)} + 4H^{+}_{(aq)} \quad 2.27$$

$$Zr^{4+}_{(aq)} + 2H_2MBP_{(org)} \rightleftharpoons Zr(MBP)_{2(org)} + 4H^{+}_{(aq)} \quad 2.28$$

Maya [51] found that the rate of formation of non strippable $Zr(MBP)_2$ species increases with increasing acidity in the organic phase, which agrees with zirconium's unique extraction distribution in highly concentrated HNO_3. All Zr that was initially extracted by a mixture of TBP and H_2MBP was completely converted to its non strippable form in less than one hour. Additionally, H_2MBP can cause the formation of gelatinous $Zr(MBP)_2 \cdot H_2O$ precipitates in the aqueous phase [51]. So H_2MBP, as a degradation product of both TBP and HDBP, can disrupt the equilibrium of zirconium that is distributed between the two phases and causes an elevated distribution ratio of Zr [51, 52]. This strong retention of Zr in the organic phase can have a detrimental effect on the reprocessing of UNF in extraction processes. With ^{95}Zr and its daughter ^{95}Nb in contact with TBP, a significant amount of TBP can degrade to H_2MBP, allowing for even more zirconium to be extracted as a non strippable form. Thus, a deleterious cycle of the degradation of TBP and extraction/retention of ^{95}Zr in the organic phase occurs. This decreases the partitioning of U and Pu from other elements in reprocessing by reducing the concentration of TBP necessary for their extraction [17].

There are additional reactions that affect the extraction of zirconium in UNF reprocessing. Technetium is a fission product present in UNF in significant quantities as the heptavalent pertechnetate ion, TcO_4^- [44]. TcO_4^- is reasonably extracted from 1 $mol \cdot L^{-1}$ HNO_3 at high TBP concentrations ($\geq$ 30%) and 25°C [53]. However, a synergistic effect occurs with technetium and zirconium as complexation occurs between Zr^{4+} and TcO_4^- ions and the co-extraction of the two metals is enhanced (Equation 2.29) [54].

$$Zr^{4+}_{(aq)} + 3NO^{-}_{3\,(aq)} + TcO^{-}_{4\,(aq)} + 2TBP_{(org)} \rightleftharpoons Zr(NO_3)_3(TcO_4) \cdot 2TBP_{(org)} \quad 2.29$$

Zirconium can also form insoluble precipitates with molybdenum as the $Zr(MoO_4)_2 \cdot nH_2O$ complex, particularly at low acidity [44]. Molybdenum is formed in UNF during the

fission process of uranium and ^{95}Mo is also the granddaughter of ^{95}Zr (Equation 2.22). The formation of this precipitate is undesirable as it complicates reprocessing by introducing solids to a liquid-liquid extraction system.

In reviewing zirconium's role in typical UNF reprocessing conditions, Zr is well extracted both as the tetranitrate and mono- and dihydrolyzed species (Equations 2.24-2.26). The extraction is enhanced at high HNO_3 concentrations and a distribution maximum is not observed for increasing HNO_3. ^{95}Zr causes the radiolytic degradation of TBP, which results in Zr·MBP species forming in the organic phase that cannot be stripped back to the aqueous phase. To minimize the extraction of zirconium, contact between the aqueous and organic phases should occur at 30°C and low acidity, when the distribution of Zr is at a minimum [55]. However, zirconium tends to form insoluble precipitates with Mo, particularly at low acidity. Therefore, controlling Zr in separation streams is a significant technical challenge but is crucial in achieving effective separation of numerous elements in the reprocessing of UNF. If time is not of the essence, the fuel rods can cool for more several years so that ^{95}Zr and ^{95}Nb decay to stable ^{95}Mo prior to the dissolution of the fuel.

2.1.3.2 Cerium

Cerium is produced in UNF as a fission product of ^{235}U and is one of the most abundant fission products in low-enriched uranium fuel immediately upon removal of the UNF rods from the reactor [44]. Both ^{141,144}Ce isotopes undergo β and are of concern in terms of reprocessing because of their high activity. ^{141}Ce has a $t_{1/2}$ of 32.5 days with E_{max} = 435 keV whereas ^{144}Ce has a $t_{1/2}$ of 285 days with E_{max} = 319 keV. Therefore, they will contribute to the radiotoxicity and heat of UNF for several years. In acidic solutions, cerium exists in the tri- and tetravalent oxidation states. The SRP of Ce^{4+}/Ce^{3+} is +1.71 ± 0.02V versus SHE [13] and indicates that Ce^{4+} is a strong oxidizing agent. During the dissolution of UNF by HNO_3, Ce^{4+} can form, which is readily extracted by TBP (Equation 2.30). Under PUREX reprocessing conditions, Ce^{4+} is quickly reduced to Ce^{3+} using ferrous sulfamate However, when AHA is added to the scrub section of UREX, it

can react with either oxidation state of cerium. AHA will reduce Ce^{4+} to Ce^{3+} and form $Ce(AHA)^{2+}$, $Ce(AHA)_2^{+}$, $Ce(AHA)_3$ complexes [56]. Therefore, the reactivity of cerium with AHA must be considered if AHA is to be used in UREX.

$$Ce^{4+}_{(aq)} + 4NO^{-}_{3\,(aq)} + 2TBP_{(org)} \rightleftharpoons Ce(NO_3)_4 \cdot 2TBP_{(org)} \qquad 2.30$$

2.1.3.3 Cesium and Strontium

Cesium, as an alkali metal and strontium, as an alkaline earth metal exist as monovalent and divalent cations in acidic solution, respectively. Both are fission products in UNF, are poorly extracted by TBP, and can be separated from U and Pu. However, it is important to mention these two elements as they are of significant concern in terms of high-level waste (HLW) disposal. Cesium's primary isotope of interest is ^{137}Cs which has a $t_{1/2}$ of 30.07 years. ^{137}Cs emits energetic β (0.514 MeV_{max}) and γ (0.662 MeV) radiation and is one the largest fission product heat contributors in UNF [44]. Stronium's isotope of concern is ^{90}Sr ($t_{1/2}$ 28.8 years). ^{90}Sr is a pure beta emitter with β emission of 0.546 MeV_{max}. ^{90}Sr is in secular equilibrium with ^{90}Y, which has a shorter $t_{1/2}$ (64 hours) but much more energetic β emission (2.28 MeV_{max}) [9]. The $^{90}Sr/^{90}Y$ decay pair also contributes to the radiotoxicity and heat of HLW. With their intermediates half-lives, ^{137}Cs and ^{90}Sr will exist in HLW for approximately three hundred years. Therefore, there is much interest in removing these two radioisotopes from the HLW prior to long-term disposal. Several advanced reprocessing techniques have been developed to remove them from the waste stream; one of which is described in section 2.2.2.2.

2.2 Chemistry of Solvent Extraction Systems

2.2.1 PUREX

As a result of the development and production of nuclear weapons during World War II, the United States accrued tremendous quantities of wastes which contained uranium and plutonium. Therefore, a method needed to be developed to recover these elements. The extracting ability of TBP was first discovered in the United States during the Manhattan

Project in 1944 at the Oak Ridge National Laboratory (ORNL) when workers found that TBP extracted plutonium and thorium nitrates [57]. TBP extraction was first openly published by James Warf in 1949, who determined that uranyl and thorium nitrates can be extracted from nitric acid [58]. Therefore, TBP showed great promise for the recovery of uranium and plutonium from weapons production waste created during the Manhattan Project [17]. Since then, much attention has been given to TBP for UNF reprocessing and, "can be confidently asserted that more is known about TBP than any other metal extractant" [17].

Currently the most widely used extraction system for the reprocessing of UNF is the plutonium uranium extraction (PUREX) process and TBP is the key constituent in that process. Undiluted TBP has several undesirable qualities for solvent extraction, such as a density similar to that of water and a high viscosity. Pure TBP extracts most elements which does not allow for the partitioning of U and Pu from other elements present in UNF. Therefore, TBP is diluted in a hydrocarbon solvent, such as odorless kerosene or *n*-dodecane, to increase its solubility in an organic phase to extract U and Pu from moderately concentrated (3-4 $mol \cdot L^{-1}$) nitric acid solutions. TBP is a neutral extractant whose phosphoryl group forms adducts with metal salts, such as uranyl nitrate (Equation 2.4) and plutonium nitrate (Equation 2.7). In the PUREX process, TBP selectively extracts tetravalent plutonium and hexavalent uranium from nitric acid solutions, while leaving tri- and pentavalent elements, such as Am^{3+}, Cm^{3+}, and NpO_2^{+}, in the aqueous raffinate [59]. The significant extraction differences between An^{4+} and AnO_2^{2+} compared to An^{3+} and AnO_2^{+} are due to their effective cationic charges (Figure 2.6). After the extraction An^{4+} and AnO_2^{2+} metal·nitrates, plutonium is then partitioned from uranium by the selective reduction to inextractable Pu^{3+}. Ferrous sulfamate has been used to reduce tetravalent plutonium; however, this practice is not considered ideal due to the creation of solid iron wastes that cannot be evaporated or incinerated. UO_2^{2+} is not reduced by ferrous sulfamate and remains in the organic phase. Following the reduction and separation of plutonium, UO_2^{2+} and is then stripped from the organic phase by dilute nitric acid concentration as the significantly reduced concentration of nitrate ions drives Equation 2.4 to the left. Once uranium and plutonium are separated from each other, the

aqueous raffinate contains most fission products, U can then be used for fresh fuel in power reactors, Pu can be used for weapons production, and both can be used as a mixed oxide (MOX) fuel source for power reactors.

2.2.2 UREX+

Although the PUREX process has been effectively utilized by many countries throughout the past fifty years, it no longer considered an ideal extraction system because of the isolation of plutonium, the inability effectively control the oxidation state of neptunium, and the formation of solid aqueous wastes which contain trivalent actinoids and lanthanoids [60]. Therefore, research is being conducted worldwide to develop solvent extraction systems that will improve separation of TRU elements from uranium and fission products and provide better separation of UNF elements.

There are several research labs that are developing continuous separation processes that combine several extraction segments with the aim to separate key radionuclides and close the nuclear fuel cycle. In the United States, one such separation scheme called UREX+ (Figure 2.9, adapted from [61]) is being developed at the Argonne National Laboratory (ANL) under the leadership of George Vandegrift [62]. UREX+ consists of a series of several solvent extraction processes (UREX, CCD/PEG, NPEX, TRUEX, TALSPEAK) and one ion exchange operation (Tc/U) to achieve the following objectives: recovery of uranium and Tc in separate product streams, combined recovery of cesium and strontium, recovery of TRU elements, with plutonium/neptunium and americium/curium extracted in separate product streams and separated from short lived fission products. By using various extractants and reducing/complexing agents, a better control the oxidation states and flow of the elements throughout the extraction steps can be achieved.

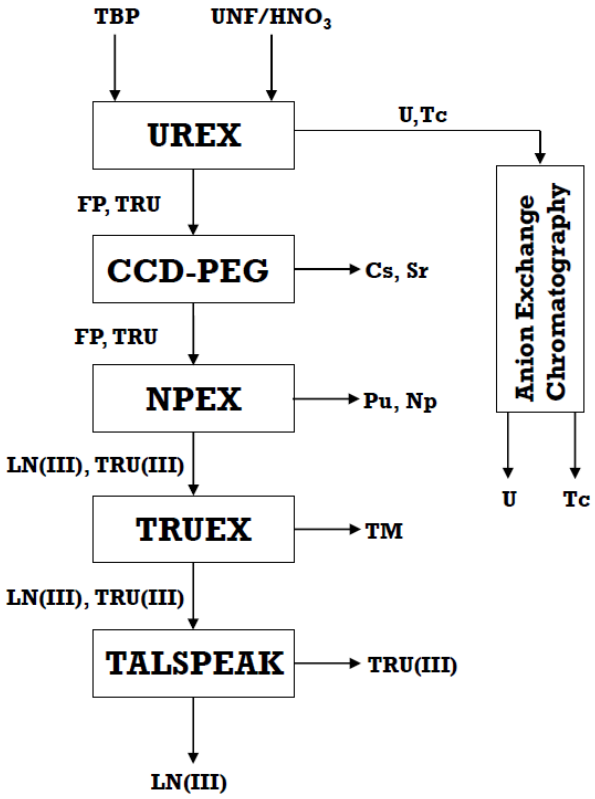

Figure 2.9: Flowchart of the UREX+ process.

2.2.2.1 UREX

The Uranium Extraction (UREX) process is being developed by Vandegrift, et. al [4] at ANL to separate Np and Pu from U. UREX uses the same organic extractant, TBP diluted in *n*-dodecane, as in PUREX. However, the two extraction processes differ in the manner in which Pu, and also Np, are separated from U. In PUREX, ferrous sulfamate has been used to reduce plutonium to its inextractable Pu^{3+} oxidation state, which allows for the separation of Pu from the extracted U. However, Fe^{2+} also rapidly reduces both NpO_2^{2+} and NpO_2^{+} to extractable Np^{4+}, but not to Np^{3+} [36]. Tetravalent neptunium is readily extracted by TBP so it remains with U in the organic phase. Therefore, ferrous sulfamate cannot be used to effectively separate neptunium from uranium in the PUREX process. On the other hand, UREX uses acetohydroxamic acid (AHA, Figure 2.10) to control the oxidation states of Pu and Np in UREX. AHA is a small hydrophilic organic ligand that reduces the high valence oxidation states of Pu to Pu^{4+} and NpO_2^{2+} to poorly

extractable NpO_2^+ [63]. AHA also forms inextractable complexes with Pu^{4+} and Np^{4+} [64, 65]. However, unlike ferrous sulfamate, AHA does not reduce NpO_2^+ to Np^{4+} [63]. Laboratory scale studies indicate that AHA significantly decreases the extraction of Pu and Np without adversely affecting the extractability of uranium [66-69]. Therefore, AHA has been chosen as the reductant and complexant in the UREX process to separate Pu and Np from U. In the United Kingdom, a similar process to UREX called Advanced PUREX, which also utilizes hydroxamic acids, is also being developed [70, 71].

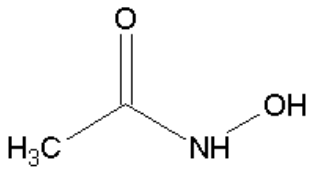

Figure 2.10: Structure of the keto form of AHA.

The UREX extraction process consists of three segments: extraction, scrub, and strip. The elements U, Pu Tc and Np (as NpO_2^{2+} and Np^{4+} as a lesser concentration) are extracted from the bulk UNF solution with 30% v/v TBP in *n*-dodecane in the initial extraction segment. Fission products, transition metals, Am^{3+}, Cm^{3+}, and NpO_2^+ are not extracted are remain in the aqueous raffinate. In the scrub segment, plutonium and neptunium that were initially extracted are partitioned from the organic phase by reducing the acidity of a fresh aqueous phase to less than 1 $mol \cdot L^{-1}$ and adding AHA to the aqueous feed. AHA reduces Pu to Pu^{4+} and NpO_2^{2+} to NpO_2^+, and forms inextractable complexes with Pu^{4+} and Np^{4+}. This scrub now contains both Pu and Np and is added to the aqueous raffinate from the initial extraction segment of UREX. Plutonium is not isolated at any point during UREX so proliferation concerns are not as significant as in PUREX. The U and Tc remaining in the product stream are stripped from the organic phase using 0.01 $mol \cdot L^{-1}$ nitric acid. Uranyl and pertechnetate (TcO_4^-) are separated using an ion exchange column. TcO_4^- is sorbed by a Reillex HPQ anion exchange resin, whereas UO_2^{2+} passes through the column. Ammonium hydroxide is used to elute the pertechnetate off the column, thus allowing for the separation of U and Tc. Uranium can then be used for the fabrication of fresh fuel for commercial power reactors or blended with Pu as a MOX fuel source.

Technetium, existing primarily as the ^{99}Tc isotope, has a long $t_{1/2}$of 214,000 years and is soluble and mobile in environmental aqueous conditions as TcO_4^- [72]. Therefore, controlling the throughput of Tc in the UREX process allows for its separation from other elements and for the conversion to its final and higher integrity waste form for long-term disposal.

2.2.2.2 CCD/PEG

The CCD/PEG process has been developed by the Idaho National Laboratory (INL) to separate Cs and Sr from the waste stream [73]. The aqueous raffinate from the UREX process, which contains most elements from the dissolved UNF except for U and Tc is directly used for CCD/PEG. As mentioned in section 2.1.3.3, Cs and Sr, existing primarily as ^{137}Cs and ^{90}Sr, are of significant concern in terms of UNF disposal because of their intermediate half-lives, heat contribution, and health concerns. In order to separate Cs and Sr from the TRU elements and other fission products, the aqueous phase from UREX, already in relatively dilute nitric acid (<1 $mol \cdot L^{-1}$), is contacted with an organic phase consisting of a mixture of chlorinated cobalt dicarbollide (CCD, Figure 2.11a) and polyethylene glycol 400 (PEG-400, Figure 2.11b) diluted in phenyltrifluoromethyl sulfone (FS-13, Figure 2.11c). CCD extracts Cs and PEG-400 extracts Sr into the organic phase. Rubidium and barium are also extracted to the organic phase to a significant extent. Any trace amounts of TRU elements extracted by either CCD or PEG-400 are scrubbed from the organic phase using moderately concentrated nitric acid. The scrub is combined with the initial aqueous raffinate from the CCD/PEG process and is then used in additional extraction processes, as described in section 2.2.2.4. Cs and Sr, along with Rb and Ba, are stripped from the FS-13 organic phase using a guanidine carbonate and diethylenetriamine pentaacetic acid (DTPA, Figure 2.13b) strip solution. The organic phase can then be cleaned and recycled for additional CCD/PEG separations. ^{137}Cs and ^{90}Sr, with half-lives of 30.07 and 28.8 years, can be stored for approximately 300 years until they have sufficiently decayed to stable ^{137}Ba and ^{90}Zr, respectively.

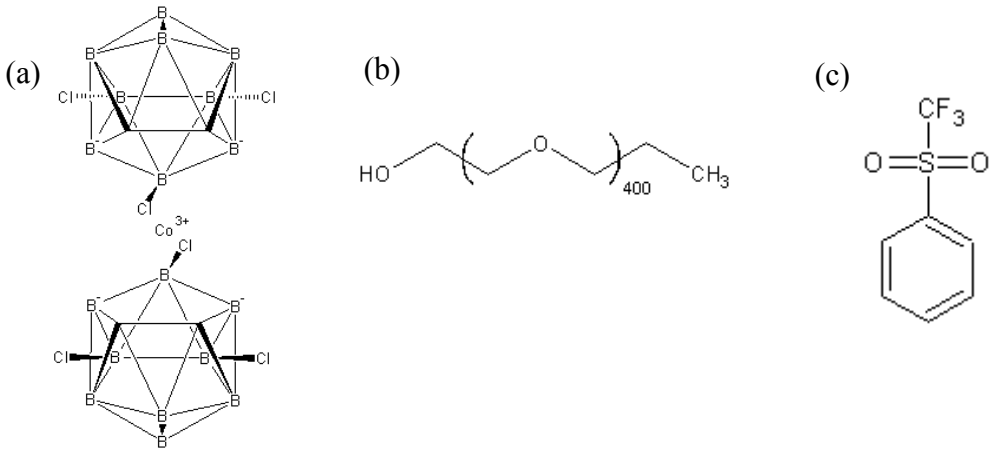

Figure 2.11: Structures of (a) CCD, (b) PEG-400, and (c) FS-13.

The Fission Product Extraction (FPEX) process has also been developed by INL as an alternative to CCD-PEG [74]. FPEX uses crown ether and calixarene extractants that are diluted in a branched aliphatic hydrocarbon diluent for the simultaneous and synergistic extraction of both Cs and Sr. Other elements of higher valency that are initially present in the aqueous feed of FPEX are not extracted.

2.2.2.3 NPEX

The aqueous raffinate from CCD-PEG (or FPEX) is adjusted for the Neptunium Plutonium Extraction (NPEX) process. The AHA that was added in UREX is destroyed by heating the solution. The acidity of the feed is also increased to facilitate in the destruction of AHA, so the hydrophilic complexes of plutonium and neptunium that formed in UREX no longer exist. Neptunium(V) is oxidized to the readily extractable NpO_2^{2+} by the addition of vanadium(V) prior to the extraction segment in NPEX. The VO_2^+/VO^{2+} reduction potential is +1.00V versus SHE [13] so vanadium(V) oxidizes NpO_2^+ to NpO_2^{2+} [75]. The adjusted aqueous feed is contacted with an organic phase consisting of 30% v/v TBP in *n*-dodecane. Neptunium and plutonium are extracted by TBP while the trivalent TRU elements, primarily Am^{3+} and Cm^{3+}, and fission products remain in the aqueous raffinate. Impurities are removed from the solvent in the scrub section by contacting the organic phase with dilute nitric acid and are combined with the

aqueous raffinate. Lastly, neptunium and plutonium are stripped from the organic phase into a fresh dilute nitric acid aqueous phase using AHA. This aqueous strip containing Pu and Np can be used in MOX fuel in power reactors for electricity production. The raffinate from NPEX is used for additional extraction schemes without any adjustment.

2.2.2.4 TRUEX

At this point in the UREX+ process, trivalent TRU elements, primarily Am^{3+} and Cm^{3+}, and most fission products, (except for Tc, Cs, and Sr), which includes the trivalent lanthanoids and transition metals, exist in the aqueous feed from the NPEX process. Trace amounts of neptunium and plutonium may exist in the feed solution as well. To partition these elements, the transuranium extraction (TRUEX) process is utilized, which was developed at ANL by Horwitz, et. al [76] that uses octyl(phenyl)-N,N-diisobutylcarboylmethyl-phosphine oxide (CMPO, Figure 2.12) and TBP as extractants for tri-, tetra-, and hexavalent actinoids from nitric acid. However, in UREX+, TRUEX is primarily used to separate the trivalent actinoids and lanthanoids from transition metals. CMPO's extracting ability comes from its phosphoryl and carbonyl groups [77], and like TBP, the metal charge must be compensated by nitrate ions in order for extraction to occur (Equation 2.31).

$$M^{3+}_{(aq)} + 3NO^{-}_{3\,(aq)} + 3CMPO_{(org)} \rightleftharpoons M(NO_3)_3 \cdot 3CMPO_{(org)} \qquad 2.31$$

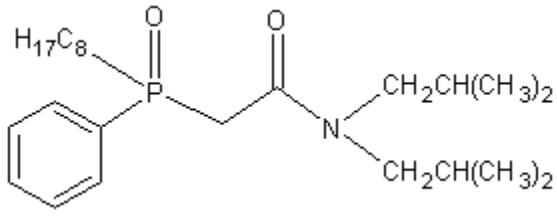

Figure 2.12: Structure of CMPO

The aqueous raffinate from NPEX is contacted with 0.2 mol·L^{-1} CMPO and 1.4 mol·L^{-1} TBP that has been diluted in *n*-dodecane. By combining TBP and CMPO, Am^{3+}, Cm^{3+}, and the trivalent lanthanoids are initially extracted to the organic phase. Transition metals would be partially extracted as well. Unique to UREX+, the TRUEX flowsheet has three scrub sections to remove transition metals and impurities from the trivalent actinoids and

lanthanoids [4]. In the first scrub section, oxalic acid is added to remove impurities, such as the transition metals, from the organic phase. In the second scrub section, moderately concentrated nitric acid is added to scrub the oxalic acid from the organic phase. In the third scrub section, the nitric acid concentration is decreased. All aqueous feeds from the scrub sections are combined, which mostly contains transitions metals, oxalic acid, and trace amounts of An^{3+} and Ln^{3+}. By increasing the pH of the aqueous feed, the trivalent actinoids and lanthanoids can be stripped from the organic phase using a weak complexant salt. Thus, the initial aqueous raffinate from the TRUEX process in UREX+ which contains transition metals and impurities, can be sufficiently separated from trivalent actinoids and lanthanoids and can be disposed of as non-TRU waste [78]. The product stream from TRUEX is used in a final solvent extraction process to separate the trivalent actinoids from the lanthanoids, as described in section 2.2.2.5.

Although the TRUEX process has been shown to be an effective extraction process in UREX+ [4], there are solubility limitations, as CMPO will separate into two organic phases when overloaded in hydrocarbon diluents [79, 80]. This results in the formation of a second organic phase and causes an increase in reprocessing complexity. To increase the load capacity of CMPO, TBP is added to increase its solubility. Remarkably, the addition of TBP decreases the extraction of Am^{3+} by CMPO in low HNO_3 concentrations (≤ 1 mol·L^{-1}) while increasing their extraction by CMPO at high HNO_3 concentrations (≥ 2 mol·L^{-1}) [77]. As such, TBP greatly increases the partitioning of trivalent actinoids and lanthanoids in TRUEX, as it aids in both their extraction at high acidity and stripping at low acidity.

2.2.2.5 TALSPEAK

The final step of UREX+ involves the separation of the trivalent actinoids from the lanthanoids, which is done by employing the Trivalent Actinide Lanthanide Separations by Phosphorus-reagent Extraction from Aqueous Komplexes (TALSPEAK) process. TALSPEAK was designed by Weaver and Kappelmann [81] at ORNL and the separation is based on the difference of the Lewis acidity of the trivalent actinoids and lanthanoids [82]. With the same oxidation state of +3 but slightly smaller radii [83], lanthanoids act

as harder Lewis acids than actinoids. This difference in their Lewis acidity is exploited in TALSPEAK in the following manner: the aqueous phase consists of a mixture of lactic acid (Figure 2.13a), ammonium lactate, and an aminopolyacetic acid, such as DTPA (Figure 2.13b), which are dissolved in a pH 3-4 buffered solution. Although lactic acid forms complexes with lanthanoids and actinoids, its primary role is to maintain the pH of the solution, as metal·DTPA complexation is greatly affected by the pH of the solution [84]. As both a nitrogen and oxygen donor, DTPA is a softer Lewis base than the small, oxygen only donating lactic acid. Since hard acid-hard base interactions are stronger than either hard acid-soft base or soft acid-hard base interactions [85], the trivalent actinoids preferentially complex with DTPA. The actual separation is based on the extraction of the lanthanoids by di-(2-ethylhexyl)phosphoric acid (HDEHP, Figure 2.13c) dissolved in *n*-dodecane. HDEHP is an acidic extractant, so unlike TBP or CMPO, the metal charge is not compensated by nitrate ions (Equation 2.32, where HDEHP is represented by *HL* for clarity). Three HDEHP dimers are necessary to extract trivalent metals.

$$M^{3+}_{(aq)} + 3H_2L_{2(org)} \rightleftharpoons M(HL_2)_{3(org)} + 3H^{+}_{(aq)} \qquad 2.32$$

The actinoid-DTPA complexes remain in the aqueous phase, while the lanthanoids are extracted by HDEHP. The small fraction of actinoids extracted to the organic phase is scrubbed by adding additional lactic acid and DTPA in the scrub section. If plutonium and neptunium still remain in the feed from TRUEX, they can also be separated from the lanthanoids using TALSPEAK. DTPA complexes with Pu(IV) and Np(IV) are stronger than DTPA complexes with either trivalent actinoids or lanthanoids. Therefore, Pu·DTPA and Np·DTPA complexes are held back with the trivalent actinoids. The lanthanoids that were extracted by HDEHP are stripped from the loaded organic phase to a highly acidic fresh aqueous phase. Most lanthanoids in UNF have shorter half-lives so they can be stored in interim waste containers until the radioactivity has decreased to sufficient levels. On the other hand, the trivalent actinoids, such as ^{241}Am and ^{244}Cm, have long half-lives and can undergo transmutation to avoid long-term waste storage. By irradiating Am and Cm with fast neutrons in a nuclear reactor, the activated elements undergo fission to create fission products of much shorter half-lives. Although most of the fission products are also radioactive, their half-lives are significantly shorter than ^{241}Am or

^{244}Cm and can remain in storage until they decay and their radioactivity becomes insignificant.

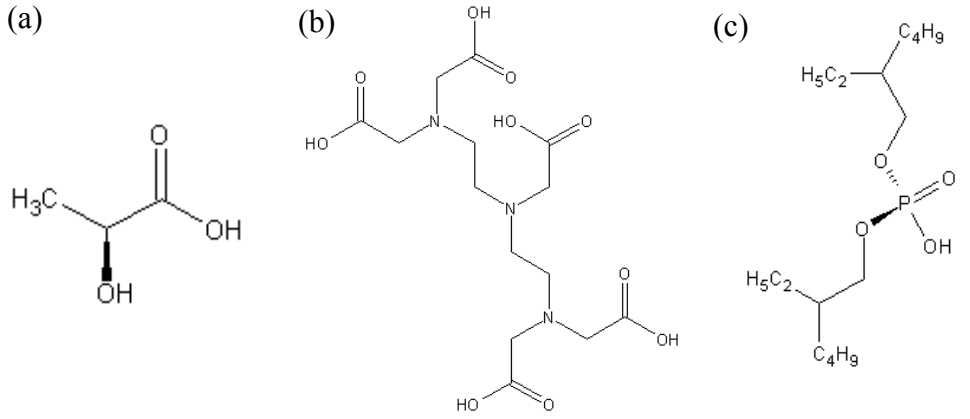

Figure 2.13: Structures of (a) lactic acid, (b) DTPA, and (c) HDEHP.

2.3 Acetohydroxamic Acid

Hydroxamic acids are di-oxygen donors with the general formula RCONHOH. They are much weaker organic acids than carboxylic acids (RCOOH), which are structurally related. Dissociation constants are pK_a = 4.75 and 9.2 for acetic acid and AHA [86], respectively. They are salt-free organic compounds that have been proposed for use in the UREX process as the reducing/complexing agent for Pu and Np [4]. "Salt-free" compounds contain only C, H, O, and N and decompose in high temperatures and/or highly acidic solutions to gases and nitrous acid. This is advantageous because, unlike using ferrous sulfamate as a reducing agent, AHA does not increase the mass of the aqueous waste of the UREX extraction process.

2.3.1 Acetohydroxamic Acid Complexation with Metals

Deprotonated hydroxamic acids, also known as hydroxamates, are bidentate ligands that have an affinity for hard metal cations and form stable complexes as five-member chelate

rings (Figure 2.14). The complexation of a metal (*M*) and ligand (*L*) is described by Equation 2.33, where where *z* is the cationic charge and *n* is a number of interacting ligands). For simplicity, a monovalent L^- anion is used. The equilibrium constant (K_n) of the complexation is related to the stability constant (β_n) of the metal·ligand complex in solution and is described by Equation 2.34. The chemistry and thermodynamics of metal·ligand complexes are described in greater detail in section 2.4.1.

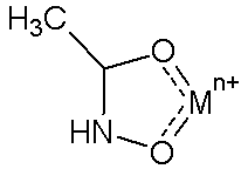

Figure 2.14: Structure of acetohydroxamate-metal complex.

$$M^{z+}_{(aq)} + nL^{-}_{(aq)} \rightleftharpoons ML^{(z-n)+}_{n\,(aq)} \qquad 2.33$$

$$\beta_1 = K_1 = \frac{\{ML^{(z-1)+}\}}{\{M^{z+}\}\{L^{-}\}} \qquad 2.34$$

As a result of the chelate effect, metal·AHA complexes are generally much stronger than complexes with related carboxylates (log β_1= 10.84 for Fe(III)·AHA, and logβ_1 = 2.8 for Fe(III)·acetate [86]) and contain two oxygen donor atoms in the chelate ring. AHA preferentially complexes with tetravalent metals in dissolved UNF because of their higher effective cationic charge compared to metals with other oxidation states (Figure 2.6). Other An oxidation states, particularly the tri- and pentavalent oxidation states, generally do not form strong complexes with AHA. The stability constants for An ions decreases along the series of effective cationic charge (Figure 2.6) [87]. See Table 2.1 for a comparison of stability constants for hydroxamate complexes of several metal cations, where μ is the ionic strength of the solution. Compared to other trivalent metals with higher atomic numbers, ferric iron forms much stronger complexes with AHA. With the same charge but smaller ionic radius than Ce^{3+} and Pu^{3+}, Fe^{3+} acts as a much stronger Lewis acid and readily complexes with AHA, as indicated by the significant differences in their stability constants. Chemically speaking, Fe^{3+} acts similarly to tetravalent actinoids so it is often used as a chemical analog to Np^{4+} and Pu^{4+}. See section 3.4.1for

acetohydroxamatoiron(III) complexation studies. The stability constants for An ions decreases along the series of their effective cationic charge (Figure 2.6) [87]. Therefore, tetravalent actinoids act as stronger Lewis acids and have a large affinity for AHA. As such, Np^{4+} and Pu^{4+} have stability constants that are orders of magnitude greater than either UO_2^{2+} or Pu^{3+}.

Table 2.1: Stability constants for acetohydroxamate complexes of various ions.

Ion	$Log_{10}\beta_1$	$Log_{10}\beta_2$	$Log_{10}\beta_3$	Reference	Note
Ce^{3+}	5.45	9.79	12.80	[56]	20°C, μ = 0.1 mol·L^{-1} NO_3^-
Pu^{3+}	5.77	11.66	14.84	[88]	22°C, μ = 2.0 mol·L^{-1} ClO_4^-
Fe^{3+}	11.00	20.93	28.75	[89]	25°C, μ = 0.1 mol·L^{-1} NO_3^-
Np^{4+}	12.46	22.22	29.89	[90]	25°C, μ = constant ClO_4^-
Zr^{4+}	12.77	23.13		[89]	25°C, μ = 1 mol·L^{-1} ClO_4^-
Pu^{4+}	14.2	24.1	32.2	[91]	22°C, μ = 2.0 mol·L^{-1} NO_3^-
UO_2^{2+}	8.22	15.30		[92]	25°C, μ = 0.1mol·L^{-1} NO_3^-

2.3.2 Reduction of Metals by Acetohydroxamic Acid

It is well known that hydroxamic acids undergo an irreversible electrochemical oxidation at positive potentials [93] according to Equation 2.35, with the intermediate product $HN(OH)_2$ slowly converting to hyponitrous acid [94].

$$RCONHOH_{(aq)} + 2H_2O_{(l)} \rightarrow RCOOH_{(aq)} + HN(OH)_{2(aq)} + 2H^+_{(aq)} + 2e^- \qquad 2.35$$

AHA oxidation has an onset potential of +0.861V versus SHE [94, 95]. Therefore, AHA is thermodynamically capable of reducing metals with reduction potentials greater than +0.861V versus SHE, which is based on spontaneity of the free energy of the reduction-oxidation reaction (Equation 2.9). By assessing the Latimer diagrams for the metals in dissolved UNF that are listed previously, it is apparent that AHA can reduce NpO_2^{2+} to NpO_2^+, NpO_2^{2+} to Np^{4+}, and the reduction of several Pu species. However, the direct reduction of NpO_2^{2+} to Np^{4+} would involve the breaking of the di-oxygen bonds and is not observed because it is less spontaneous than the rapid reduction of NpO_2^{2+} to NpO_2^+ caused by AHA [96]. The reduction of PuO_2^{2+} and/or PuO_2^+ by AHA in UREX process conditions ultimately results in either the formation of Pu^{4+}·AHA complexes or Pu^{3+} [97].

Direct reduction of UO_2^{2+} to U^{4+} has a reduction potential of +0.27 versus SHE and therefore is not reduced by AHA. By reducing NpO_2^{2+} to nearly inextractable NpO_2^{+} [63] and reducing Pu to poorly extractable Pu^{3+} [98] without affecting the extraction of UO_2^{2+} [66, 68, 99] AHA has great promise for use in the UREX process to reduce Np and Pu and allow for their effective partitioning from U.

Other reductants have also been considered to control the oxidation states of neptunium in advanced reprocessing. Table 2.2 provides a list of various reducing agents and the reduction rate of NpO_2^{2+} to NpO_2^{+}. Formohydroxamic acid (FHA), which was initially chosen as the reductant/complexant in the Advanced PUREX process in the United Kingdom, has a rate constant much greater than the other reagents. AHA is commercially available, whereas FHA is not. It should be noted that the reduction of NpO_2^{2+} by FHA is a second order process with units $mol^{-1} \cdot L \cdot sec^{-1}$. Also, all reductants listed in Table 2.2 are salt-free except for U(IV).

Table 2.2: Measured rate constants for the reduction of NpO_2^{2+} at 22°C.

Reductant	Rate constant (s^{-1})	Reference
Formohydroxamic acid	1174*	[100]
Phenyl hydrazine	44	[101]
U(IV)	15.7	[39]
Hydroxylamine	3.5	[101]
Acetaldoxime	3.0	[102]
Hydrazine	0.17	[101]
Butyraldehyde	0.001	[103]

2.3.3 Hydrolysis of Acetohydroxamic Acid

Although AHA has been chosen as the reductant and complexant to manipulate and control the oxidation states of Pu and Np in UREX, it is not particularly stable in strongly acidic solutions. Hydroxamic acids hydrolyze in acid solutions, decomposing to their respective carboxylic acid and hydroxylamine, as described by Equation 2.36 for AHA.

$$CH_3CONHOH_{(aq)} + H_3O^{+}_{(aq)} \rightarrow CH_3COOH_{(aq)} + NH_3OH^{+}_{(aq)} \qquad 2.36$$

* Reduction of NpO_2^{2+} by FHA is a second order reduction process, with units $mol^{-1} \cdot L \cdot sec^{-1}$.

The hydrolysis of AHA is initiated and catalyzed by a hydronium ion, followed by the rate limiting step when the protonated intermediate is attacked by a water molecule [104]. The rate of AHA hydrolysis is of significant importance in UREX reprocessing, as the contact time of AHA with the acidic aqueous phase is on the order of minutes. Therefore, several studies have been done to determine the kinetics of hydrolysis of AHA [105-107]. The change in AHA concentration ([AHA]) as a function of time has been defined by the following differential equation for $[HNO_3] < 3$ mol·L^{-1} and $[HNO_3] > [AHA]$ (Equation 2.37) [108], where the rate constant k of the reaction is also defined by the Arrhenius Equation (2.38).

$$-\frac{d[AHA]}{dt} = k[AHA][H^+] \qquad 2.37$$

$$k = Ae^{-\frac{E_A}{RT}} \qquad 2.38$$

The pre-exponential factor A has been determined as 3.22×10^9 mol^{-1}·L·sec^{-1} and the activation energy E_A equals 79.9 kJ·mol^{-1} for AHA [105]. The gas constant R is equal to 8.314 J·mol^{-1}·K^{-1} and T is the temperature of the reaction in Kelvins. The rate constant for the hydrolysis of AHA has been determined as 0.00181 mol^{-1}·L·sec^{-1} in 1 mol·L^{-1} HNO_3 at 25°C [107]. With a slightly smaller alkane backbone, FHA is more reactive than AHA. As such, the rate constant for the hydrolysis of FHA has been calculated as 0.016 mol^{-1}·L·sec^{-1} in HNO_3 and an E_A equal to 77.9 kJ·mol^{-1} [105].

To minimize the hydrolysis of AHA, the acidity of the aqueous feed during the scrub section of UREX when AHA is added is reduced to less than 1 mol·L^{-1} nitric acid [4]. By doing so, the hydrolysis of AHA is kept to a minimum while the complexation of Pu and Np with AHA is enhanced. An added benefit of lowering the acidity is that the extraction of the pertechnetate ion by TBP is increased. Furthermore, zirconium is poorly extracted by TBP at low nitric acid concentrations [49]. On the other hand, uranyl remains sufficiently extracted by TBP, even at the lower scrub acidity. Therefore, by lowering the acidity during the scrub section of UREX enhances the partitioning of Pu and Np from U and Tc.

Although the hydrolytic degradation of AHA is detrimental for the separation of Pu and Np from U and Tc in the scrub section of UREX, this instability of AHA becomes beneficial in later steps. Following the separation of Pu and Np from the organic phase of UREX, AHA can be destroyed by either increasing the acidity or raising the temperature of the aqueous raffinate. As a salt-free reagent, AHA is destroyed and gaseous products evolve which leave the aqueous stream and do not contribute to the mass of the waste. This artifact of AHA is significantly different than the ferrous sulfamate that has been used in PUREX. Ferrous sulfamate cannot be evaporated or incinerated without leaving behind solid residues that contributes to the volume of the waste.

2.4 Chemical Thermodynamics

2.4.1 Complexation Thermodynamics

The strength of the metal-ligand complex is defined as the stability constants (β) of a metal-ligand complexes formed in an aqueous phase, initially stated as Equation 2.34 but restated here for reference. The braces {} denote the molar activity, which describes the effective concentration of a species *i* in solution and is defined by Equation 2.40, where γ_i is the unitless activity coefficient, C_i is the molar concentration, and the A_i is the activity of the species.

$$\beta_1 = K_1 = \frac{\{ML^{(z-1)+}\}}{\{M^{z+}\}\{L^-\}} \tag{2.39}$$

$$A_i = \gamma_i \cdot C_i \tag{2.40}$$

Knowledge of the stability constant of complexes is important in actinoid chemistry and depends on the oxidation state of a particular metal, the complexing ligand itself, and the solution ionic strength and temperature. Some metals interact with more than one ligand and the $\beta_n s$ of these multi-coordinated complexes are equal to the product of the equilibrium constants (K_n) of the stepwise formation of each metal-ligand complex (Equation 2.41). For systems where γ_i of some species are unknown or neglected, the true

stability constant cannot be determined. However, the conditional stability constants (β_n') can be determined from the molar concentrations of each species (Equation 2.42).

$$\beta_n = K_1 \cdot K_2 \cdot \ldots \cdot K_n = \frac{\{ML_n^{(z-n)+}\}}{\{M^{z+}\}\{L^-\}^n} \quad 2.41$$

$$\beta_n' = \frac{[ML_n^{(z-n)+}]}{[M^{z+}][L^-]^n} \quad 2.42$$

The thermodynamics of the complexation chemical in aqueous solutions can be measured either calorimetrically or determined using the temperature dependence of the stability constants measured at various temperatures. For example, the enthalpy of complexation reaction, ΔH_n^o, can be determined as a slope of Van't-Hoff plot for β_ns of metal-ligand complexes:

$$\frac{d \log_e(\beta_n)}{dT} = \frac{-\Delta H_n^o}{RT} \quad 2.43$$

By plotting $\log_e(\beta_n)$ versus T^{-1}, the slope of the line will be equal to $-\Delta H_n^o \cdot R^{-1}$. Then both the free Gibbs energy, ΔG_n^o, and the entropy change, ΔS_n^o, of complexation can also be determined:

$$\Delta G_n^o = -RT \ln \beta_n \quad 2.44$$

$$\Delta G_n^o = \Delta H_n^o - T\Delta S_n^o \quad 2.45$$

2.4.2 Complexation Modeling and Ion Interactions

There are also several modeling programs for calculating complexation constants. One such program is Stability Quotients from Absorption Data (SQUAD) [109]. SQUAD is a computational program designed to calculate molar extinction coefficients and stability constants from spectrophotometric values of solutions at equilibrium. SQUAD uses a non-linear least squared approach and an iterative process that refines the output coefficients and constants. By inputting entire spectra from several solutions with varying metal·ligand concentration ratios, SQUAD can accurately determine the molar extinction

coefficients and stability constants of interest. A more recent computation program is Hyperquad [110], which also calculates stability constants. In addition to analyzing spectrophotometric data, Hyperquad can also analyze data from potentiometric and NMR experiments to calculate stability constants [111].

Precise thermodynamic information on ionic interactions can be obtained only in the presence of an inert electrolyte (such as perchlorate) of sufficiently high concentration so that ionic activity coefficients can be considered constant throughout the measurements. These measurements can only be considered for these particular conditions used. Therefore, the activity of solutes in non-inert electrolytic solutions must be considered, as the values for activity coefficients are essential if equilibrium and stability constants are to be corrected for changes in background medium. The Specific Ion Interaction Theory (SIT) program [112] estimates the activity coefficients of single ions in relatively high electrolyte solutions. SIT was developed from the Extended Debye –Hückel theory [113] and accurately estimates the γ_i of a ion with z integer charge in a solution with an ionic strength of μ (Equation 2.46):

$$\log_{10}(\gamma_i) = z_i^2 \frac{0.51\sqrt{\mu}}{1+1.5\sqrt{\mu}} + \sum_k \varepsilon_{ik} m_k \qquad 2.46$$

where ε is the interaction coefficient and m is the molal concentration of each ion k in solution. The SIT theory differs from the Extended Debye –Hückel by considering the interaction coefficients between the various ions present in solution. By doing so, the SIT theory can estimate the activity coefficient of an ion over a wide range of ionic strengths, whereas the Extended Debye –Hückel can only provide accurate activity coefficients for solutions with $\mu \leq 1$ mol·kg^{-1}. Therefore, the SIT program will be used to correct the ionic strength when possible.

2.5 Extraction Thermodynamics

2.5.1 Extraction Thermodynamics

Solvent extraction is the basis for the separation of various elements in the extraction schemes described in section 2.2, and refers to the distribution of a solute between two

immiscible liquid phases. In UNF reprocessing, these phases are typically an aqueous and organic phase that are placed in contact with one another and mixed with banks of mixer-settlers, centrifugal contactors, or pulsed columns [114]. In these extraction schemes, the aqueous phase is acidic and the organic solvent consists of an extracting ligand X dissolved in a diluent so a low solubility of organic solvent in aqueous phase is assured. If initially present in the aqueous phase, the metal cation (M^{z+}) interacts with an acidic extracting ligand and is extracted to the organic phase (Equation 2.47). For simplicity, any dimerization of the extracting ligand has been omitted. The metal, ligand, and other solutes eventually distribute between the two phases, with the equilibrium constant of the extraction (K_{ex}) is defined by Equation 2.48. Molar concentrations are used to define K_{ex}, rather than the activity of each species, which is typical convention. To define K_{ex} for activity, the γ_i must be known for each species and multiplied by their respective molar concentrations (Equation 2.40).

$$M_{(aq)}^{z+} + zHX_{(org)} \rightleftharpoons MX_{(org)} + zH_{(aq)}^{+} \tag{2.47}$$

$$K_{ex} = \frac{[MX]_{org}[H+]_{aq}^{z}}{[M^{z+}]_{aq}[HX]_{org}^{z}} \tag{2.48}$$

The distribution ratio (D) of the solute is defined as the ratio of "the total analytical concentration of the solute in the extract to its total analytical concentration in the other phase" (Equation 2.49) [115]. Therefore, D of a metal distributed between two phases can be related to the equilibrium extracting ligand (Equation 2.50).

$$D = \frac{\sum[M]_{org}}{\sum[M]_{aq}} \tag{2.49}$$

$$K_{ex} = D\frac{[H^{+}]_{aq}^{z}}{[HX]_{org}^{z}} \tag{2.50}$$

Some ligands used in the extraction schemes described in section 2.2 are neutral extractants whereas others are not. For example, TBP is a neutral extractant so the charge of the cationic metal must be compensated in order for extraction to occur. In PUREX and UREX, the metal charge is balanced by the coordination of the metal with several

nitrate ions; examples of which are described by Equations 2.18 and 2.19. In TALSPEAK, HDEHP is an acidic extractant so the metal charge is not compensated by counter anions (Equation 2.32).

2.5.2 Extraction Modeling

There are several programs for modeling solvent extraction systems and simulation of extraction processes: SXLSQI by the radioseparation group of ORNL [116], SX-Solver by the Pacific Northwest National Laboratory [117, 118] or the Argonne Model for Universal Solvent Extraction (AMUSE) code by ANL [119]. The AMUSE code models the UREX process and other related solvent extraction processes and defines many of the process streams that are integral to the design of the systems model [120]. All these programs use a database of activity coefficients of species in the aqueous and organic phases, stability constants of metals with ligands in the aqueous phase, and stability constants with extracting agents in the organic solvent. Therefore, before or during the solvent extraction modeling, data inputted into the code must be accurate. Advanced modeling programs, such as AMUSE and SXLSQI, also use other physicochemical characteristics such as density, volatility, and solubility data to correct the activity coefficients, particularly those from the organic phase.

2.6 Chemical Kinetics

2.6.1 Chemical Kinetics

Knowledge of a radioisotope's decay kinetics is necessary for its identification. The reactivity of metals with reducing and complexing agents can also described by the chemical kinetics of the reaction. The rate of a reaction of an irreversible process can be expressed in terms of the decrease of concentration of any reactant (A) or an increase of any product (X):

$$aA \rightarrow xX \qquad 2.51$$

The rate of concentration change at any time t during the reaction is defined by Equation 2.52, where k is the rate constant of the reaction. The manner in which the rate of reaction

varies with the concentration of the reacting substance is described by the order of the reaction (α) [121]. It should be noted that the stoichiometric coefficient (*a*) is not necessarily equal to the order of reaction and α must be experimentally determined from the reaction kinetics.

$$-\frac{d[A]}{dt} = k \cdot [A]^{\alpha} \qquad 2.52$$

For a first order reaction such as radioactive decay, where α equals 1, integration of 2.52 provides an equation that predicts the time dependence of the concentration of *A* relative to its initial concentration $[A]_o$.

$$[A] = [A]_o \cdot e^{-kt} \qquad 2.53$$

The reduction of NpO_2^{2+} by AHA is more complicated than a first-order reaction. The reduction can be described by a generic reaction (Equation 2.54), where *A* represents NpO_2^{2+}, *B* represents AHA, and *X* represents the reduced neptunium species, NpO_2^{+}.

$$aA + bB \rightarrow xX \qquad 2.54$$

The rate of reduction of *A* can be described by the differential Equation 2.55, where it is assumed that the reaction is second order overall and first order with respect to both *A* and *B*.

$$-\frac{d[A]}{dt} = k[A][B] \qquad 2.55$$

A two-to-two stoichiometric ratio (*a*:*b* = 2:2) occurs for the reduction of NpO_2^{2+} by AHA [122]. The fact that the stoichiometric coefficients are equals allows for the simplification of Equation 2.55. If *y* is defined as the concentration of *A* or *B* that has disappeared for a given time *t* because of the progression of Equation 2.54, the amount of *A* remaining is $[A] = A_o - y$ and the amount of *B* remaining is $[B] = B_o - y$:

$$-\frac{d([A]_o - y)}{dt} = \frac{dy}{dt} = k([A]_o - y)([B]_o - y) \qquad 2.56$$

Integration of 2.56 is a non-trivial calculation, but is provided in Laidler [121] and is defined by Equation 2.57. By knowing the initial concentration of *A* and *B*, and the

concentration of one the reactants that have disappeared at a given time *t*, the rate constant of the reaction can be determined. Equation 5.3 used in the determination of the rate constant for the reduction of NpO_2^{2+} by AHA is derived from Equation 2.57.

$$\frac{1}{[B]_o - [A]_o} \cdot \ln \frac{[A]_o \cdot ([B]_o - y)}{[B]_o \cdot ([A]_o - y)} = k \cdot t \qquad 2.57$$

2.6.2 Kinetic Modeling

A model developed by Martin Precek of Oregon State University based on the Runge-Kutta fourth order (RK4) method [123] is used to approximate kinetic data from absorbance spectra of a given wavelength. The model has been used to successful determine the reduction and complexation kinetics of Pu^{4+} in the presence of AHA from Vis-NIR spectroscopy [98]. It is based on the numeric integration of a set of differential equations (Equation 2.58) to determine both the rate constant of the reaction and the order of reaction of each reactant.

$$\frac{d[A_i]}{dt} = \sum_{m=1}^{m=M} (c_{im} \cdot k_m \cdot \prod_{j=1}^{j=n} [A_j]^{\alpha mj}) \qquad 2.58$$

The model calculates the concentration of each reacting species as a function of time. Manually selected variables c_{im} and α_{im}, typically of integer or half integer values, are used to optimize the rate constant k_m of each *m* reaction. A mathematical solution to the set of differential equations can be determined, where each reaction was proportional to the concentration of reactants present, each raised to a certain power. The calculated concentrations of absorbing species are comparable to their experimental concentrations determined from the absorption spectra and the Beer-Lambert law. Calculated rate constants can be optimized using a least-squares method performed by the Microsoft Excel Solver add-in.

3 COMPLEXATION CHEMISTRY OF ZIRCONIUM(IV), URANIUM(VI), AND IRON(III) WITH ACETOHYDROXAMIC ACID

Brent S. Matteson, Peter Tkac, and Alena Paulenova

Separation Science and Technology
Taylor & Francis Group
270 Madison Avenue
New York, NY 10016

Separation Science and Technology, 2010. *Accepted for publication.*

3.1 Abstract

The complexation of zirconium(IV), uranium(VI), and iron(III) with acetohydroxamic acid (AHA) has been analyzed spectrophotometrically in various ionic strengths at 25°C. Arsenazo III (AAIII) was used as an indicator for unbound zirconium. The SQUAD computational program was employed to evaluate the stability constants. Conditional stability constants of four zirconium complexes $Zr(AAIII)^{3+}$, $Zr(AAIII)_2^{2+}$, $Zr(AHA)^{3+}$, and $Zr(AHA)_2^{2+}$ were determined in 1 mol·L^{-1} $HClO_4$ as log β' = 5.09, 10.29, 12.78, and 23.13, respectively. Conditional stability constants of $UO_2(AHA)^+$, $Fe(AHA)^{2+}$, $Fe(AHA)_2^+$, and $Fe(AHA)_3$, in 0.1 mol·L^{-1} HNO_3 were calculated as log β_1' = 8.32, 11.00, 20.93, and 28.75, respectively.

3.2 Introduction

Used nuclear fuel (UNF) has been reprocessed for decades in countries such as France, Russia, Japan, and the United Kingdom in order to separate actinoids from fission products and other elements. The PUREX process is the most widely used method, which extracts uranium and plutonium using tri-n-butyl phosphate (TBP) diluted in kerosene from UNF dissolved in nitric acid. Recent attention has been given to advanced reprocessing schemes in order to increase proliferation resistance, create a sustainable energy source by recovering uranium resources from UNF, and minimize the amount of radioactive waste that would be required for long term geologic storage. To meet these criteria, the UREX+ process has been developed by the Advanced Fuel Cycle Initiative [124]. Acetohydroxamic acid (AHA) has been proposed for use in UREX to effectively separate neptunium and plutonium from uranium. Hydroxamic acids are salt-free compounds with the general formula RC(=O)NHOH [125] and are much weaker organic acids than carboxylic acids (RC(=O)OH), yet are structurally related. Dissociation constants for acetic acid and AHA at I = 1 mol·L^{-1} and 25 ^oC are pK_a = 4.58 and 9.07, respectively [86]. AHA is a di-oxygen donor with a high affinity for hard cations. In acidic solutions, the deprotonated species (AHA^-) forms stable complexes as five-member chelate rings [126].

Zirconium is an important metal in the nuclear industry, as it is used for fuel cladding because of its low neutron cross section and its alloys are resistant to corrosion. Zirconium is also a fission product and produced in significant amounts in UNF [5]. During UNF dissolution zirconium can co-precipitate with molybdenum and plutonium [127], but can also exist as both the extractable Zr^{4+} and $Zr(OH)^{3+}$ ions and inextractable $Zr_3(OH)_4^{8+}$ species during reprocessing. In addition, a synergistic effect occurs with technetium, as complexation occurs between Zr^{4+} and TcO_4^- ions and the co-extraction of the two metals is enhanced [54]. Also, uncomplexed zirconium can be extracted as strongly as the actinoids [128]. Therefore, controlling the flow of Zr in separation streams is crucial to achieve effective separation during advanced reprocessing of UNF.

Zirconium exists in a greater quantity in UNF than neptunium [5] and the reactivity of Zr with AHA must be considered in advanced reprocessing schemes if AHA were to be effectively used as a reductant/complexant for Np. Despite the importance of Zr and similarities with tetravalent actinoids, the complexation of Zr(IV) with AHA has not been studied to date. Therefore, we provide an initial study of the complexation of Zr^{4+} with AHA. In this paper we report the conditional stability constants of $Zr(AAIII)^{3+}$, $Zr(AAIII)_2^{2+}$, $Zr(AHA)^{3+}$, and $Zr(AHA)_2^{2+}$ calculated with SQUAD (Stability Quotients from Absorbance Data) [129] using experimentally determined spectrophotometric absorption data.

Uranium is the most abundant element in UNF and its recovery is of major interest for reprocessing. Previous studies show that AHA forms complexes with uranyl [92, 130], yet AHA has little effect on the extraction of uranium by TBP [131], whereas AHA can strip Pu back into the aqueous phase [132]. Thus, the use of AHA for advanced reprocessing of UNF is very promising. However, only a limited number of $UO_2(AHA)^+$ studies that determined the stability constants of $UO_2(AHA)^+$ have been published [91, 92, 133]. Therefore, we provide additional data of the complexation of uranyl with AHA using spectrophotometric analysis. Conditional stability constants of $UO_2(AHA)^+$ in 0.1 and 1.0 $mol \cdot L^{-1}$ NO_3^- and ClO_4^- in pH 1.0 and 25°C are determined by the SQUAD program.

With the aim to confirm the validity of our approach and for comparison with previously publish data, the complexation of AHA with iron(III) was also studied. Acetohydroxamic acid forms strong complexes with iron(III) which can be monitored by observing the intense color of the complex formation. Conditional stability constants of $Fe(AHA)^{2+}$, $Fe(AHA)_2^{+}$, and $Fe(AHA)_3$ in 0.1 mol·L^{-1} NO_3^- and pH 1.0 at 25°C are reported and compared with previously reported values [134, 135].

3.3 Experimental

3.3.1 Materials

All reagents used were of analytical grade and used without further purification.

Thenoyltrifluroracetone (TTA, 99%, Acros Organics) was kept in darkness at 4°C and dissolved in xylene (Mallinckrodt, Inc.) immediately prior to any extraction experiments.

Arsenazo III, (AAIII, 2,7-Bis(2-arsonophenylazo)-1,8-dihydroxynaphthalene-3,6-disulfonic acid, VWR Scientific Co.) was dissolved in water. A stock concentration of $6.0x10^{-3}$ mol·L^{-1} AAIII was determined by spectrophotometric titrations using a uranyl nitrate standard (Inorganic Ventures, Inc.).

Acetohydroxamic Acid (AHA, Toronto Research Chemicals) was kept at -18 ^oC, dissolved in water when needed, and was the final component added in order to minimize hydrolytic degradation in acidic solutions.

Iron Nitrate ($Fe(NO_3)_3·9H_2O$, Alfa Aesar) was dissolved in 0.5 mol·L^{-1} nitric acid.

Uranyl Nitrate ($UO_2(NO_3)_2$, Mallinckrodt, Inc.) was dissolved in either 1 mol·L^{-1} nitric acid or 1 mol·L^{-1} perchloric acid, depending on the nature of the subsequent experiments.

Zirconium oxychloride ($ZrOCl_2·8H_2O$, Fisher Scientific Co.) was dissolved in 10 mol·L^{-1} perchloric acid.

Ionic strength (I) of solutions was adjusted using stock solutions of either nitric acid and lithium nitrate or perchloric acid and sodium perchlorate, prepared from HNO_3 (70%, Fisher Scientific Co.), $LiNO_3$ (Alfa Aesar), $HClO_4$ (70%, Mallinckrodt Baker, Inc.), and $NaClO_4·H_2O$ (EMD Chemicals, Inc.). The acid concentration was determined by a pH-metric titration with standardized sodium hydroxide (Mettler-Toledo DL58 Titrator).

Distilled, deionized water (Barnstead, 18 MΩ·cm resistivity) was used for all experiments.

3.3.2 Sample Preparation and Transfer of Solution

Required volumes of stock solutions (except for AHA) were brought to 25°C in a temperature controlled water bath. Solutions were made in small plastic vials with pipettes calibrated to assure accurate transfer of preheated solutions. A small volume of AHA was added last, which did not affect the solution temperature. Each vial contained a total solution volume of 2 mL. Vials were placed in a temperature controlled mixer for 3 minutes at 1000 rpm. Vials for the iron and uranium experiments were taken immediately after mixing for spectroscopic analysis. Solutions of the Zr/AAIII/AHA experiments were returned to the water bath for 20 minutes to assure complete complexation.

3.3.3 UV-Vis Spectroscopy

All optical experiments were performed using an Ocean Optics QE65000 spectrometer and an Ocean Optics DH-2000-BAL light source. The prepared samples were transferred to 1-cm quartz cuvettes and placed in a temperature controlled cuvette holder.

3.3.4 Identification of Zr(IV) Species

To determine the species of zirconium in our experiments, TTA dissolved in xylene was used as an extractant of zirconium. 5.0×10^{-5} mol·L^{-1} Zr(IV) in 1 mol·L^{-1} $HClO_4$ was extracted by various concentrations of TTA at 25°C, and the concentration of zirconium not extracted by TTA was determined by monitoring the Zr(AAIII) complex using absorption spectroscopy. A slope of 3.7 was determined for the linear regression for the plot of the log(D) versus the log([TTA]) , where D is the ratio of the concentration of zirconium in the TTA phase to the concentration of zirconium in the aqueous phase. The slope indicates that in the acidic solutions of our experiments zirconium exists primarily as the Zr^{4+}ion, and not as zirconyl ZrO^{2+} [136, 137].

3.3.5 Computation of Stability Constants

Absorption spectra from a given set of experiments were introduced into a modified version of SQUAD (Stability Quotients from Absorbance Data), a program designed to calculate stability constants from absorbance data using a nonlinear least-squares approach [129]. SQUAD simultaneously processes numerous spectra and refines several stability constants from a set of experiments of a metal-ligand solution. Absorption spectra data were converted to [8D10.4] Fortran format using a simple Java program. The absorption spectra were incorporated into the SQUAD input files as a refined parameter, which were then used to determine the stability constant of the metal complex upon convergence of the program. The pK_as of AHA at 25°C (9.33 at I = 0.1 mol·L^{-1}, 9.07 at I 1.0 = mol·L^{-1}, and 9.02 at I = 2.0 mol·L^{-1} [86]) were added to each appropriate input file. The baseline from each experiment was also included to each input file.

SQUAD calculates a number of statistical parameters, including the standard deviation of the absorbance data, $s_{DATA,}$ and the standard deviation of each refined stability constant, s_{CONST}. SQUAD s_{DATA} values determined were all $\leq$ 0.01 and all s_{CONST} were considerably less than 1% of the calculated stability constant. These values are indicative of a good fit and suggest that the correct model had been found by SQUAD [129]. The uncertainty of the calculated stability constants include error associated with the experiments themselves and were calculated using Equation 3.1 [27]:

$$s_{\log\beta} = \sqrt{s_{CONST}^2 + \sum_i s_i^2} \qquad 3.1$$

where $s_{log\beta}$ is the uncertainty of a given stability constant and s_i is an estimation of the error associated with the experiments (*e.g.* pH, ionic strength, reagent concentration, and AHA hydrolytic degradation). Calculated $s_{log\beta}$ values are listed with their associated stability constants in tables I, II, and V.

3.4 Results and Discussion

3.4.1 Fe(III)·Acetohydroxamate Complexes

Iron(III) can form up to three mononuclear complexes with AHA^-, as described by Equation 3.2. In order to obtain absorbance spectra useful for the determination of stability constants in SQUAD, distinct concentration ratio ranges of Fe(III) and AHA were determined from the Hyperquad Simulation and Speciation (HySS) program [110] and previous literature [134, 135]. Critically assessed equilibrium data indicated that the formation of $Fe(OH)^{2+}$ only becomes significant above pH 2.17 [13, 135, 138]. Therefore, the hydrolysis of Fe(III) was not of consideration in HySS, as the pH of all solutions was 1 and the concentration of the ferric ion was low. The concentration ranges used are listed in Table 3.1 and their corresponding spectra are shown in Figure 3.1. Peak maxima shift from 503nm for the mono complex, 465nm for the bis complex, and 425nm for the tris complex. Spectral points for all concentration ratios in the wavelength range of 350-700nm were inputted into the SQUAD program and stability constants for the mono, bis, and tris complexes (Equation 3.3) were determined simultaneously upon convergence of the program.

$$Fe^{3+} + nAHA^- \rightleftharpoons Fe(AHA)_n^{3-n} \qquad 3.2$$

$$\beta_n' = \frac{[Fe(AHA)_n^{3-n}]}{[Fe^{3+}][AHA^-]^n} \qquad 3.3$$

Conditional stability constants of the $Fe(AHA)^{2+}$, $Fe(AHA)_2^+$, and $Fe(AHA)_3$ complexes were determined in 0.1 mol·L^{-1} HNO_3, 0.1 mol·L^{-1} NO_3^-, and 25 °C as log β_n' = 11.00 ± 0.03, 20.93 ± 0.01, and 28.75 ± 0.01 respectively. The values are listed in Table 3.1 and are comparable with Andrieux, et. al [135] (log β_n = 10.94, 20.68, and 28.26 at 25°C for $0 \leq pH \leq 1.00$ and $NO_3^- \approx 0.1$ mol·L^{-1}, calculated from their published data using 9.33 [86] as the pK_a for AHA at I = 0.1 mol·L^{-1}). Our values are also in agreement with other published data [86, 139]. Molar extinction coefficients were also determined by SQUAD and listed in Table 3.1. These values agree fairly well with previously published values [134].

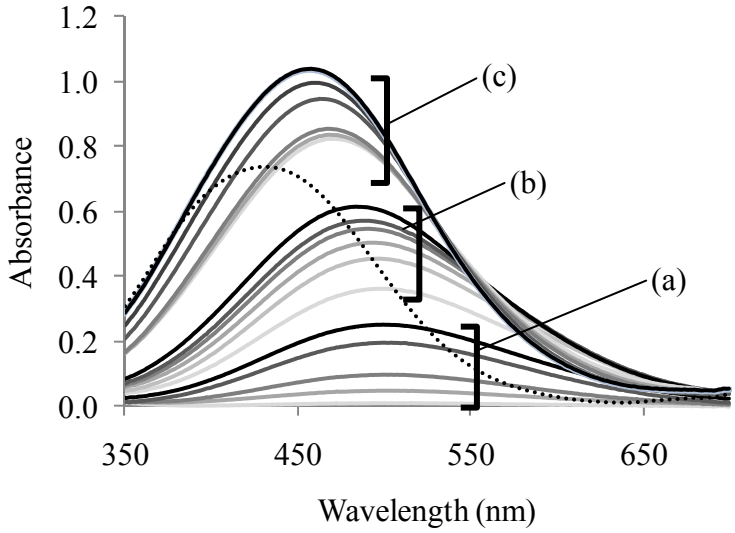

Figure 3.1: Absorbance spectra of $Fe(AHA)_n^{3-n}$ complexation.

Studied system: 0.1 mol·L^{-1} HNO_3, I = 0.1 mol·L^{-1} NO_3^-, and T = 25°C. Concentration ratio regions of Fe(III):AHA are a) 1000:1 – 50:1, b) 1:2 – 1:35, and c) 1:1,000 – 1:1,500. The dashed line is spectrum of a Fe(III):AHA ratio of 1:16,000.

Table 3.1: Conditional stability constants and molar extinction coefficients for $Fe(AHA)_n^{3-n}$.

Experiments: 0.1 mol·L^{-1} HNO_3, I = 0.1 mol·L^{-1} NO_3^-, and 25°C.

[Fe(III)] (mol·L^{-1})	**[AHA]$_{init}$ (mol·L^{-1})**	**Fe(III):AHA**	**Species of Interest**
1.00×10^{-2}	1.00×10^{-5} – 1.00×10^{-3}	1000:1 – 50:1	$Fe(AHA)^{2+}$
5.00×10^{-4}	1.00×10^{-3} – 1.75×10^{-2}	1:2 – 1:35	$Fe(AHA)^{2+}$ & $Fe(AHA)_2^+$
5.00×10^{-4}	8.00×10^{-2} – 7.5×10^{-1}	1:160 – 1:1,500	$Fe(AHA)_2^+$ & $Fe(AHA)_3$
7.50×10^{-5}	1.2×10^{0}	1:16,000	$Fe(AHA)_3$

Complex	**logβ_n' (this paper)**	**logβ_n' (ref. [135])***	**ε $Fe(AHA)_n^{3-n}$ (mol^{-1}·L·cm^{-1}) (this paper)**	**ε $Fe(AHA)_n^{3-n}$ (mol^{-1}·L·cm^{-1}) (ref. [135])**	**ε $Fe(AHA)_n^{3-n}$ (mol^{-1}·L·cm^{-1}) (ref. [134])**
$Fe(AHA)^{2+}$	11.00 ± 0.03	10.94	1.073×10^3 ± 40 at 503nm	1.01×10^3 at 510nm	1.13×10^3 at 501nm
$Fe(AHA)_2^+$	20.93 ± 0.01	20.68	1.960×10^3 ± 60 at 465nm	1.65×10^3 at 465nm	1.98×10^3 at 465nm
$Fe(AHA)_3$	28.75 ± 0.01	28.26	2.005×10^3 ± 80 at 425nm	3.63×10^3 at 420nm	2.41×10^3 at 426nm

3.4.2 U(VI)·Acetohydroxamate Complex

The uranyl cation begins to hydrolyzes in aqueous solutions above pH 2 [16], so the hydrolysis of uranyl was not of concern for this study, as the pH of all solutions was kept at 1. The concentration ranges of uranyl and AHA are listed in Table 3.2 and their corresponding spectra are shown in Figure 3.2. Neither a bathochromic shift nor isosbestic points were observed, but a significant change in spectra occurred as the absorbance ratio of the three peak maxima at 400, 411, and 422nm changed as the ratio of U(VI):AHA changed. A total of four sets of experiments were performed: 0.1 mol·L^{-1} HNO_3 in ionic strengths of 0.1 and 1.0 mol·L^{-1} NO_3^- and 0.1 mol·L^{-1} $HClO_4$ in ionic strengths of 0.1 and 1.0 mol·L^{-1} ClO_4^-. Spectral points for all concentration ratios for a given set of experiments in the wavelength range of 350-600nm were inputted into SQUAD and the conditional stability constant (Equation 3.5) was determined upon

*Note: Conditional stability constants for Andrieux at 25°C for $0 \le pH \le 1.00$ and $NO_3^- \approx 0.1$ mol·L^{-1} were calculated from their published data for comparative purposes using 9.33 as the pK_a for AHA at I = 0.1 mol·L^{-1}.

convergence of the program. Uranyl nitrate stability constants [140] were also included in the input files.

$$UO_2^{2+} + AHA^- \rightleftharpoons UO_2(AHA)^+ \quad 3.4$$

$$\beta_1' = \frac{[UO_2(AHA)^+]}{[UO_2^{2+}][AHA^-]} \quad 3.5$$

Conditional stability constants of the $UO_2(AHA)^+$ complex and molar extinction coefficients of the 411nm absorption peak for the four sets of experiments are provided in Table 3.2. Our results are in good agreement with Koide et. al [92] who calculated log β_1 as 8.22 ± 0.03 in I = 0.1 mol·L^{-1} at 25°C by potentiometric titrations. Koide et. al [92] also determined log β_2 as 15.30 ± 0.07.

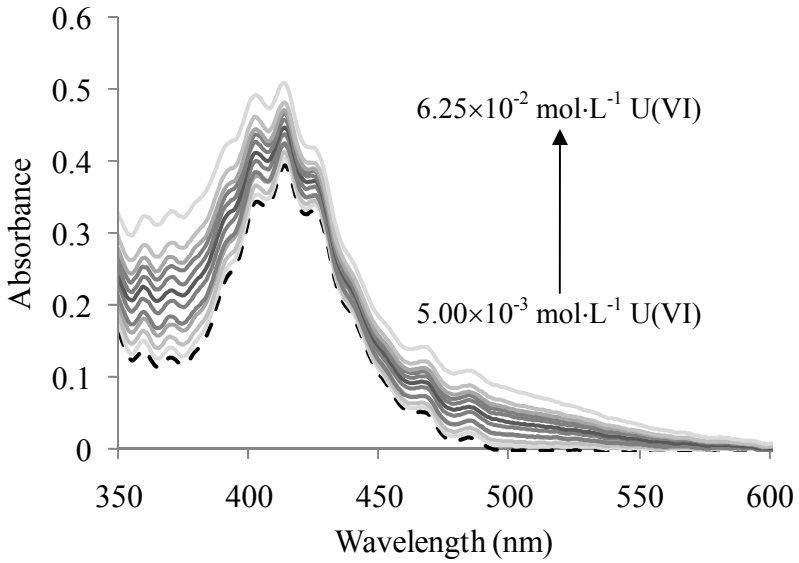

Figure 3.2: Absorbance spectra of $UO_2(AHA)^+$ complexation.

Studied system: 0.1 mol·L^{-1} HNO_3, I = 1.0 mol·L^{-1} NO_3^-, 6.25×10^{-2} mol·L^{-1} AHA, and T = 25°C. The dashed line is the spectrum of 5.00×10^{-2} mol·L^{-1} uranyl nitrate in the absence of AHA.

Table 3.2: Conditional stability constants and molar extinction coefficients for $UO_2(AHA)^+$.

Experiment temperature: 25°C.

$[UO_2^{2+}]$ ($mol \cdot L^{-1}$)	**[AHA] ($mol \cdot L^{-1}$)**	**U(VI):AHA**
6.25×10^{-2}	$2.00\times10^{-2} - 9.00\times10^{-2}$	0.32:1 – 1.44:1
$5.00\times10^{-3} - 6.25\times10^{-2}$	5.00×10^{-2}	10:1 – 0.80:1

Acidity ($mol \cdot L^{-1}$)	**I ($mol \cdot L^{-1}$)**	**$\log\beta_1$'**	**ε $UO_2(AHA)^+$ at 411nm ($mol^{-1} \cdot L \cdot cm^{-1}$)**
0.1 HNO_3	0.1 NO_3^-	8.32 ± 0.02	58.0 ± 0.7
0.1 HNO_3	1.0 NO_3^-	8.05 ± 0.09	50.3 ± 1.1
0.1 $HClO_4$	0.1 ClO_4^-	8.19 ± 0.06	69.1 ± 0.7
0.1 $HClO_4$	1.0 ClO_4^-	8.07 ± 0.05	60.0 ± 1.0
HNO_3	0.1 NO_3^-	8.22 ± 0.03	Ref. [92]*

3.4.3 Zr(IV)·Acetohydroxamate Complexes

Little has been investigated of the complexation of hydroxamic acids with Zr(IV). The complexation of Zr(IV) with benzohydroxamic acid (BHA) was studied, with stability constants calculated as $\log\beta_1$ for $Zr(BHA)^{3+}$ as 12.43 and $\log\beta_2$ for $Zr(BHA)_2^{2+}$ as 24.08 [141]. The limited published material of Zr(IV) with hydroxamic acids is in part due to the tendency of Zr(IV) to form hydrolyzed and polymerized species in aqueous solutions. This could lead to inconsistent results when determining stability constants of unhydrolyzed Zr(IV)-hydroxamate species. Therefore, the hydrolysis and polymerization of zirconium were considered throughout this study.

3.4.3.1 Hydrolysis of Acetohydroxamic Acid and its Complexes

Preliminary experiments showed that the ligand-exchange reaction of Zr(AAIII) with AHA is relatively slow and needed 20 minutes to achieve the complete exchange of the AAIII ligand for AHA. The significant difference of absorbance of the Zr(AAIII) complex in 1 and 2 $mol \cdot L^{-1}$ ClO_4^- shown in Figure 3.3 is due to the change in

* Note: Koide, et. al determined $UO_2(AHA)^+$ stability constant using potentiometric titration at 25°C.

concentration of the ionic media itself [142, 143]. AHA undergoes hydrolytic degradation under acidic conditions, forming acetic acid and hydroxylamine (Equation 3.6) [104].

$$CH_3C(=O)NHOH + H_2O + H^+ \rightarrow CH_3COOH + NH_3OH^+ \quad 3.6$$

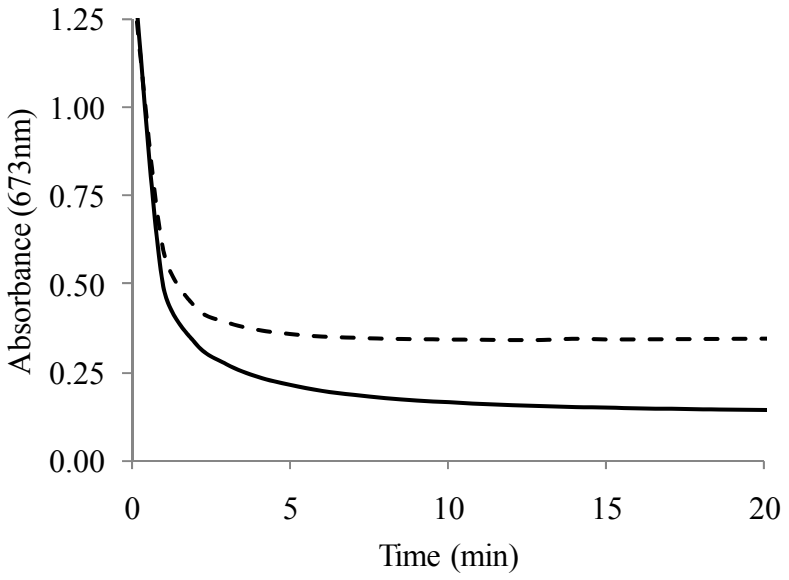

Figure 3.3: Absorbance of Zr/AAIII 673nm peak as a function of time.

Time zero is just prior to the addition of AHA. $[Zr^{4+}]_{tot}$ = 5.0×10^{-5} mol·L^{-1}, [AAIII] = 1.25×10^{-4} mol·L^{-1}, [AHA] = 0.113 mol·L^{-1}, $[HClO_4]$ =1 mol·L^{-1} Solid line: I = 1.0 mol·L^{-1} ClO_4^-. Dashed line: I = 2.0 mol·L^{-1} ClO_4^-.

We found no study of the hydrolytic degradation of AHA in such a low acid concentration as 1 mol·L^{-1} perchloric acid and varying ionic strengths published to date. For comparison, previous nitric acid studies [99, 106] determined that the half life of AHA in 1 mol·L^{-1} decreases as the $[NO_3^-]$ increases. On the other hand, Carrott et al. [95] did not find any appreciable difference in the degradation of AHA in 1 mol·L^{-1} HNO_3 and I = 1 - 6.99 mol·L^{-1} $NaNO_3$ during the experiment. Nonetheless, in this study the half life of the AHA hydrolytic degradation in 1 mol·L^{-1} $HClO_4$ with I = 2 mol·L^{-1} ClO_4^- at 25 ^oC was estimated as 415 minutes using Alyapyshev's 1.5 mol·L^{-1} $HNO_3/LiNO_3$ data [106]. This corresponds to an AHA degradation of 3.3%. The half-life of AHA in 1 mol·L^{-1} $HClO_4$, without any additional ClO_4^-, was calculated as 513 minutes at 25^oC using the $t_{1/2}$ data previously reported [106] for the hydrolytic degradation of AHA at perchloric acid

concentrations of ≥1.5 mol·L^{-1} and extrapolating back to 1 mol·L^{-1} $HClO_4$. This corresponds to approximately 2.7% of AHA degradation after 20 minutes of contact time.

Initial AHA concentrations ($[AHA]_{init}$) were corrected for the 20 minutes of total contact time with the perchloric acid. The reaction was assumed to be first order with respect to both [AHA] and [H^+] and is independent of the AHA concentration. Both the initially prepared $[AHA]_{init}$, which assumes no AHA degradation, and the corrected concentrations $[AHA]_{corr}$, were entered into separate SQUAD input files. SQUAD results indicate that no significant differences exist between the stability constants of $Zr(AHA)^{3+}$ and $Zr(AHA)_2^{2+}$ complexes for the $[AHA]_{init}$ and $[AHA]_{corr}$, as the stability constant obtained for $[AHA]_{corr}$ was within the uncertainty of the stability constant calculated for the $[AHA]_{init}$. The inconsequential differences between the two sets of stability constants could be due to the formation of the Zr(AHA) complex itself, as previous Np(IV)-AHA complexation studies by Andrieux, et. al [90] confirmed the previous suggestion [106] that the formation of the chelation ring protects against the acid-catalyzed hydrolysis of AHA. However, further investigation of the complexation of Zr^{4+} with AHA is needed to confirm this postulation.

3.4.3.2 Hydrolysis of Zr^{4+} in Aqueous Solutions

Zr^{4+} can also form hydrolyzed monomeric and polymeric species in acidic solutions. Previous studies [16, 46] postulated that trimeric ($Zr_3(OH)_4^{8+}$ or $Zr_3(OH)_5^{7+}$) and tetrameric ($Zr_4(OH)_8^{8+}$) species begin to form at approximately 5.0×10^{-4} mol·L^{-1} zirconium solutions in 1 mol·L^{-1} perchloric acid. More recently, Ekberg et al. [47] determined that the monomeric hydrolyzed species $Zr(OH)^{3+}$, $Zr(OH)_2^{2+}$, $Zr(OH)_3^{+}$, and $Zr(OH)_4$ and polymeric species $Zr_2(OH)_6^{2+}$, $Zr_3(OH)_4^{8+}$, and $Zr_4(OH)_8^{8+}$ exist in acidic solutions, and the solubility of Zr^{4+} in solution is highly dependent on acid strength and metal concentration.

The speciation distribution for 5.0×10^{-5} mol·L^{-1} Zr^{4+} in 1 mol·L^{-1} $HClO_4/NaClO_4$ at 25°C was created by inputting the Zr hydrolysis stability constants determined by Ekberg et al

[47] (Table 3.3) into the HySS program. At pH = 0.0 and $[Zr^{4+}]_{total}$ = 5.0×10^{-5} mol·L^{-1}, both the unhydrolyzed Zr^{4+} and $Zr(OH)^{3+}$ hydrolyzed species exist in solution Figure 3.4, whereas polymeric species dominate at pH > 1 and higher metal concentrations ($[Zr^{4+}]_{total}$ = 10^{-3} mol·L^{-1}). Similar results were also determined by Davydov et al. [144]. To calculate the abundance of polymeric hydrolyzed species that form at higher ionic strengths, zirconium stability constants [47] were adjusted by the Specific Ion Interaction Theory [112]. The corrected zirconium stability constants at 2 mol·L^{-1} ClO_4^- were inputted into the HySS program. It was determined that the relative abundance of hydrolyzed species increased with increasing ionic strength. However, at an ionic strength of 2 mol·L^{-1} ClO_4^-, pH 0.0, and at the highest $[Zr^{4+}]$ used in our experiments of 7.00×10^{-5} mol·L^{-1}, the greatest abundance of any polymeric species, $Zr_3(OH)_4^{8+}$, was only 1.2×10^{-2} %. The other polymeric species formed in minute amounts under these solution conditions, as $Zr(OH)^{3+}$ was the only monomeric hydrolyzed species that formed with any significance. However, as shown in Figure 3.4 and Figure 3.5, the modeling program HySS confirmed that when a strong complexing ligand, such as AAIII or AHA, are added to the aqueous solution, all zirconium hydrolyzed species concentrations become insignificant because the hydroxyl groups on zirconium are replaced with covalently bound organic ligands.

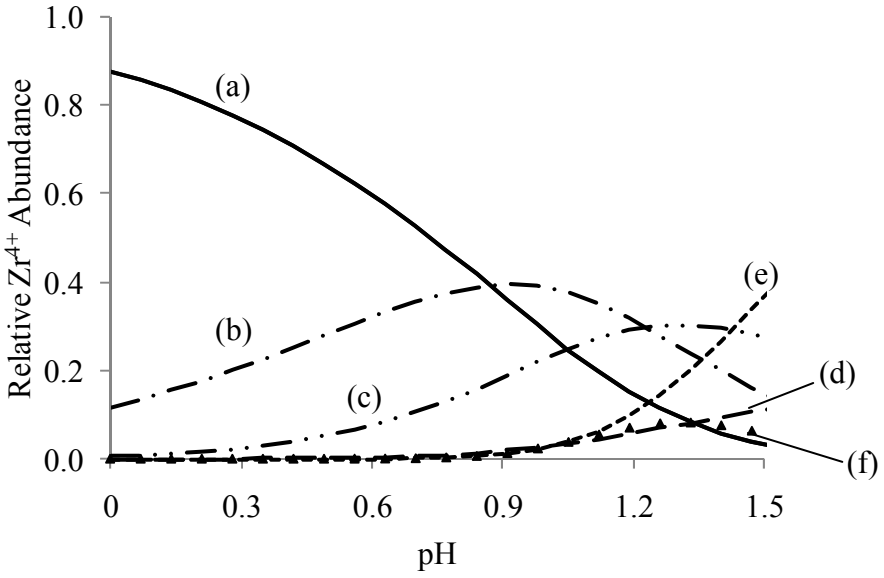

Figure 3.4: Speciation distribution diagram of Zr^{4+}.

Studied system: pH 0-1.5 $HClO_4$, 25 °C, $[Zr^{4+}]_{total} = 5.0\times10^{-5}$ mol·L^{-1}. (a) Zr^{4+}, (b) $Zr(OH)^{3+}$, (c) $Zr(OH)_2^{2+}$, (d) $Zr(OH)_3^{+}$, (e) $Zr_2(OH)_6^{2+}$, and (f) $Zr_4(OH)_8^{8+}$. Other possible Zr^{4+}-species such as $Zr(OH)_4$ and $Zr_3(OH)_4^{8+}$ have relative molar fractions ≤ 0.015 under these conditions and are not shown for clarity.

Table 3.3: Hydrolysis constants of Zr^{4+}.

I = 1 mol·L^{-1} ClO_4^- at 25°C as reported by Ekberg, et. al [47] using potentiometry and solvent extraction.

Species	**Log K_H (25 °C)**
$Zr(OH)^{3+}$	-0.87 ± 0.05
$Zr(OH)_2^{2+}$	-2.1 ± 0.2
$Zr(OH)_3^{+}$	-4.0 ± 0.3
$Zr(OH)_4$	-6.7 ± 0.3
$Zr_2(OH)_6^{2+}$	-2.42 ± 0.13
$Zr_3(OH)_4^{8+}$	4.1 ± 0.5
$Zr_4(OH)_8^{8+}$	5.2 ± 0.2

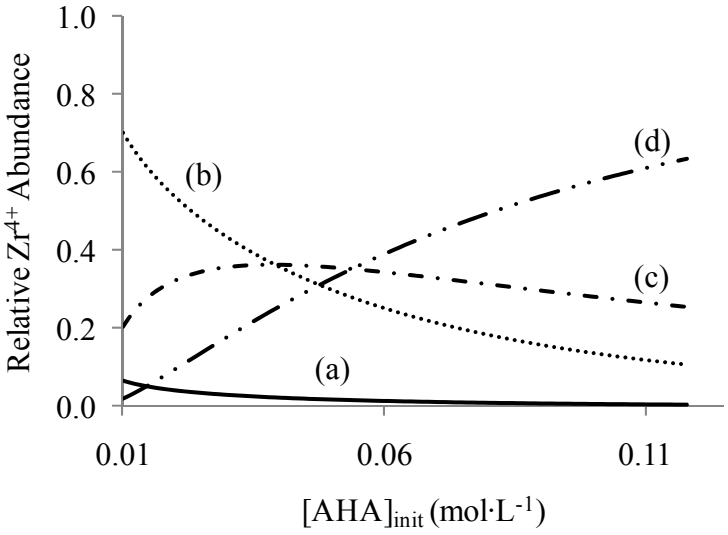

Figure 3.5: Speciation distribution diagram of Zr^{4+} in aqueous solutions of AHA.

$[Zr^{4+}]_{total} = 5.0\times10^{-5}$ mol·L^{-1}, $[AAIII]_i = 1.25\times10^{-4}$ mol·L^{-1}, and $[AHA]_{init} = 0.005 - 0.113$ mol·L^{-1} in 1 mol·L^{-1} $HClO_4$, 1 mol·L^{-1} ClO_4^-, and 25°C. (a) $Zr(AAIII)^{3+}$: (b) $Zr(AAIII)_2^{2+}$: (c) $Zr(AHA)^{3+}$: (d) $Zr(AHA)_2^{2+}$. Zr_{free} abundance was ≤ 1% for the studied AHA concentration range.

3.4.3.3 Complexation of Zr with Arsenazo III

AAIII is a brightly colored chelate anion used as an indicator to detect metals and their complexes that are spectroscopically silent. It is widely used for analytical spectroscopy of zirconium [145, 146], actinoids [147, 148], and rare earth elements [149]. Zr^{4+} and its complexes with AHA lack an absorbance peak in the visible spectral range but zirconium will form complexes with AAIII (Equation 3.7) yielding an absorption peak that can be measured by monitoring changes in the 650-700 nm region with a maximum at 673 nm, (Figure 3.6).

$$Zr^{4+} + mAAIII^- \rightleftharpoons Zr(AAIII)_m^{4-m} \qquad 3.7$$

The absorbance of free AAIII (520-540nm) at the absorbance maxima of the Zr(AAIII) complex is negligible, as shown by the dotted line in Figure 3.6. Previous studies [150] show that the composition of the complex depends on the ratio of AAIII and Zr^{4+} in solution, with a 1:1 Zr:AAIII ratio when Zr^{4+} is in excess and a 1:2 Zr:AAIII ratio when AAIII is in excess. In order to determine the Zr:AAIII ratio of our experiments, a Job's

method experiment was performed with the sum of the $[Zr^{4+}]_{init}$ and [AAIII] concentrations equal to 5.0×10^{-5} mol·L^{-1} at 25°C and 1 mol·L^{-1} $HClO_4$. At this total concentration, a maximum absorbance at the 673 nm peak occurred at a ratio of 0.62 (Figure 3.7). A ratio of 0.50 would indicate that a 1:1 complexation ratio of Zr:AAIII, whereas a 0.66 ratio would indicate a 1:2 Zr:AAIII complexation ratio. Therefore, with a ratio of 0.62 our data indicates that both 1:1 and 1:2 Zr:AAIII ratios are present, but with the 1:2 complex in a greater relative abundance. Experiments were performed where the $[Zr^{4+}]_{init}$ and [AAIII] varied, as listed in Table 3.4. Absorption spectral data for all experiments were inputted into SQUAD, along with the pK_as of AAIII [86], to simultaneously determine the molar extinction coefficients for the $Zr(AAIII)^{3+}$ and $Zr(AAIII)_2^{2+}$ complexes at 673 nm. Results are provided in Table 3.5. It is important to note that the molar extinction coefficients reported in this paper for 1 and 2 mol·L^{-1} perchloric acid are significantly smaller than the molar coefficients for Zr-AAIII comp1exes originally determined by Savvin for a 9 mol·L^{-1} solution of HCl [143]. However, Muk and Radosavljevic [151] determined that the absorbance of the Zr(AAIII) complex in 1 mol·L^{-1} $HClO_4$ is approximately 6 times less than the absorbance in 6 mol·L^{-1} $HClO_4$ for Zr^{4+} and AAIII concentrations similar to our experiments. Therefore, we attribute the lower molar extinction coefficients to the lower acid concentration used in our experiments.

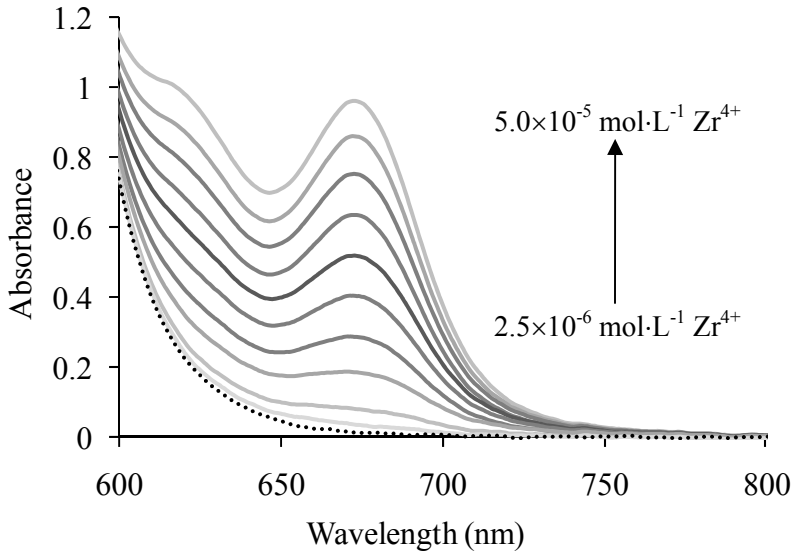

Figure 3.6: Absorbance spectra of Zr^{4+}/AAIII.

1 mol·L^{-1} $HClO_4$, 1 mol·L^{-1} ClO_4^-, and 25 °C. [AAIII] = 1.25×10^{-4} mol·L^{-1}. $[Zr^{4+}]_{total}$ = 2.5×10^{-6} – 5.0×10^{-5} mol·L^{-1} except for dotted line, where $[Zr^{4+}]_{total}$ = 0.0 mol·L^{-1}.

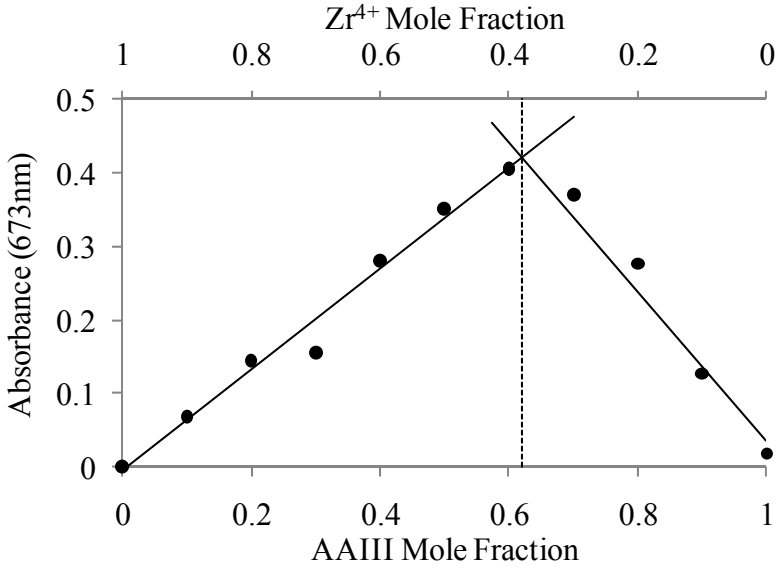

Figure 3.7: Job's method experiment of Zr^{4+} and AAIII

Total concentration of 5.0×10^{-5} mol·L^{-1}. The AAIII mole fraction was determined as 0.62.

Table 3.4: Reagent concentrations ranges for Zr^{4+}/AAIII/AHA experiments.

[Zr^{4+}] (mol·L^{-1})	**[AAIII] (mol·L^{-1})**	**[AHA] (mol·L^{-1})**
$2.50\times10^{-6} - 5.00\times10^{-5}$	1.25×10^{-4}	0
5.00×10^{-5}	$1.00\times10^{-5} - 1.25\times10^{-4}$	0
0	$1.00\times10^{-5} - 1.25\times10^{-4}$	0
5.00×10^{-5}	1.25×10^{-4}	$5.00\times10^{-3} - 1.13\times10^{-1}$
$1.00\times10^{-5} - 7.00\times10^{-5}$	1.25×10^{-4}	4.00×10^{-2}

3.4.3.4 Complexation of Zr with AHA

Zr(AHA) complexes and their conditional stability constants are described by Equations 3.8 and 3.9.

$$Zr(AAIII)_m^{4-m} + nAHA^- \rightleftharpoons Zr(AHA)_n^{4-n} + mAAIII^- \quad 3.8$$

$$\beta'_n = \frac{[Zr(AHA)_n^{4-n}]}{[Zr(AAIII)_m^{4-m}][AHA^-]^n} \quad 3.9$$

$Zr(AHA)_n^{4-n}$ complexes do not absorb light in the visible region. However, the addition of AHA to a Zr(AAIII) solution decreases the $Zr(AAIII)^{3+}$ complex by forming $Zr(AHA)_n^{4-n}$ species. AAIII is replaced by AHA^- because acetohydroxamic acid forms much stronger complexes with Zr^{4+} than AAIII, as indicated by the large difference in their conditional stability constants. The absorbance of the $Zr(AAIII)^{3+}$ complex in the 650-700 nm spectral range decreased with increasing [AHA], (Figure 3.8). Thus, the complexation of AHA with Zr^{4+} can be observed by monitoring the changes of absorption of $Zr(AAIII)^{3+}$. Reagent concentrations ranges for the Zr^{4+}/AAIII/AHA experiments are provided in Table 3.4.

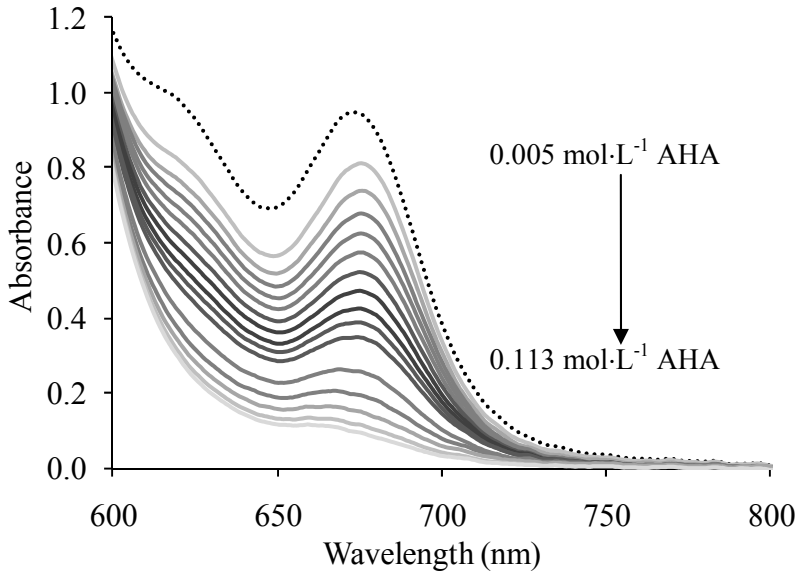

Figure 3.8: Absorbance spectra of Zr^{4+}/AAIII/ AHA

1 mol·L^{-1} $HClO_4$, 1 mol·L^{-1} ClO_4^-, and 25 °C. $[Zr^{4+}]_{total}$ = 5.0×10^{-5} mol·L^{-1} and [AAIII] = 1.25×10^{-4} mol·L^{-1}. [AHA] = 0.005 – 0.113 mol·L^{-1} except for dashed line, where [AHA] = 0.0 mol·L^{-1}.

Table 3.5: Conditional stability constants and extinction coefficients of Zr·AAIII and AHA.

$Zr(AAIII)^{3+}$, $Zr(AAIII)_2^{2+}$, $Zr(AHA)^{3+}$, and $Zr(AHA)_2^{2+}$ and molar extinction coefficients of Zr(AAIII) species in 1 mol·L^{-1} $HClO_4$, I = 1-2 mol·L^{-1} ClO_4^-, and 25°C.

Species	**Logβ' 1.0 mol·L^{-1} ClO_4^-**	**ε $Zr(AAIII)_m^{4-m}$ ($mol^{-1}\cdot L\cdot cm^{-1}$) at 673nm**	**Logβ' 2.0 mol·L^{-1} ClO_4^-**	**ε $Zr(AAIII)_m^{4-m}$ ($mol^{-1}\cdot L\cdot cm^{-1}$) at 673nm**
$Zr(AAIII)^{3+}$	5.09 ± 0.07	$2.96\times10^4 \pm 1.29\times10^3$	5.27 ± 0.08	$2.77\times10^4 \pm 9.26\times10^2$
$Zr(AAIII)_2^{2+}$	10.29 ± 0.09	$2.05\times10^4 \pm 3.17\times10^3$	10.34 ± 0.09	$2.08\times10^4 \pm 2.94\times10^2$
$Zr(AHA)^{3+}$	12.77 ± 0.02	-	12.82 ± 0.09	-
$Zr(AHA)_2^{2+}$	23.13 ± 0.03	-	23.61 ± 0.06	-

The conditional stability constants of $Zr(AAIII)_m^{4-m}$ and $Zr(AHA)_n^{4-n}$ for m and n = 1 and 2 were calculated using SQUAD under the assumption that no Zr polymerized species existed in solution, which was based on the HySS results described above. Speciation distribution diagrams indicate that only Zr^{4+}, $Zr(AAIII)^{3+}$, $Zr(AAIII)_2^{2+}$, $Zr(AHA)^{3+}$ and $Zr(AHA)_2^{2+}$ species were present, even when all hydrolyzed species were considered in HySS (Figure 3.5). See Table 3.5 for calculated conditional stability constants for $Zr(AHA)^{3+}$, and $Zr(AHA)_2^{2+}$ in 1 mol·L^{-1} $HClO_4$, I = 1 and 2 mol·L^{-1} ClO_4^-, and 25°C. No

Zr hydrolyzed species existed in any solution containing either AAIII or AHA this study, as the [Zr^{4+}] was low (on the order of 10^{-5} mol·L^{-1}) and the acidity was high (1 mol·L^{-1}). This finding agrees with Zielen and Connick [46], who also found that in the perchloric acid range of 1 to 2 mol·L^{-1} the principal zirconium species at low zirconium concentrations is the unhydrolyzed monomer, Zr^{4+}. Also, under all solution conditions, the concentrations of AAIII and AHA^- were high compared to the negligible amount of hydroxide ions present in solution needed to form zirconium hydrolyzed species. Therefore, hydrolyzed zirconium species did not form and interfere with the Zr(AAIII) and Zr(AHA) complexation because of the initial reagent concentrations chosen for all experiments.

Overall, it was confirmed that zirconium forms strong complexes with AHA, which have stability constants nearly as large as for tetravalent plutonium-AHA complexes (logβ = 14.2 ± 0.2 and 24.1 ± 0.2 for $Pu(AHA)^{3+}$ and $Pu(AHA)_2^{2+}$, respectively [91]). Both plutonium and zirconium-AHA complexes are much stronger than uranyl-AHA complexes, as evident by the significant differences in their stability constants. With the formation of particularly strong hydrophilic complexes of $Pu(AHA)_n^{4-n}$, acetohydroxamic acid significantly decreases the distribution of plutonium between the aqueous and TBP phases [64, 99, 152]. The same is also true for zirconium, as AHA decreases the distribution of Zr^{4+} by TBP [153] by forming strong $Zr(AHA)_n^{4-n}$ complexes. On the contrary, uranyl-AHA complexes are much weaker than both the plutonium and zirconium-AHA complexes, since their stability constants differ by six orders of magnitude. The significant differences of the stability constants are in part due to their effective cationic charges. Tetravalent Pu has a charge of 4+, whereas UO_2^{2+} has an effective charge of +3.2, with uranium being partially shielded by the two oxygen atoms [20]. This causes plutonium to be a stronger Lewis acid, allowing for the formation of stronger complexes with organic and inorganic ligands. Since the $UO_2(AHA)^+$ complex is much weaker, acetohydroxamic acid has little effect on the stripping of uranyl nitrate under UREX process conditions [66]. Therefore, the utilization of AHA in the UREX process results in a greater retention of plutonium and zirconium in the aqueous phase and effective separation from uranium.

3.5 Conclusion

The conditional stability constants of the mono- and di-acetohydroxamate complexes of zirconium have been determined by spectrophotometric analysis in 1 $mol \cdot L^{-1}$ $HClO_4$ aqueous solutions at various ionic strengths and 25°C. Zr^{4+} and AAIII form 1:1 and 1:2 complexes and neither monomeric nor polymeric hydrolyzed Zr^{4+} species formed under experimental conditions. Conditional stability constants for $UO_2(AHA)^{+}$, $Fe(AHA)^{2+}$, $Fe(AHA)_2^{+}$, $Fe(AHA)_3$, $Zr(AAIII)^{3+}$, $Zr(AAIII)_2^{2+}$, $Zr(AHA)^{3+}$, and $Zr(AHA)_2^{2+}$ were determined at 25°C. It has been shown that zirconium-AHA complexes are much stronger than uranyl-AHA complexes, with their stability constants differing by six orders of magnitude. Therefore, AHA is a promising complexant to separate zirconium from uranium in the UREX process.

3.6 Acknowledgements

We express our gratitude to Lin Kong for his work of the uranium spectroscopy experiments. We thank Peter Sprunger for creating a Java program to align the SQUAD input files.

The research was performed under financial support of the Office of Civilian Radioactive Waste Management Graduate Fellowship Program administered by Oak Ridge Institute for Science and Education and USDOE NERI Program, Award 054657.

4 COMPLEXATION CHEMISTRY OF ZIRCONIUM(IV) WITH ACETOHYDROXAMIC ACID IN NITRIC ACID

4.1 Introduction

All previous zirconium complexation studies with arsenazo III (AAIII) and acetohydroxamic acid (AHA) were performed in perchloric acid (section 3.4.3). Since perchlorate does not complex with metals, it was used to minimize the complexity of the Zr·AAIII and Zr·AHA system. UNF is dissolved in nitric acid; for that reason, we expect $Zr(NO3)_n^{4-n}$ complexes will form in solution and subsequently compete with AHA for available Zr binding sites. Therefore, additional spectrophotometric experiments were performed in nitric acid to determine whether zirconium nitrate complexation may affect the formation of Zr·AAIII and Zr·AHA complexes. SQUAD [129] was used to determine conditional stability constants of the Zr complexes.

4.2 Experimental

All materials (except for acid), sample preparation, and visible spectroscopy were performed in the same manner as described in section 3.3. Experimental concentrations for the Zr·AAIII and Zr·AAIII·AHA experiments are provided in Table 10.7 and

.

Acidity of stock solutions were adjusted using nitric acid, prepared from HNO_3 (68% EMD Chemicals GR ACS grade). The acid concentration was determined by a pH-metric titration (Mettler-Toledo DL58 Titrator) with sodium hydroxide standardized by potassium hydrogen phthalate (Analytical Reagent, Mallinckrodt). Distilled, deionized water (Barnstead, 18 MΩ·cm resistivity) was used for all experiments.

4.3 Results

4.3.1 Zirconium Nitrate Complexation

Nitrate anions readily coordinate with Zr. Formation constants have previously been determined [136, 154], with accepted values [86] for the first four $Zr{\cdot}NO_3$ complexes at 20°C and an ionic strength of 4.0 $mol{\cdot}L^{-1}$ (Table 4.1). Ionic strength of these experiments (1.0 $mol{\cdot}L^{-1}$ NO_3^-) was corrected (SIT [112]). The zirconium nitrate formation constants for a 1.0 $mol{\cdot}L^{-1}$ NO_3^- ionic strength were added to SQUAD input files.

Table 4.1: Zirconium nitrate formation constants.

Species	**log K_n (I = 4.0 $mol{\cdot}L^{-1}$) [86]**	**log K_n (I = 1.0 $mol{\cdot}L^{-1}$) Calculated from SIT**
$Zr(NO_3)^{3+}$	+0.34	+0.65
$Zr(NO_3)_2^{2+}$	+0.10	-0.08
$Zr(NO_3)_3^{+}$	-0.30	-1.09
$Zr(NO_3)_4$	-0.80	-2.31

4.3.2 Zirconium·Complexation with Arsenazo III

The stability constants of Zr·AAIII complexes were calculated for use in later Zr·AHA complexation studies. Zr·AAIII complexes were monitored using visible spectroscopy (Figure 4.1 and Figure 4.2). Two sets of experiments were performed: one with constant [AAIII] of 3.0×10^{-5} $mol{\cdot}L^{-1}$ and varying $[Zr^{4+}]$, and the other with constant $[Zr^{4+}]$ of 3.0×10^{-5} $mol{\cdot}L^{-1}$ and varying [AAIII]. Conditional stability constants were determined from 400-750nm spectral data from for all experiments. A background spectrum, which only included 1.0 $mol{\cdot}L^{-1}$ HNO_3, and the $Zr{\cdot}NO_3$ formation constants for a 1.0 $mol{\cdot}L^{-1}$ NO_3^- ionic strength were included.

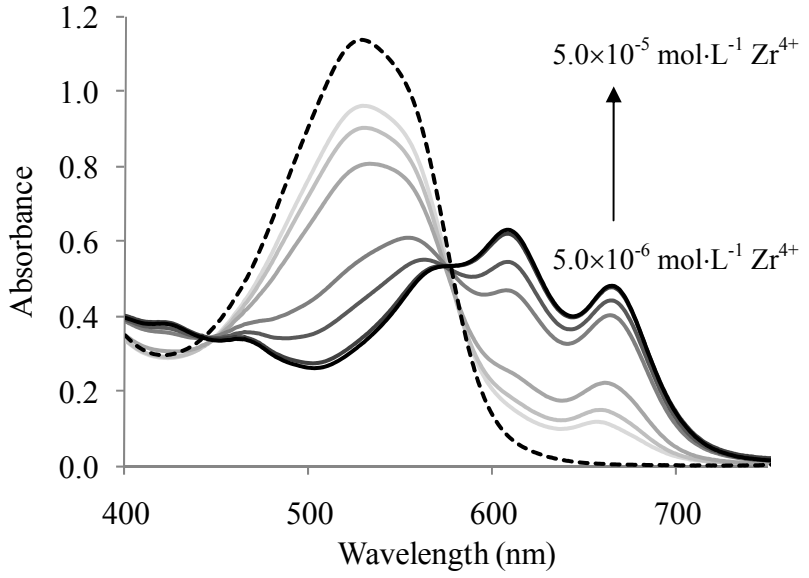

Figure 4.1: Absorbance spectra of Zr·AAIII system ($\Delta[Zr^{4+}]$).

[AAIII] = 3.0×10^{-5} mol·L^{-1} and [Zr^{4+}] = 5.0×10^{-6} – 5.0×10^{-5} mol·L^{-1} (solid lines) and [Zr^{4+}] = 0.0 mol·L^{-1} (dashed line).

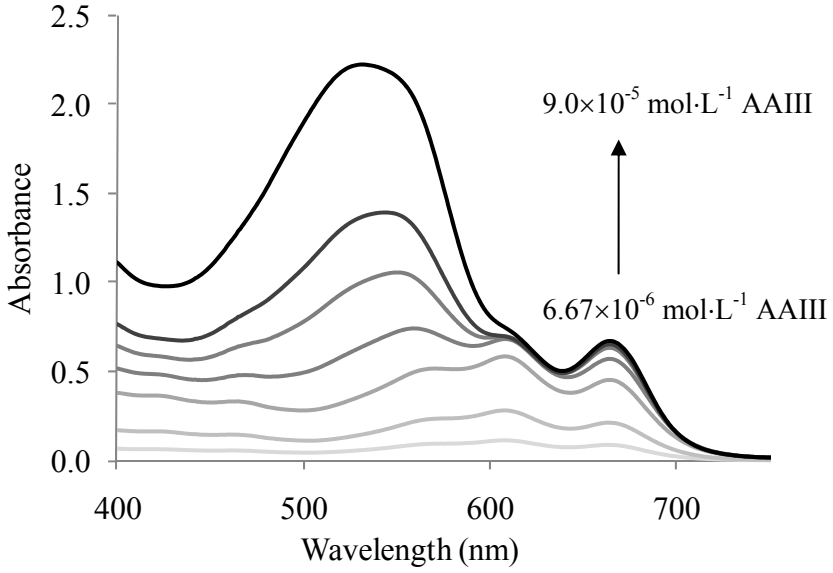

Figure 4.2: Absorbance spectra of Zr·AAIII system (Δ[AAIII]).

[Zr^{4+}] = 3.0×10^{-5} mol·L^{-1} and [AAIII] = 6.67×10^{-6} – 9.0×10^{-5} mol·L^{-1}.

The conditional stability constants for $Zr(AAIII)^{3+}$ and $Zr(AAIII)_2^{2+}$ and associated molar extinction coefficients were simultaneously determined (Table 4.2). Conditional stability constants in 1 $mol \cdot L^{-1}$ perchloric acid are 5.09 ± 0.07 and 10.29 ± 0.09 for $Zr(AAIII)^{3+}$ and $Zr(AAIII)_2^{2+}$ (section 3.4.3.3), whereas in 1 $mol \cdot L^{-1}$ nitric acid they are 4.96 ± 0.08 and 10.02 ± 0.15.

The conditional stability constants determined for Zr·AAIII in 1 $mol \cdot L^{-1}$ nitric acid were used in determining the speciation of the solutions used in the experiments. The hydrolysis constants of all hydrolyzed and polymerized zirconium species (Table 3.3), zirconium nitrates (Table 4.1), and the pKa of nitric acid (-1.44, [155]) were inputted in HySS. Speciation diagrams for the concentration ranges of both zirconium arsenazo III experiments are provided (Figure 4.3 and Figure 4.4). Zirconium nitrate species are present in solution of both experiments, explaining the slight decrease in conditional stability constants for Zr·AAIII complexes in nitric acid compared to perchloric acid. Nitrate ions and AAIII compete for Zr binding sites, whereas non-complexing perchlorate anion does not bind to Zr. In the nitric acid system the Zr·AAIII complex is not quite as prevalent for a given Zr:AAIII concentration ratio, hence the lower stability constant.

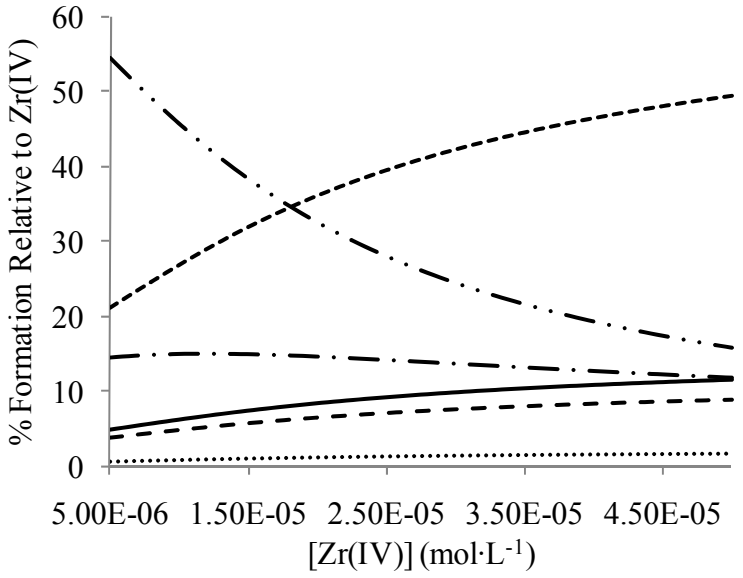

Figure 4.3: Speciation distribution diagram of Zr^{4+} in HNO_3 ($\Delta[Zr^{4+}]$).

System: 1 mol·L^{-1} HNO_3, 25 °C, $[Zr^{4+}]_{total}$ = 5.0×10^{-6} - 5.0×10^{-5} mol·L^{-1}, [AAIII] = 3.0×10^{-5} mol·L^{-1}. Zr^{4+} (solid line), $Zr(OH)^{3+}$ (dotted line), $Zr(NO_3)^{3+}$ (narrow dashed line), $Zr(NO_3)_3^{2+}$ (medium dashed line), $Zr(AAIII)^{3+}$ (· – ·), and $Zr(AAIII)_2^{2+}$ (·· – ··).

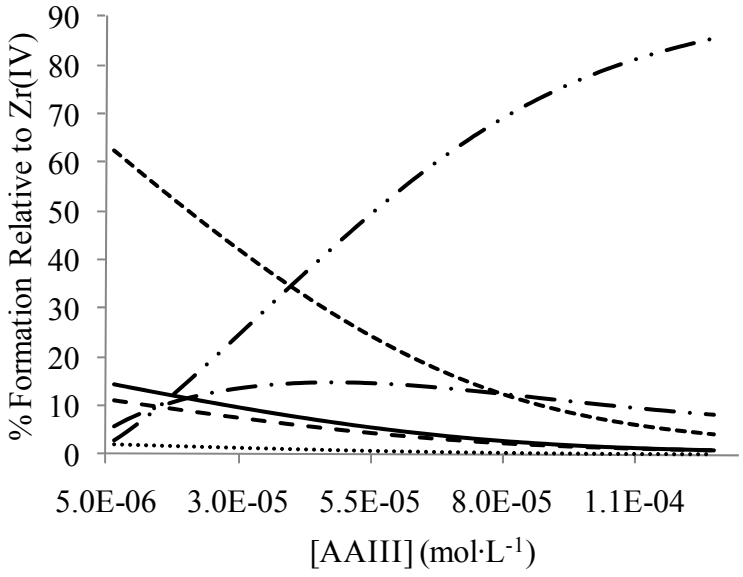

Figure 4.4: Speciation distribution diagram of Zr^{4+} in HNO_3 (Δ[AAIII]).

System: 1 mol·L^{-1} HNO_3, 25 °C, $[Zr^{4+}]_{total}$ = 3.0×10^{-5} mol·L^{-1}, [AAIII] = 6.7×10^{-6} – 1.2×10^{-4} mol·L^{-1}. Zr^{4+} (solid line), $Zr(OH)^{3+}$ (dotted line), $Zr(NO_3)^{3+}$ (narrow dashed line), $Zr(NO_3)_3^{2+}$ (medium dashed line), $Zr(AAIII)^{3+}$ (· – ·), and $Zr(AAIII)_2^{2+}$ (·· – ··).

4.3.3 Zirconium Complexation with AHA

AHA forms strong complexes with Zr, which competes with AAIII for zirconium binding sites. As a much stronger Lewis base, AHA replaces AAIII and the characteristic 673nm peak of the Zr·AAIII complex decreases. This enables monitoring of Zr·acetohydroxamate complexation.

Two sets of experiments were performed: one with constant [AAIII] and [Zr^{4+}] of 3.0×10^{-5} mol·L^{-1} and varying [AHA], and the other with constant [AAIII] of 3.0×10^{-5} mol·L^{-1}, constant [AHA] of 0.02 mol·L^{-1}, and varying [Zr^{4+}] (Figure 4.5 and Figure 4.6).

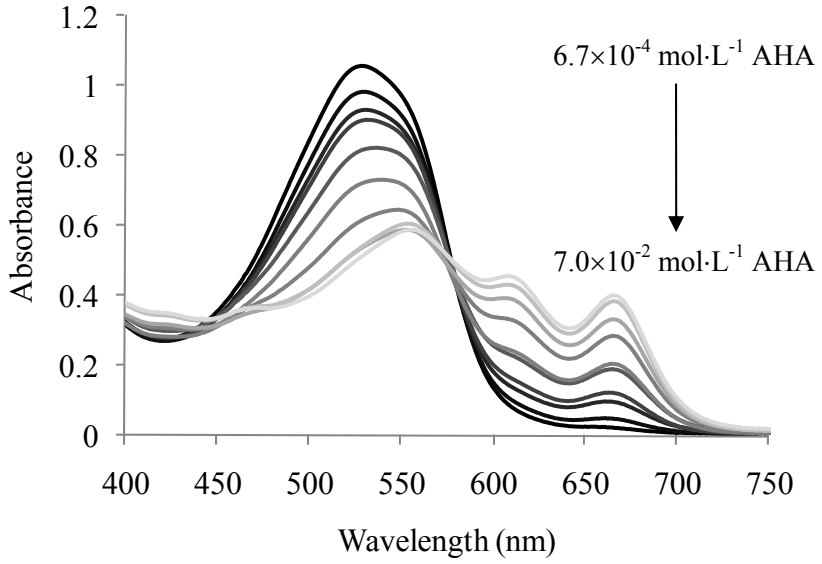

Figure 4.5: Absorbance spectra of Zr/AAIII/AHA system (Δ[AHA]).
[AAIII] = 3.0×10^{-5} mol·L^{-1}, [Zr^{4+}] = 3.0×10^{-5} mol·L^{-1}, [AHA] = 6.7×10^{-4} – 7.0×10^{-2} mol·L^{-1}.

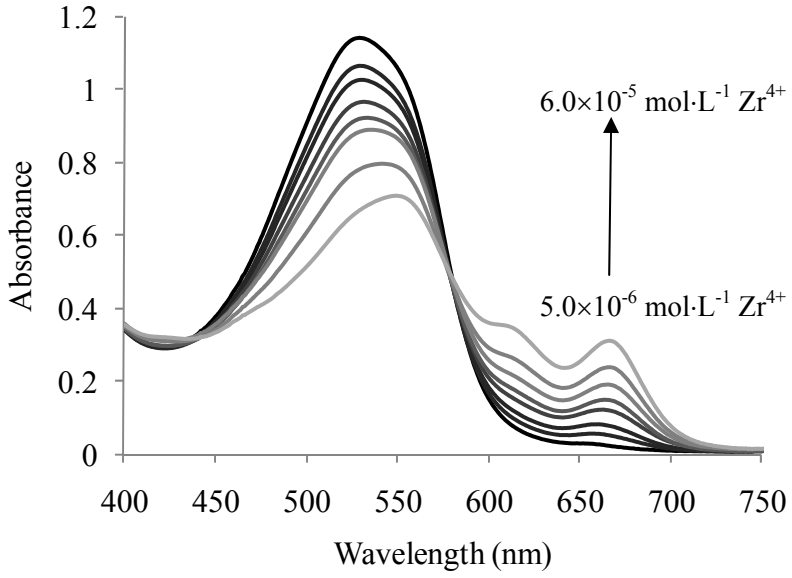

Figure 4.6: Absorbance spectra of Zr/AAIII/AHA system ($\Delta[Zr^{4+}]$).
[AAIII] = 3.0×10^{-5} mol·L^{-1}, [Zr^{4+}] = 5.0×10^{-6} - 6.0×10^{-5} mol·L^{-1}, [AHA] = 1.0×10^{-2} mol·L^{-1}.

Conditional stability constants for $Zr(AHA)^{3+}$ and $Zr(AHA)_2^{2+}$ were determined from 400-750nm spectral data from for all experiments (Table 4.2). A background spectrum, which only included 1.0 mol·L^{-1} HNO_3, and the $Zr{\cdot}NO_3$ formation constants for a 1.0 mol·L^{-1} NO_3^- ionic strength were included. Molar extinction coefficients for Zr·AHA were not determined since the complexes are spectroscopically silent. Conditional stability constants of Zr·AHA complexes in nitric acid were slightly less than those of the perchloric acid studies (Table 3.5) which is attributed to complexation of Zr^{4+} and NO_3^- that occurs in the nitric acid. This indicates that AHA will readily complex with Zr present in UNF dissolved in nitric acid. Calculated Zr·AHA conditional stability constants are large compared to most other metal·AHA constants (Table 2.1). Therefore, the reactivity of AHA with Zr must be considered if AHA is to be used in advanced reprocessing schemes such as UREX.

Table 4.2: Conditional stability constants of Zr·AAIII and Zr·AHA complexes.

Molar extinction coefficients of Zr·AAIII complexes.

Species	Logβ' 1.0 mol·L^{-1} NO_3^-	ε $Zr(AAIII)_m^{4-m}$ (mol^{-1}·L·cm^{-1}) at 673nm
$Zr(AAIII)^{3+}$	4.96 ± 0.08	$1.50\times10^4 \pm 3.49\times10^2$
$Zr(AAIII)_2^{2+}$	10.02 ± 0.15	$3.14\times10^4 \pm 2.50\times10^3$
$Zr(AHA)^{3+}$	12.67 ± 0.10	-
$Zr(AHA)_2^{2+}$	22.78 ± 0.07	-

The Zr·AHA conditional stability constants in 1 mol·L^{-1} nitric acid were used to determine the speciation of the solutions used in the experiments (Table 4.2). The formation constants of all hydrolyzed and polymerized zirconium species (Table 2.1), zirconium nitrates (Table 4.1), the pKa of nitric acid (-1.44, [155]), and the Zr·AAIII stability constants were inputted in HySS. $Zr\cdot NO_3$ species are prevalent in the solutions, explaining the slight decrease of the Zr·AHA stability constants in nitric acid compared to the perchloric acid system.

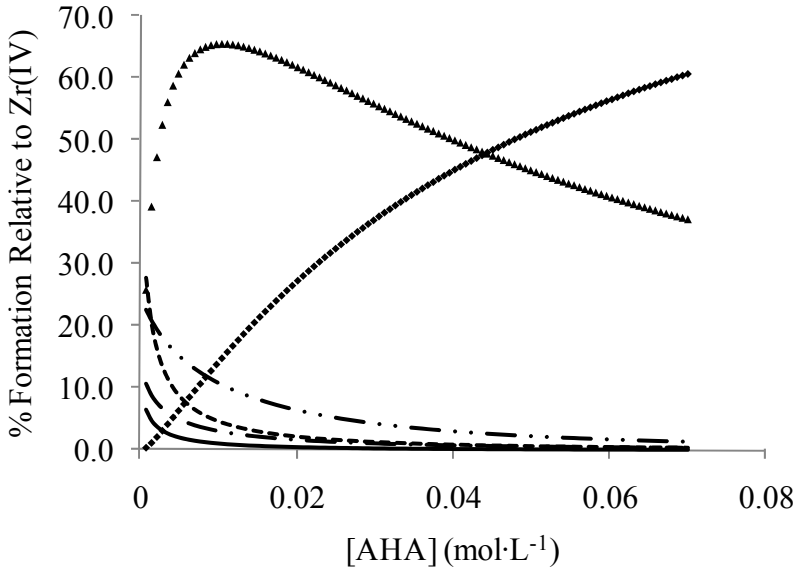

Figure 4.7: Speciation distribution diagram of Zr^{4+} in HNO_3 (Δ[AHA]).

System: 1 mol·L^{-1} HNO_3, 25 °C, $[Zr^{4+}]_{total}$ = 3.0×10^{-5} mol·L^{-1}, [AAIII] = 3.0×10^{-5} mol·L^{-1}, [AHA] = 7.0×10^{-2} – 6.7×10^{-4} mol·L^{-1}. Zr^{4+} (solid line), $Zr(OH)^{3+}$ (dotted line), $Zr(NO_3)^{3+}$ (narrow dashed line), $Zr(AAIII)^{3+}$ (· – ·), and $Zr(AAIII)_2^{2+}$ (·· – ··), $Zr(AHA)^{3+}$ (▲), and $Zr(AHA)_2^{2+}$ (■).

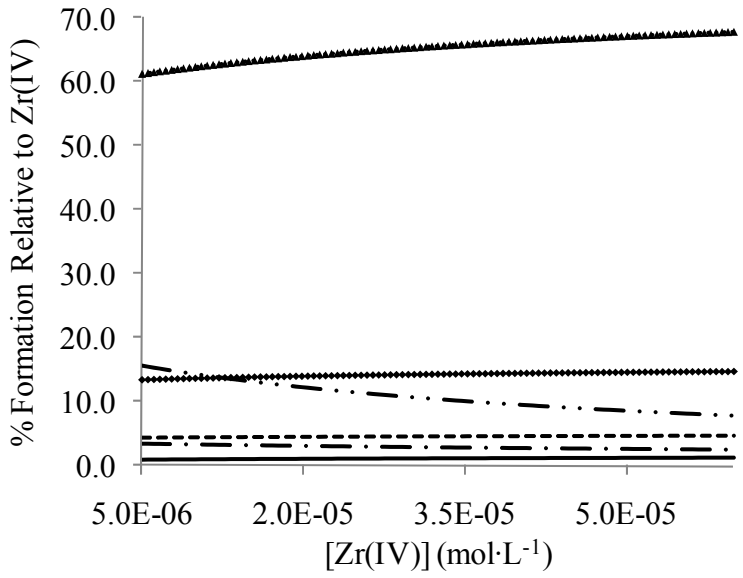

Figure 4.8: Absorbance spectra of Zr/AAIII/AHA system ($\Delta[Zr^{4+}]$).

System: 1 mol·L^{-1} HNO_3, 25 ^{o}C, $[Zr^{4+}]_{total}$ = 5.0×10^{-6} - 6.0×10^{-5} mol·L^{-1}, [AAIII] = 3.0×10^{-5} mol·L^{-1}, [AHA] = 1.0×10^{-2} mol·L^{-1}. Zr^{4+} (solid line), $Zr(OH)^{3+}$ (dotted line), $Zr(NO_3)^{3+}$ (narrow dashed line), $Zr(AAIII)^{3+}$ (· – ·), and $Zr(AAIII)_2^{2+}$ (·· – ··), $Zr(AHA)^{3+}$ (▲), and $Zr(AHA)_2^{2+}$ (♦).

5 A STUDY OF THE KINETICS OF THE REDUCTION OF NEPTUNIUM(VI) BY ACETOHYDROXAMIC ACID IN PERCHLORIC ACID

Brent S. Matteson, Martin Precek, and Alena Paulenova

Material Science and Engineering

Elsevier

3251 Riverport Lane

Maryland Heights, MO 63043

Material Science and Engineering, volume 9, 2010, *Published.*

5.1 Abstract

The kinetics of reduction of NpO_2^{2+} to NpO_2^{+} by acetohydroxamic acid in 1 mol·L^{-1} perchloric acid media at 10 and 22°C were studied. The reaction rate was monitored using stopped-flow and standard infrared spectroscopy. Under conditions such that acetohydroxamic acid was in excess relative to Np, the reduction rate of NpO_2^{2+} is described by the following:

$$-\frac{d[NpO_2^{2+}]}{dt} = k[NpO_2^{2+}][AHA] \qquad 5.1$$

where k = 2.57×10^3 mol^{-1}·L·sec^{-1} at 10°C. However, when neptunium is in a significant molar excess relative to acetohydroxamic acid, the reduction mechanism is dictated by two distinct reactions. An initial and incomplete reduction occurs as the result of the oxidation of AHA, while a slower and partial reduction of NpO_2^{2+} is likely caused by the oxidation products of AHA. The reaction rate of this first-order mechanism was calculated as 3.7×10^{-4} sec^{-1} at 10°C and 0.001 sec^{-1} at 22°C.

5.2 Introduction

For several decades, used nuclear fuel (UNF) from commercial power reactors has been reprocessed in order to recovery uranium and plutonium. The PUREX process is the most utilized method worldwide and uses a tri-n-butyl phosphate/kerosene organic phase to separate desired products from UNF dissolved in nitric acid. Although the United States does not currently recycle its commercial UNF, recent attention [156] has been given to advanced reprocessing schemes in order to effectively and economically separate uranium and technetium from plutonium, neptunium, other minor actinides, and fission products to reduce the heat load and minimize the amount of radioactive waste requiring long-term geologic storage. In order to meet these requirements, the UREX+ process scheme [157] has been developed by Argonne National Laboratory and other national laboratories under the Advance Fuel Cycle Initiative. Acetohydroxamic acid (AHA) has been proposed as a salt-free reagent to effectively separate neptunium and plutonium from uranium. It has been shown that hydroxamic acids can greatly reduce the

extractability of neptunium and plutonium without affecting the extraction of uranium [66] by reducing hexavalent NpO_2^{2+} and PuO_2^{2+} [105] to their inextractable pentavalent oxidation states and forming inextractable complexes with Np^{4+} [158] and Pu^{4+} [159]. Unlike the reduction of NpO_2^{2+} by Fe^{2+} or U^{4+} [39], further reduction of NpO_2^{+} to Np^{4+} by hydroxamic acids has not been observed [63]. This can be partially explained by the difference in redox potentials, as the standard redox potentials of NpO_2^{2+}/NpO_2^{+} and NpO_2^{+}/Np^{4+} are 1.24 V and 0.66 V, respectively [13].

A previous kinetics study [122] of the reduction of NpO_2^{2+} to NpO_2^{+} by AHA in HNO_3 indicated that AHA reduces NpO_2^{2+} much slower than formohydroxamic acid (FHA) [100], despite the structural similarities of AHA and FHA. However, our preliminary results indicate that AHA is able to reduce NpO_2^{2+} at a much higher rate than previously reported [122]. Therefore, an additional investigation was necessary to better understand the mechanism in which AHA reduces NpO_2^{2+} and provide rate constants for the reduction of NpO_2^{2+} by AHA in $HClO_4$.

5.3 Experimental

5.3.1 Materials

All chemical reagents were of analytical grade and used without further purification. Distilled, deionized water (Barnstead, 18 MΩ·cm resistivity) was used for all experiments.

Acetohydroxamic acid (AHA, Toronto Research Chemicals) was kept in a freezer at -18 °C. In order to minimize the hydrolytic degradation of AHA, aqueous solutions were prepared shortly before experiments.

Acidity of solutions was adjusted using stock solutions of perchloric acid prepared from concentrated $HClO_4$ (60% w/w, Mallinckrodt Baker, Inc.). The acid concentration in used for the Np solutions was determined by a pH-metric titration with standardized sodium hydroxide.

Neptunium was received as $^{237}NpO_2$ from Argonne National Laboratory and dissolved in a slight molar excess of hydrogen peroxide and 8 $mol \cdot L^{-1}$ nitric acid. Confirmation of the

tetravalent oxidation state was determined using Vis-NIR spectroscopy. In order to remove any transuranic impurities, the Np solution was added to a prepared BioRad AG1 ×10 1 cm anion exchange column. The column was rinsed with a solution of 8 $mol \cdot L^{-1}$ nitric acid, 0.3 $mol \cdot L^{-1}$ hydrazine monohydrate, and 2 $g \cdot L^{-1}$ hydroquinone. Np was stripped from the column using 0.36 $mol \cdot L^{-1}$ hydrochloric acid and its isotopic purity was confirmed using thin-window HPGe γ spectroscopy. Any organic impurities were destroyed by concentrated nitric acid and hydrogen peroxide. The clean solution was evaporated to dryness, whereupon concentrated perchloric acid was added and fumed multiple times under an infrared heat lamp. Confirmation of the hexavalent oxidation state was determined by Vis-NIR spectroscopy.

In order to maintain a constant solution temperature during all experiments, an external water bath (Julabo CF31 Cryo-Compact Circulator) was used to control the desired temperature using an external probe connected to either the cuvette holder or the stopped-flow sample chamber. The water bath submerged drive syringes were filled with solutions for the stopped- flow experiments and given sufficient time to equilibrate to the appropriate temperature.

5.3.2 Neptunium Solution Speciation

Initial NpO_2^+ and NpO_2^{2+} concentrations were determined by NIR spectroscopy immediately prior to any reduction experiment. An OLIS rapid scanning monochromator (RSM) [160] with a 1cm glass cuvette, xenon arc lamp, and InGaAs detectors were used to monitor their absorbances (NpO_2^+: 980nm, $\varepsilon = 395\ mol^{-1} \cdot L \cdot cm^{-1}$. NpO_2^{2+}: 1223nm, $\varepsilon = 45\ mol^{-1} \cdot L \cdot cm^{-1}$) [36]. All neptunium solutions contained ≥ 95% NpO_2^{2+}. Two systems were studied: a) varying an excess $[AHA]_o$ (where the subscript naught represents the initial concentration of the species of interest) relative to constant $[NpO_2^{2+}]_o$ and $[HClO_4]$, and b) varying an excess $[NpO_2^{2+}]_o$ relative to constant $[AHA]_o$ and $[HClO_4]$.

5.3.3 Stopped-Flow NIR Spectroscopy

Solutions of NpO_2^{2+} in 2 mol·L^{-1} $HClO_4$ and AHA in H_2O were prepared immediately prior to the experiments and loaded into two separate syringes. Due to the 1:1 volume mixing of the stopped-flow (SF) apparatus, the concentration of Np, $HClO_4$, and AHA in the two syringes were twice that of the reaction conditions during the experiments. The reduction of NpO_2^{2+} was monitored by observing the increase in absorbance of NpO_2^{+} using an OLIS RSM spectrometer and SF mixing unit. A reference spectrum containing 1 mol·L^{-1} $HClO_4$ was collected and, when necessary, baseline corrections were determined from the absorbance at 950nm. For the 10°C experiments, a stable baseline was difficult to obtain due to water condensation formation on the exterior of the glass sample chamber. To alleviate this problem, the sample chamber enclosure was continuously purged with nitrogen gas during all experiments at 10°C.

The initial concentrations of each species for the experiments are listed in Table 5.1. Each experiment was performed six times. The first two experiments were necessary to remove any air bubbles in the system and the subsequent four experiments were used for analysis. Using optical gratings with 600 lines/mm and a blaze wavelength of 1000 nm, the OLIS RSM spectrometer is capable of capturing 1000 scans per second over a wavelength range of approximately 200nm with a resolution of 0.7nm and a response delay of 4ms. The rapid scanning and short response delay of this system was essential to monitor the rapid increase in the NpO_2^{+} absorption peak, as most reactions were complete within seconds of initial contact between neptunium and AHA. The measured data were evaluated using both the 4^{th} order Rung-Kutta Numerical Integrator, as described earlier [161], and Equation 5.3.

5.3.4 Long Term Kinetic Experiments

Reactions in which $[NpO_2^{2+}]_o$ was significantly greater than $[AHA]_o$ took a much longer time to achieve a constant NpO_2^{+} absorption peak than experiments where $[AHA]_o$ was in excess. Two distinct reactions were observed: a fast reaction occurred upon mixing of Np and AHA, and an additional and comparably slow reduction of NpO_2^{2+} was observed. To

monitor the slow reduction, kinetic experiments where $[NpO_2^{2+}]_o \geq [AHA]_o$ were performed using an OLIS RSM in a 1cm glass cuvette by monitoring both the decrease of the NpO_2^{2+} and increase of the NpO_2^{+} absorption peaks. Experiments were performed at 10°C and 22°C. Reference spectra of 1 mol·L^{-1} $HClO_4$ were collected prior to all experiment and, when necessary, baseline corrections were determined from the absorbance at 950nm. A solution of AHA was added to the cuvette containing Np and $HClO_4$. The spectrophotometer began scanning immediate following the addition of AHA.

Experimental conditions for these kinetic experiment involving an excess of $[NpO_2^{2+}]_o$ relative to $[AHA]_o$ in constant $[HClO_4]$ are given in Table 5.1. Each experiment was performed until the NpO_2^{+} absorption peak reached a maximum. Spectra were captured at scan rate of 400nm/min with a wavelength range of 400nm and a resolution of 1nm. Each experiment was repeated three times for reproducibility of results.

Table 5.1: Reaction conditions of NpO_2^{2+} reduction by AHA

Experimental conditions: 1 mol·L^{-1} perchloric acid, 10°C.

Stopped-flow Kinetic Experiments			***Long Term Kinetic Experiments***		
$NpO_2^{2+}{}_o$:AHA_o	**$[NpO_2^{2+}]_o$ (mol·L^{-1})**	**$[AHA]_o$ (mol·L^{-1})**	**$NpO_2^{2+}{}_o$:AHA_o**	**$[NpO_2^{2+}]_o$ (mol·L^{-1})**	**$[AHA]_o$ (mol·L^{-1})**
1:1	4.95×10^{-4}	5.0×10^{-4}	1:1	1.85×10^{-3}	1.84×10^{-3}
1:2	4.95×10^{-4}	1.0×10^{-3}	2:1	1.48×10^{-3}	7.43×10^{-4}
1:4	4.95×10^{-4}	2.0×10^{-3}	4:1	1.66×10^{-3}	4.01×10^{-4}
1:8	4.95×10^{-4}	4.0×10^{-3}	8:1	1.75×10^{-3}	2.19×10^{-4}

5.4 Results and Discussion

5.4.1 Stopped-Flow Reduction Experiments

The reduction of NpO_2^{2+} was studied at different initial concentrations of the acetohydroxamic acid ($[AHA]_o = 5\times10^{-4} – 4\times10^{-3}$ mol·L^{-1}), keeping $[NpO_2^{2+}]_o$, $[HClO_4]$, and temperature constant at 5×10^{-4} mol·L^{-1}, 1 mol·L^{-1} and 10°C, respectively. The progress of reaction from each experiment is displayed in Figure 5.1.

Colston et. al. [100] observed a pseudo 2nd order reaction for the reduction of NpO_2^{2+} by formohydroxamic acid at a constant and excess concentration of nitric acid. We determined that the reaction is first order with respect to AHA. The initial rate constants were determined from the slope of the $[NpO_2^{+}]$ as a function of time for the first 10 msec of the reaction. The plot of the initial rate constants as a function of $[AHA]_o$ gives a slope of 1.19 ± 20%. Chung and Lee [122] determined that the reaction is also first order with respect to NpO_2^{2+}. Applying this to AHA, for a constant H^+ concentration, we obtain:

$$\frac{-d[NpO_2^{2+}]}{dt} = k'[NpO_2^{2+}][AHA] \qquad 5.2$$

where $k' = k[H^+]^{\gamma}$. According to Colston [100], Equation 5.3 can be used to determine the rate constant of the reaction, as a plot of the left hand side of the equation as a function of time should give a straight line with the slope of the equal to the rate constant, k'.

$$\left(\frac{1}{[NpO_2^{2+}]_o - [AHA]_o}\right)\left(\ln\frac{[NpO_2^{2+}]_o - [NpO_2^{+}]_t}{[AHA]_o - [NpO_2^{+}]_t} - \ln\frac{[NpO_2^{2+}]_o - [NpO_2^{+}]_o}{[AHA]_o - [NpO_2^{+}]_o}\right) = k't \qquad 5.3$$

Equation 5.3 assumes a one to one stoichiometric ratio between NpO_2^{2+} and AHA. While we found this to be true for experiments where AHA was in excess, it was not the case for experiments with an excess of NpO_2^{2+}. It should be noted that the initial pentavalent neptunium concentration ($[NpO_2^{+}]_o$) was included in Equation 5.3. As stated by both this work and [100], the initial neptunium solution was not entirely NpO_2^{2+}, but contained a small percentage of NpO_2^{+}. Since the only variable on the left hand side (LHS) of Equation 5.3 is $[NpO_2^{+}]_t$ (where the subscript t represents the concentration of the species of interest at a given time in the reaction) the plot cannot go through the origin without correcting for the $[NpO_2^{+}]_o$. Also, since we were monitoring the reduction of NpO_2^{2+} by following the increase of the absorbance of NpO_2^{+}, it is important to only consider the NpO_2^{+} that was produced as a result of the reduction of NpO_2^{2+}. We processed the data by both Equation 5.3 and the RK4 method. Rate constants from both methods are listed in Table 5.2. Although the values from both methods were similar, we concluded that the results from the RK4 data analysis are more reliable. Using Equation 5.3 for calculating the rate constant of the reaction is highly dependent on the chosen time interval. This is

caused by the fact that the vast majority of NpO_2^{2+} is reduced in the presence of an excess of AHA within a few seconds. Near the completion of the reduction of NpO_2^{2+}, the absorption of NpO_2^{+} approaches equilibrium and while the signal remains relatively stable and behaves asymptotically towards a peak maximum, there is a small fluctuation in the absorbance. The magnitude of this fluctuation is exacerbated when the neptunium concentrations are calculated from the absorption values and inputted into Equation 5.3. Conversely, the RK4 method is able to accurately process the absorbance values from the entire length of reaction and is independent of the time interval chosen for determining the rate constant.

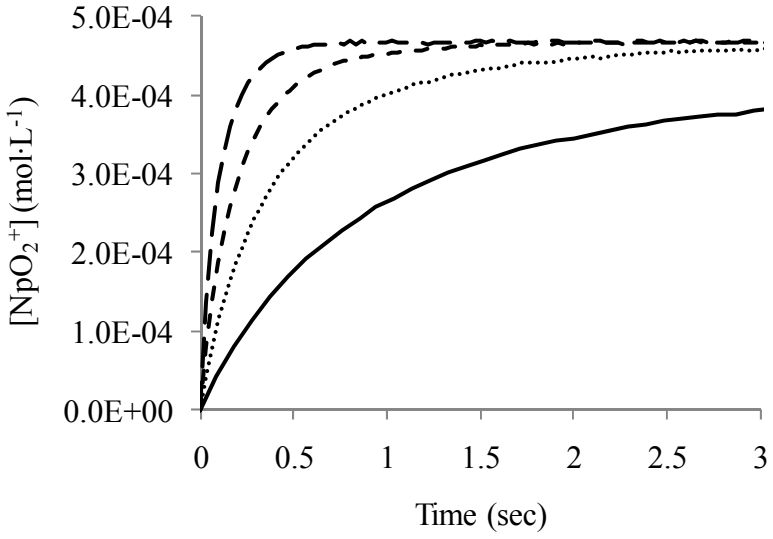

Figure 5.1: NpO_2^{+} concentration measured by stopped-flow and IR spectroscopy.

$[NpO_2^{2+}]_o$:$[AHA]_o$ = 1:1 (solid line), 1:2 (dotted line), 1:4 (narrow dashes), 1:8 (wide dashes). $HClO_4$ = 1 mol·L^{-1} at 10°C.

Table 5.2: Rate constants of stopped-flow NpO_2^{2+} reduction by AHA.

1 mol·L^{-1} perchloric acid at 10°C.

$NpO_2^{2+}{}_o$: AHA_o	**k (mol^{-1}·L·sec^{-1}) Equation 5.3**	**k (mol^{-1}·L·sec^{-1}) RK4**	**initial rate (mol·L^{-1}·sec^{-1})**
1:1	2483 ± 3.4%	2364 ± 2.9%	0.0005 ± 8.0%
1:2	2831 ± 2.0%	2754 ± 1.6%	0.0011 ± 6.0%
1:4	2638 ± 4.1%	2586 ± 4.2%	0.0029 ± 4.9
1:8	2541 ± 0.5%	2548 ± 0.6%	0.0058 ± 6.6%
Averages	2623 ± 2.5%	2563 ± 2.3%	-

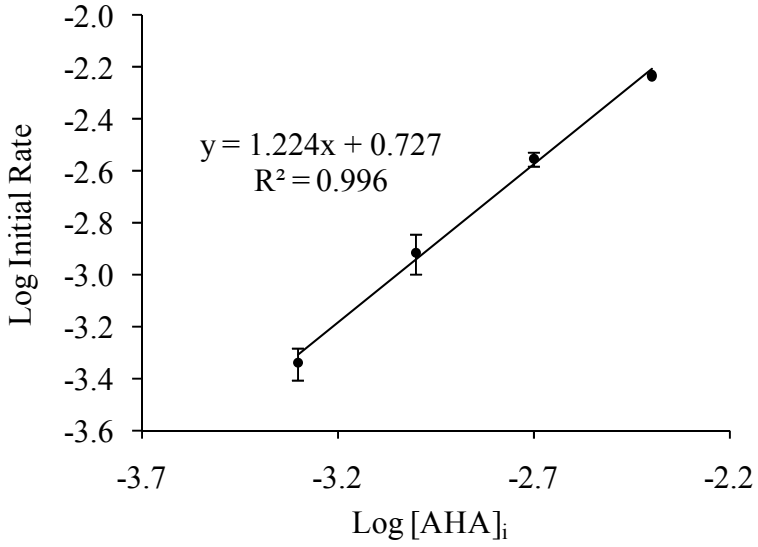

Figure 5.2: Observed initial rates for the reduction of NpO_2^{2+} by AHA

1 mol·L^{-1} $HClO_4$ at 10°C. The initial rate was determined by the change in $[NpO_2^{+}]$ for the first 10 msec of the reaction

Also, the RK4 method is able to determine the stoichiometry and reaction order with respect to each species. Second order rate constants calculated using Equation 5.3 were compared with rate constants calculated from the RK4 method for experiments where $[AHA]_o \geq [NpO_2^{2+}]_o$ and are in agreement. The rate constant for the reduction of NpO_2^{2+} by AHA in 1 mol·L^{-1} perchloric acid at 10°C was calculated by the RK4 method as 2563 mol^{-1}·L·sec^{-1}± 2.3%. This value is much greater than 191.2 ± 11.2 mol^{-1}·L·sec^{-1} at 25°C as determined by Chung and Lee [122]. Contrary to their data, in which approxiately 2 data points per second were collected, our data are collected with a frequency of 1000 data per second, and we can observe the near-immediate growth of the NpO_2^{+} absorption peak. As shown in Figure 5.1, the reaction is nearly complete within one second.

5.4.2 Long Term Kinetic Experiments

The reduction of NpO_2^{2+} was studied at varying $[NpO_2^{2+}]_o$:$[AHA]_o$ ratios (1:1 – 8:1) at temperatures of 10 and 22°C while keeping $[HClO_4]$ constant at 1 mol·L^{-1}. For ratios of 1:1 and 2:1, complete reduction of NpO_2^{2+} was observed within seconds of initial mixing between Np and AHA. This is not surprising, however, as hydroxamic acids are known to

undergo a two-electron oxidation process [93]. The results for the 4:1 and 8:1 ratio greatly differ from the 1:1 and 2:1 experiments.

The growth of the NpO_2^+ absorption peak, caused by the reduction of NpO_2^{2+}, is initially rapid and over 50% of NpO_2^{2+} is reduced. However, the reaction then proceeds to equilibrium at a much slower rate. See Figure 5.3 for the reduction of NpO_2^{2+} at an 8:1 ratio at 10 and 22°C. This differs greatly from the SF experiments, where $[AHA]_o$ was in molar excess relative to $[NpO_2^{2+}]_o$ and the reduction is complete within seconds (Figure 5.1). It is assumed that AHA is immediately consumed by the reduction of NpO_2^{2+} to NpO_2^+ and that the oxidation products of AHA are responsible for the slow reduction of the additional NpO_2^{2+} that remained the cuvette, as described below.

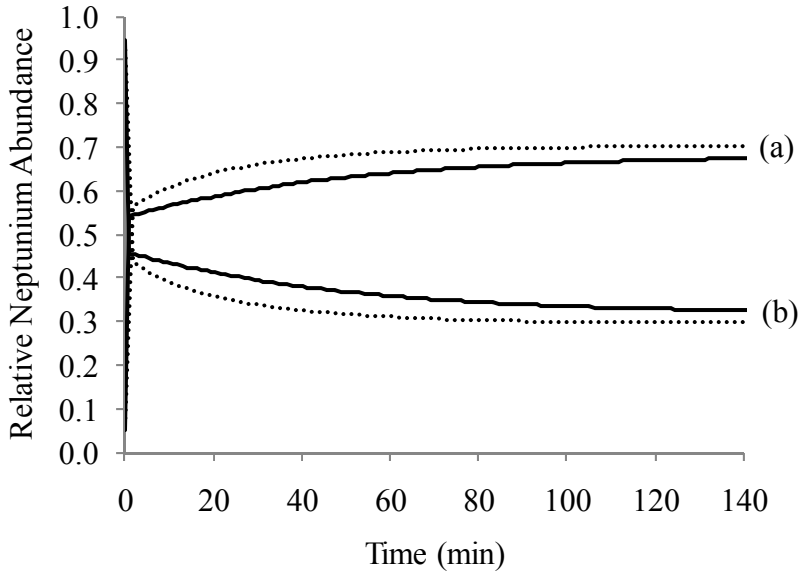

Figure 5.3: NpO_2^+ and NpO_2^{2+} abundance as a function of time.

Relative abundance of NpO_2^+ (a) and NpO_2^{2+} (b) at 10°C (solid line) and 22°C (dotted line) for $[NpO_2^{2+}]_o$:$[AHA]_o$ = 8:1, monitored at 980 nm for NpO_2^+ at 1 minute intervals. $[NpO_2^{2+}]$ was determined from $([NpO_2^+]_f - [NpO_2^+]_t)$. $[HClO_4]$ = 1 mol·L^{-1} and t = (0) is immediately prior to the addition of AHA.

Complete reduction was observed within 2 hours at 22°C and 3 hours at 10°C. The subscript f is used to designate the concentration of the species of interest at the completion of the reaction (when no change in absorbance is observed). Additional

reduction to Np^{4+} was not observed, even after several hours of contact time between the two phases.

First order reduction kinetics of NpO_2^{2+} was observed by plotting $\ln([NpO_2^+]_f-[NpO_2^+])$ as a function of time, which is shown in Figure 5.4. $[NpO_2^+]_f$ is the equilibrium concentration of NpO_2^+. Experiments were performed three times for both 4:1 and 8:1 $[NpO_2^{2+}]_o$: $[AHA]_o$ ratios and at 10 and 22°C. Analyses of the Np(V) concentration as a function of time plots for experiments where AHA was in significant excess indicate that the reaction rate of the initial rapid reaction is first order with respect to Np(VI) – the decrease of Np(VI) could be described by a pseudo-first order process. Therefore, it can be expected that the overall reduction reaction in the rapid phase must consist of two consecutive steps. The first step (reduction of the first Np(VI) by AHA) would be the slower rate determining step and the second step is a much more rapid reduction of another Np(VI) by a very reactive single-electron oxidation product of AHA. Nonetheless, conclusive evidence of the mechanism cannot be determined from the measured experimental data because the instantaneous concentration of AHA cannot be monitored directly and simultaneously by UV-VIS spectroscopy.

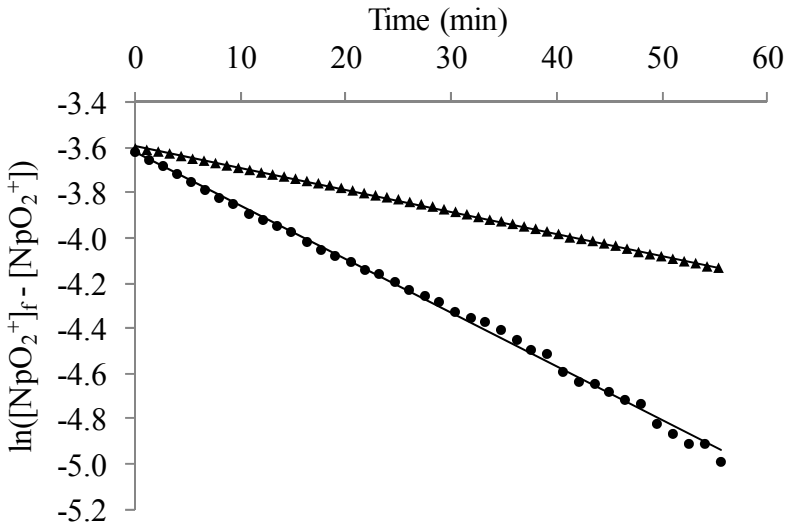

Figure 5.4: First order reduction kinetics of NpO_2^{2+}.

Represented by the plot of the $\ln([NpO_2^+]_f - [NpO_2^+])$ as a function of time. $[NpO_2^{2+}]_o$: $[AHA]_o$ = 8:1. Temperature = 10°C (triangles) and 22°C (circles) in 1 $mol \cdot L^{-1}$ $HClO_4$.

The rate constants for both ratios were determined to be $4x10^{-4}$ sec^{-1} in 10°C and 0.001 sec^{-1} in 22°C and 1 $mol \cdot L^{-1}$ $HClO_4$. The rate constant determined for the reduction of NpO_2^{2+} when $[NpO_2^{2+}]_o$:$[AHA]_o$ is 4:1 and 8:1 is orders of magnitude slower than the rate constant determined when $[NpO_2^{2+}]_o \leq [AHA]_o$. It is believed that the oxidation product(s) of AHA are responsible for the slow reduction of NpO_2^{2+}. According to Grossi [162], the oxidation products of hydroxamic acids are ultimately their respective carboxylic acid and nitrous oxide, as a result of the cleavage of the NHOH group. Applying this to AHA, the following is a possible redox reaction between NpO_2^{2+} and AHA:

$$4NpO_2^{2+} + 2CH_3CONHOH + H_2O \rightarrow 4NpO_2^{+} + 2CH_3COOH + N_2O + 4H^{+} \qquad 5.4$$

As an oxidation product of AHA, acetic acid could potentially cause the reduction of NpO_2^{2+}. Patil, et. al [163] found that acetic acid in $HClO_4$ can slightly reduce NpO_2^{2+}, whereas Choppin, et. al [164] did not find any reduction of NpO_2^{2+} by acetic acid within 24 hours. We performed an experiment where $[NpO_2^{2+}]_o$:$[CH_3COOH]_o$ was 1:10 in 1 $mol \cdot L^{-1}$ $HClO_4$ and 22°C and found no significant reduction of NpO_2^{2+} during a four hour time period. So although acetic acid is likely present in our reaction as a result of the oxidation of AHA, it is not responsible for the slow reduction of NpO_2^{2+} observed following the consumption of AHA.

Since Grossi [162] suggested that hydroxamic acids cleave at the C-N bond, we initially postulated that acetaldehyde could be responsible for the slow reduction of NpO_2^{2+}. Kolarik and Schuler [165] determined that aldehydes, particularly butyraldehyde, are able to reduce NpO_2^{2+}. However, they found that the effectiveness of aldehydes as reducing agents diminishes with decreasing size of the aliphatic group. We performed an experiment where $[NpO_2^{2+}]_o$:$[CH_3CHO]_o$ was 1:10 in 1 $mol \cdot L^{-1}$ $HClO_4$ and 10°C and did not find any significant reduction of NpO_2^{2+} over the course of three hours, thereby determining that acetaldehyde was not responsible for the slow reduction of NpO_2^{2+}.

For the experiments where $[NpO_2^{2+}]_o \geq [AHA]_o$, we do not believe that the hydrolysis products of AHA, acetic acid and hydroxylamine, are responsible for the reduction of

NpO_2^{2+}, since the observed reduction kinetics of NpO_2^{2+} (0.001 sec^{-1}) is much slower than previously reported by Koltunov [166] for a direct reduction by hydroxylamine (3.5 sec^{-1}). It has been previously shown [106] that hours are necessary to hydrolyze AHA in nitric and perchloric acid media. In these experiments where AHA is the limiting reagent, the initial and fast reduction of NpO_2^{2+} ceases within seconds and is limited by the oxidation of AHA. Also, Therefore, we doubt that hydroxylamine is causing the observed slow reduction of NpO_2^{2+}.

The complete mechanism of the oxidation of hydroxamic acids and the reactivity of its oxidation products with actinides are not definitively known. Previous data report that various radicals form as the result of the oxidation of hydroxamic acids. Boyland and Nery [167] suggested that acyl (RCO•) and nitroxyl (HNO•) radicals are formed as a result of the oxidation of hydroxamic acids:

$$RCONHOH \rightarrow RCONHO\bullet \rightarrow RCO\bullet + NHO\bullet \qquad 5.5$$

Nitroxyl radicals can then dimerize to hyponitrous acid ($H_2N_2O_2$) [168]. Glennon et. al [93] determined that hydroxamic acids can act as a two electron reductant and they can undergo an irreversible electrochemical oxidation at a positive potential:

$$RCONHOH + 2H_2O \rightarrow RCOOH + H_3NO_2 + 2H^+ + 2e^- \qquad 5.6$$

forming the intermediate product azinic acid (H_3NO_2). Azinic acid is then converted to $H_2N_2O_2$ [94]. Hyponitrous acid could be responsible for the additional reduction of NpO_2^{2+} that was observed during the slow kinetic reactions, as $NO/½H_2N_2O_2$ has a standard reduction potential of 0.71 V [13] that is lower than the standard reduction potential of 1.24 V [13] of the Np(VI)/Np(V) couple.

In summary, the oxidation of hydroxamic acids is a complicated and not fully understood process. Reactive intermediates such as radicals are likely formed and may be responsible, in part, for the slow reduction of NpO_2^{2+} that we observed when AHA is in a significant molar deficit compared to NpO_2^{2+}. It is important to state that this mechanism was not determined experimentally by us but was postulated based on our results and previously published findings [93, 94, 167, 168]. Although this study describes the

reduction of NpO_2^{2+} by AHA in perchloric acid, further studies are necessary to fully understand the mechanism in which hydroxamic acids and their oxidation products reduce NpO_2^{2+}.

5.5 Conclusion

Using a stopped-flow mixing apparatus and NIR spectroscopy, it was determined that the reduction of NpO_2^{2+} by AHA is faster than previously reported. When there is a sufficient amount of AHA to completely reduce NpO_2^{2+} to NpO_2^{+} (beginning at a $[NpO_2^{2+}]_o$:$[AHA]_o$ ratio of 2:1), the reduction is very fast and completed within seconds. AHA can act as a two electron reductant, as determined in experiments where the ratio $[NpO_2^{2+}]_o$:$[AHA]_o$ was 2:1 and greater; however, additional experiments need to be performed to elucidate the true stoichiometry of the reaction. In experiments where AHA is in a significant molar deficit ($[NpO_2^{2+}]_o$:$[AHA]_o$ = 4:1 & 8:1), the reaction is initiated by the partial reduction of NpO_2^{2+} by the consumption of AHA. However, a slow reduction of NpO_2^{2+} continues for hours until a final equilibrium is established. The exact reaction mechanism is unknown; however, it is likely that hyponitrous acid plays some role in the reduction of NpO_2^{2+}.

5.6 Acknowledgements

The research was performed under financial support of the Office of Civilian Radioactive Waste Management Graduate Fellowship Program administered by Oak Ridge Institute for Science and Education. Financial support was also provided by the NERI DOE-07-14289 grant.

6 KINETICS OF THE REDUCTION OF NEPTUNIUM(VI) BY ACETOHYDROXAMIC ACID IN NITRIC ACID

6.1 Introduction

Reduction of hexavalent neptunium in perchloric acid, discussed in Chapter 5, was an important starting step to approach the redox chemistry of Np without additional reactions possible in the system. To evaluate an effect of the high nitrate and nitric acid concentration conditions typical for the UNF solutions where complexation of metals with nitrate anions is possible, additional experiments were performed in HNO_3 to determine nitrate effects on NpO_2^{2+} reduction by AHA.

6.2 Experimental

All chemicals (except for acid) and stopped-flow NIR spectroscopy (except for the light source) are described in section 5.3. A schematic of the OLIS stopped flow apparatus is provided in Figure 11.1.The temperature of the reaction was controlled at 10°C. Experimental concentrations are provided in Table 11.2.

Acidity of stock solutions were adjusted using stock solutions of nitric acid, prepared from HNO_3 (68% EMD Chemicals GR ACS grade). The acid concentration was determined by a pH-metric titration (Mettler-Toledo DL58 Titrator) with sodium hydroxide standardized by potassium hydrogen phthalate (Analytical Reagent, Mallinckrodt). Distilled, deionized water (Barnstead, 18 MΩ·cm resistivity) was used for all experiments.

Purified Np stock solution was prepared for all subsequent NpO_2^{2+} reduction experiments. To adjust Np to its hexavalent oxidation state, a glass electrochemical two-cell setup was used. Each cell contained equal volumes of 4 $mol \cdot L^{-1}$ HNO_3 and Np in 4 $mol \cdot L^{-1}$ HNO_3. The non-radioactive cell contained the counter and reference electrode (saturated Ag/AgCl), whereas the neptunium containing cell had a coiled platinum wire

electrode. A positive 1200mV potential versus Ag/AgCl was applied using a potentiostat (BASi epsilon E2) for one hour. Following oxidation, the solution contained >99% NpO_2^{2+}, which was verified using Vis-NIR spectroscopy (Figure 6.1). This solution was used for all subsequent NpO_2^{2+} reduction experiments. Each experiment was repeated a minimum of four times.

In the Np reduction experiments detailed in Chapter 5, a Xe arc lamp was used as the light source. Although Xe lamps are a very stable light source over the visible region, they exhibit an irregular line spectrum in the near-infrared (NIR) region at the same location as the NpO_2^{+} absorption peak, causing an increase in baseline error (Figure 11.2). A tungsten light source was used in the NpO_2^{2+} reduction experiments in HNO_3 and provided a smooth output and a maximum intensity at 1000nm (Figure 11.3). This afforded greater signal intensity in the NIR region and less background noise.

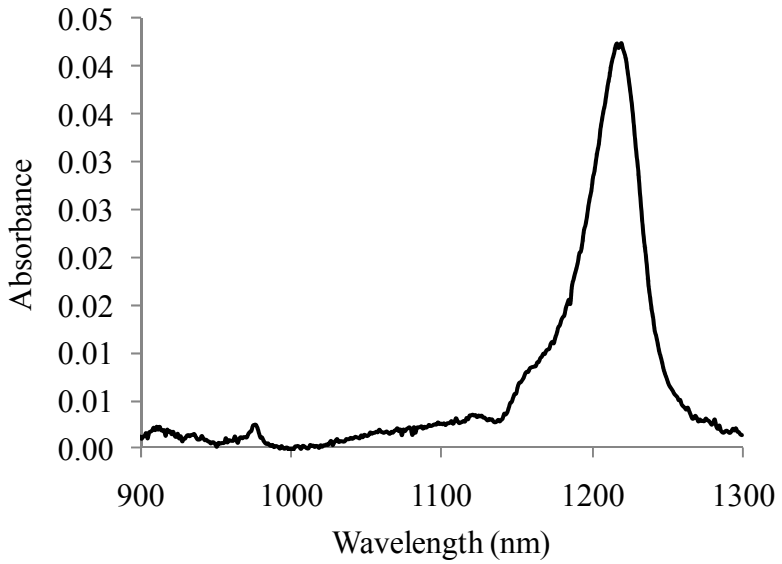

Figure 6.1: Absorbance spectrum of neptunium(VI) in HNO_3.
System: 1 mol·L^{-1} HNO_3, 25 ^{o}C, $[Np]_{total} = 9.5\times10^{-4}$ mol·L^{-1}.

6.3 Results

Absorbance of the growth of NpO_2^+ was used to monitor the reduction of NpO_2^{2+} by AHA in 1 mol $\cdot L^{-1}$ HNO_3 (Figure 6.2).

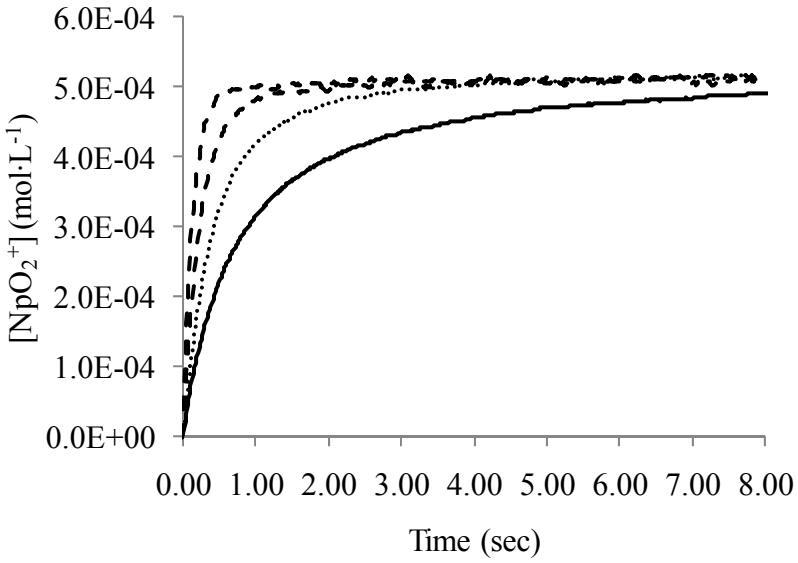

Figure 6.2: NpO_2^+ concentration measured by stopped-flow and NIR spectroscopy.

Concentration calculated from measure absorbance at 978nm. $[NpO_2^{2+}]_o$:[AHA] = 1:1 (solid line), 1:2 (dotted line), 1:4 (narrow dashes), 1:8 (wide dashes). HNO_3 = 1 mol$\cdot L^{-1}$ at 10°C.

Rate constants for the reduction of NpO_2^{2+} were calculated by both RK4 (section 2.6.2) and Equation 5.3 (Table 6.1). The average rate constant for all nitric experiments (2521 ± 23% $mol^{-1}\cdot L\cdot sec^{-1}$) is within experimental error of the average rate constant for all perchloric acid experiments (2563 ± 2.3% $mol^{-1}\cdot L\cdot sec^{-1}$). A change of the NpO_2^{2+}:AHA mole ratio resulted in differing rate constants of the Np reduction. The greater the AHA relative to initial NpO_2^{2+} concentration resulted in a smaller rate constant. This is not consistent with our reduction experiments in perchloric acid.

Results indicate RK4 is an appropriate modelling tool for determining rate constants and orders of reaction (Figure 6.3). Rate constants calculated by RK4 and Equation 5.3 were found to be equal for a given mole ratio (Table 6.1). Calculated values from the left hand

side (LHS) of Equation 5.3 were plotted against time and shown for comparison of analysed data (Figure 6.4).

Table 6.1: Rate constants of NpO_2^{2+} reduction by AHA in HNO_3.

1 mol·L^{-1} nitric acid at 10°C.

Expt. Number	**Mole Ratio** $[NpO_2^{2+}]_o$**:[AHA]**	**RK4 Calculation k' (mol^{-1}·L·sec^{-1})**	**Equation** 5.3 **k' (mol^{-1}·L·sec^{-1})**
1	1:1	2731 ± 1.7%	2806 ± 2.1%
2	1:2	2418 ± 1.8%	2431 ± 4.5%
3	1:4	2053 ± 6.7%	2103 ± 7.4%
4	1:8	1655 ± 4.5%	1692 ± 2.7%
5	1:8	2567 ± 3.0%	2585 ± 8.0%
6	1:2	2716 ± 2.4%	2671 ± 4.2%
7	1:1	3511 ± 6.7%	3531 ± 10.3%
Average		2521 ± 23%	2546 ± 23%

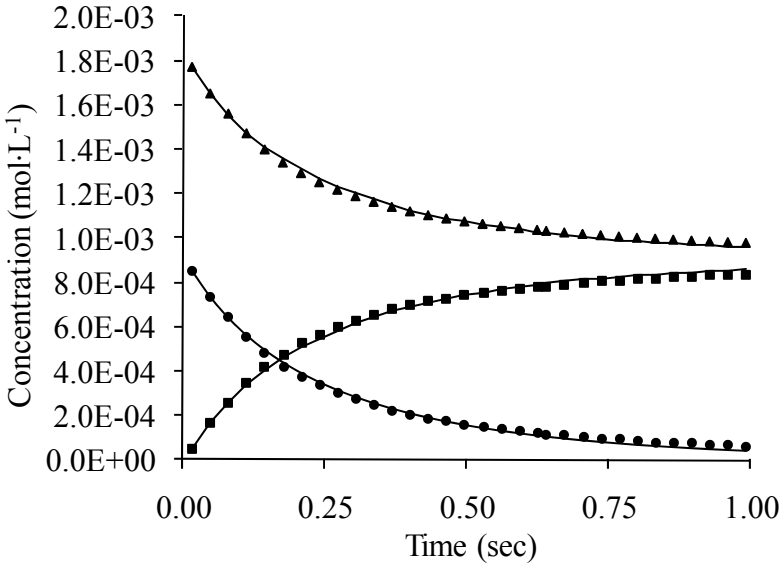

Figure 6.3: RK4 output of NpO_2^{2+} reduction.

$[NpO_2^{2+}]$o:[AHA] = 1:2. 1 mol·L^{-1} HNO_3 and 10°C. Rate constant calculated as 2698 mol^{-1}·L·sec^{-1}. Symbols represent experimental data: circles = NpO_2^{2+}, squares = NpO_2^{+}, and triangles = AHA. Lines are the concentration output from RK4.

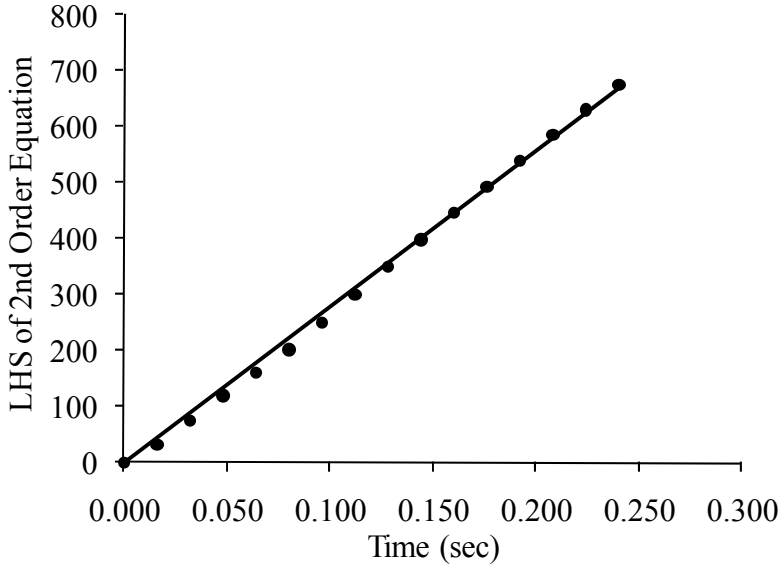

Figure 6.4: Plot of left hand side (LHS) of Equation 5.3 versus time.

$[NpO_2^{2+}]o$:[AHA] = 1:2. 1 $mol \cdot L^{-1}$ HNO_3 and 10°C. Rate constant calculated as 2774 $mol^{-1} \cdot L \cdot sec^{-1}$ (R^2 = 0.9974). Circles are calculated values from Equation 5.3 and the line is the linear regression of the data.

7 THE EXTRACTION OF METALS BY TRIBUTYL PHOSPHATE FROM NITRIC ACID

7.1 Introduction

Solvent extraction is the basis for the separation of key elements in the reprocessing of UNF and refers to the distribution of a solute between two immiscible phases. In the PUREX process, uranium and plutonium are separated from most other elements present in dissolved UNF. In advanced reprocessing techniques, such as UREX+, several solvent extraction processes are utilized in conjunction to partition specific elements to various waste streams [157]. These schemes propose closing the nuclear fuel cycle and provide a sustainable fuel source for electricity generation while extending the capacity of a long-term geologic repository. However, prior to implementation on an industrial scale, a complete understanding of the extraction, redox, and complexation chemistry of these processes is imperative.

In UREX, AHA is used as a reductant and complexant to control the oxidation states of neptunium and plutonium for their partitioning from uranium. However, AHA is also reactive with other elements present in dissolved UNF. Therefore, the extraction behavior of these metals in the presence of AHA must be studied if AHA will be used in UREX. In this chapter, the effect of AHA on the extraction of selected metals by TBP from a nitric acid aqueous phase has been studied. The distribution ratios of these metals in the presence and absence of AHA is reported and discussed.

7.2 Experimental

7.2.1 Materials

All reagents were of analytical grade and used without further purification. Experiments were performed at room temperature (22±2 °C) unless otherwise noted.

Acidity of stock solutions were adjusted using stock solutions of nitric acid, prepared from HNO_3 (68% EMD Chemicals GR ACS grade). The acid concentration was determined by a pH-metric titration (Mettler-Toledo DL58 Titrator) with sodium hydroxide standardized by potassium hydrogen phthalate (Analytical Reagent, Mallinckrodt). Distilled, deionized water (Barnstead, 18 MΩ·cm resistivity) was used for all experiments.

Acetohydroxamic Acid (AHA, Toronto Research Chemicals) was kept at -18 ^{o}C, dissolved in water when needed, and was the final component added in order to minimize hydrolytic degradation in acidic solutions. It was found by Alypyshev et. al [106] in our laboratory that AHA appreciably hydrolyzes over the course of an hour in two phase extraction systems. Therefore, the initial 0.4 mol·L^{-1}concentration of AHA was corrected based on his findings and the according concentration used in the experiment

Tri-n-butyl phosphate (TBP, 99+%, Mallinckrodt Inc.) was used as the extractant for all extraction experiments and diluted with *n-dodecane* (99+%, Alfa Aesar).

Ultima Gold AB (PerkinElmer, Inc.) was used as a liquid scintillation counting (LSC) cocktail for all LSC experiments.

Thorium nitrate ($Th(NO_3)_4$, Fisher Scientific Co.) was dissolved in 0.1 mol·L^{-1}. Thorium was assumed to exist as its natural isotopic abundance of 100% ^{232}Th.

Zirconium oxychloride ($ZrOCl_2 \cdot 8H_2O$, Fisher Scientific Co.) was dissolved in 0.1 mol·L^{-1} nitric acid.

Ceric ammonium nitrate ($(NH_4)_2Ce(NO_3)_6$, Matheson Coleman & Bell Manufacturing Chemists) was dissolved in 0.1 mol·L^{-1} nitric acid.

Uranyl nitrate ($UO_2(NO_3)_2$, Mallinckrodt, Inc.) was dissolved in 0.5 mol·L^{-1} nitric acid. Uranium was assumed to exist as its natural isotopic abundance.

Ferrous Chloride ($FeCl_2$, Aldrich Chemical Company, Inc.) was dissolved in 0.2 mol·L^{-1} hydrochloric acid and used to reduce neptunium to its tetravalent oxidation state.

Hydroxylamine Hydrochloride ($NH_2OH \cdot HCl$, Mallinckrodt Inc.) was prepared as 1.0 mol·L^{-1} in water and used to aid in the reduction of neptunium.

Neptunium nitrate ($^{237}Np(NO_3)_4$) was received from ANL and dissolved in 1 mol·L^{-1} nitric acid. ^{237}Np is often prepared from its parent ^{241}Am so prior to any neptunium extraction experiments, the amount of americium present in the solid sample needed to be

quantified. High purity germanium γ spectrometry (HPGe, Princeton Gamma-Tech N-type coaxial detector, 59 × 59 mm crystal, 41% relative efficiency) was used to determine if any ^{241}Am existed in the sample. A thin beryllium window (0.51 mm thickness, 5 mm detector-window distance) was used to measure the low energy γ emission from ^{237}Np (29 and 86 keV) and ^{241}Am (59.5 keV). The two main peaks of ^{237}Np were prominently featured in the spectrum, whereas the 59.5 keV peak of ^{241}Am was not observed above background level. Therefore, neptunium could be used for extraction experiments without further purification.

The entire 5.5 mg sample of $Np(NO_3)_4$ was completely dissolved in 1 mol·L^{-1} HNO_3. The oxidation state speciation of neptunium was determined using Vis-NIR spectroscopy A UV-Vis-NIR range of 200-1000 nm was monitored by a fiber optic system spectrometer (QE65000, OceanOptics, Inc.) with combined deuterium/halogen light source (DH-2000 BAL, OceanOptics, Inc.). The diode-array detector of the QE65000 spectrophotometer permitted simultaneously monitoring of absorbance on all selected wavelength within a 200-1000nm range. Special optical glass cuvettes with a usable wavelength range of 320-2500nm were used for all experiments (Starna Cells, Inc.) The temperature of cuvette holder was controlled to 22 ± 0.02°C (Quantum Northwest, Inc.). The initially dissolved neptunium stock solution consisted of pentavalent oxidation state in 1 mol·L^{-1} HNO_3, which was confirmed by the existence of its characteristic 617 and 980nm absorption peaks. Ferrous chloride and hydroxylamine hydrochloride were used to reduce neptunium to its tetravalent oxidation state, as it is well known that Fe^{2+} is a strong reducing agent and will rapidly reduce both NpO_2^+ and NpO_2^{2+} [36]. A slight molar excess of $FeCl_2$ and $NH_2OH{\cdot}HCl$ were added to a 4 mol·L^{-1} HNO_3 solution containing neptunium, whereupon a UV-Vis spectrum indicated that only Np^{4+} existed in solution. However, ferric iron needed to be removed prior to any extraction experiments involving acetohydroxamic acid, as Fe^{3+} which results from the neptunium reduction, and any unreacted Fe^{2+}, form complexes with AHA [56, 135]. The aqueous phase was contacted with 30% v/v TBP diluted in *n*-dodecane to extract Np^{4+} while leaving all iron in the aqueous phase. Np^{4+} was stripped from the organic phase using a fresh aqueous phases consisting of 1.0 mol·L^{-1} HNO_3. Once stripped, the solutions were combined and

evaporated to near dryness and the acidity was adjusted back to 4 mol·L^{-1} HNO_3. The Np^{4+} concentration was determined using Vis-NIR spectroscopy.

7.2.2 Extraction Procedure

The organic phase, which consisted of 30% v/v (1.1 mol·L^{-1}) TBP diluted in *n*-dodecane, was pre-equilibrated with the nitric acid concentration pertinent to the subsequent extraction experiment. A threefold volume excess of the nitric acid solution was added to the organic phase and mixed for one hour at room temperature. The organic phase was removed, whereupon a fresh aqueous phase was added and the mixing was repeated. A total of three pre-equilibrations of each organic phase were performed. Metal salts were individually dissolved in nitric acid and aliquots were added to solutions containing varying concentrations of nitric acid and AHA. When AHA was included in the experiment, it was always the final component added just prior to contact between the two phases to minimize hydrolytic degradation. The two phases were contacted and shaken for 60 minutes in a temperature controlled mixer (22 ± 0.5 °C).

7.2.3 Metal Equilibrium Determination

Both thorium and uranyl nitrates used in these experiments are in secular equilibrium with their daughter progeny occurring from the parent radioactive decay chains. A non-radioactive method was needed to discern between Th, U, and their daughter progeny to determine the equilibrium concentration of Th and U after extraction. Inductively coupled plasma atomic emission spectroscopy (ICP-AES, Varian Liberty 150) was chosen to determine the concentration of all metals except Np at equilibrium. Following mixing and separation, the aqueous phase was diluted to 1% w/w HNO_3. A peristaltic pump delivered the sample that was atomized by a nebulizer and introduced to the plasma torch of the ICP-AES. As the result of the interaction of the atomized sample and plasma, the metal loses and recombines with electrons which cause the release of electromagnetic radiation that is specific to each element. The emission lines of interest are listed in Table 7.1. Calibration curves for each metal are listed in Chapter 12. Error associated with each metal concentration was determined from the ICP-AES. Errors from sample preparation

(solid dissolution and sample dilution for analysis) were also included. The metal distribution ratio for a given extraction experiment was determined using Equation 7.1. The metal concentration extracted to the organic phase was not determined directly using ICP-AES so Equation 2.49 could not be used to directly determine the distribution ratio of the extracted metal. Instead, the equilibrium organic phase metal concentration was assumed to equal the difference between the initial ($M_{init,aq}$)and final ($M_{final,aq}$) aqueous metal concentrations determined using ICP-AES.

$$D = \frac{[M_{org}]}{[M_{aq}]} = \frac{[M_{init,aq}] - [M_{final,aq}]}{[M_{final,aq}]} \qquad 7.1$$

Table 7.1: ICP-AES emission lines for studied metals.

Metal	Emission Line (nm)
Cerium	404.1
Thorium	283.7
Uranium	367.0
Zirconium	343.8

For the neptunium extraction experiments, 50 μL of the neptunium solution was added to 2 mL solutions containing varying concentrations of nitric acid. When used, AHA was the final component added to minimize hydrolytic degradation. The final AHA concentration was 0.4 mol·L^{-1}, which was a 50x molar excess compared to the initial Np^{4+} concentration in the aqueous phase. The organic phase consisted of 30% v/v TBP dissolved in *n*-dodecane that was pre-equilibrated with HNO_3. The two phases of equal volume were mixed for ten minutes using a vortex shaker (3000 revolutions·min^{-1}). A small aliquot of 50 μL from each phase was added to glass vials. The neptunium concentration of each phase was determined using the 29 and 86 keV peaks of ^{237}Np measured with a sodium iodide (NaI) γ spectrometer (Cobra Auto-Gamma II, Packard, Inc., 3 inch crystal, 40% detector efficiency, annular geometry). Each vial was counted for 10 minutes of live time.

7.3 Results and Discussion

7.3.1 Uranium

Uranium is by far the most abundant element present in UNF. About 96% of fuel removed from a light water power reactor consists of ^{238}U. Reactor fuel is enriched to 3-5% fissile ^{235}U, but still contains 0.8% ^{235}U after several years of fission within the reactor. The recovery uranium is a main objective of UNF reprocessing as both ^{235}U and ^{238}U can be reused for the fabrication of fresh reactor fuel. When dissolved, the uranium concentration in UNF is significant at 361 $g \cdot L^{-1}$ (1.5 $mol \cdot L^{-1}$) [5]. Uranyl (Equation 2.4), along with tetra- and hexavalent plutonium, are readily extracted by TBP and was the basis for use of TBP in the PUREX process. UREX also uses TBP to initially separate uranium from plutonium, neptunium, and most fission products present in UNF. However, the two extraction schemes differ by the proposed use of AHA to control the oxidation states of neptunium and plutonium. In order to achieve effective partitioning of uranium from other transuranic elements, AHA cannot significantly affect the extraction of uranium. As discussed in section 3.4.2, AHA forms relatively weak complexes with UO_2^{2+}. If the formation of hydrophilic $UO_2 \cdot$AHA complexes are minimal, AHA should not adversely affect the extraction of uranyl nitrate. Therefore, an initial study was performed to determine the effect of AHA on uranyl extraction.

For the extraction experiments, 0.27 $mol \cdot L^{-1}$ $UO_2(NO_3)_2$ was dissolved in 1-6 $mol \cdot L^{-1}$ nitric acid. Uranium concentrations of both organic and aqueous phases were determined using ICP-AES. Results of the extraction of uranyl nitrate by 30% v/v TBP in *n*-dodecane are shown in Figure 7.1. They are compared with Alcock [169], who used 4.8 and 19% TBP for the extraction of 0.5-1.0 $g \cdot L^{-1}$ uranyl nitrate initially present in the aqueous phase. A higher percentage of TBP used in conjunction with an aliphatic diluent increases the extractability of metals [39], and is indicative of the results shown.

Additional experiments were performed where 0.4 $mol \cdot L^{-1}$ AHA was added to an aqueous phase containing 0.27 $mol \cdot L^{-1}$ $UO_2(NO_3)_2$ in nitric acid varying from 1-6 $mol \cdot L^{-1}$. AHA

was added just prior to contact of the two phases, whereupon an equal volume of the phases were mixed for 60 minutes. Uranium concentrations of both organic and aqueous phases were determined using ICP-AES. Results are shown in Figure 7.1 and indicate that AHA does not affect the extraction of $UO_2(NO_3)_2$ by TBP, as the distribution ratios are within experimental error for all 6 aqueous acid concentrations. This provides insight to the effect of AHA in the UREX process. AHA decreases the extractability of both neptunium and plutonium (section 7.3.5.2 and [68]), but does not decrease the extraction of uranyl nitrate. Therefore, AHA can be used in the advanced reprocessing of UNF to partition plutonium and neptunium from uranium.

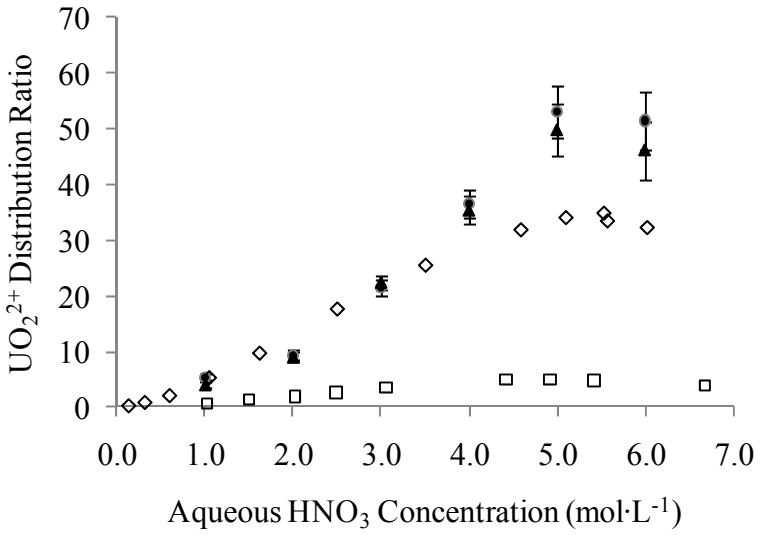

Figure 7.1: Extraction of uranyl nitrate by TBP.

$UO_2(NO_3)_2$ by 30% v/v TBP in *n*-dodecane as a function of nitric acid concentration in the presence (▲) and absence of AHA (●). Data from Alcock et. al [169] for the extraction of $UO_2(NO_3)_2$ by 4.8% (□) and 19% (◊) TBP in kerosene.

7.3.2 Thorium

In acidic solutions, thorium exists exclusively as Th^{4+},so oxidation state control was not necessary. Thorium is extracted as a neutral solvate by TBP from nitrate media (Equation 2.14) [17].

For the extraction experiments, 2.2×10^{-3} mol·L^{-1} $Th(NO_3)_4$ was dissolved in nitric acid varying from 0.1-6.0 mol·L^{-1} HNO_3. The thorium concentration in the aqueous phase was determined using ICP-AES. Our results, using 30% v/v TBP in *n*-dodecane as the organic phase, are in a good agreement with previously published data, which used differing dilutions of TBP in kerosene [31], as shown in Figure 7.2. A higher percentage of TBP used in conjunction with a kerosene diluent increases the extractability of metals [39]. The results fit with previously published data, as the calculated distribution ratios are greater than the 19% v/v TBP/kerosene extraction system but less than the 48% v/v TBP/kerosene extraction system. TBP's exceptional ability to extract metals is one reason why it is diluted in a hydrocarbon diluent. Many elements, including the heavy trivalent lanthanoids, are extracted by pure TBP from strong nitric acid [170].

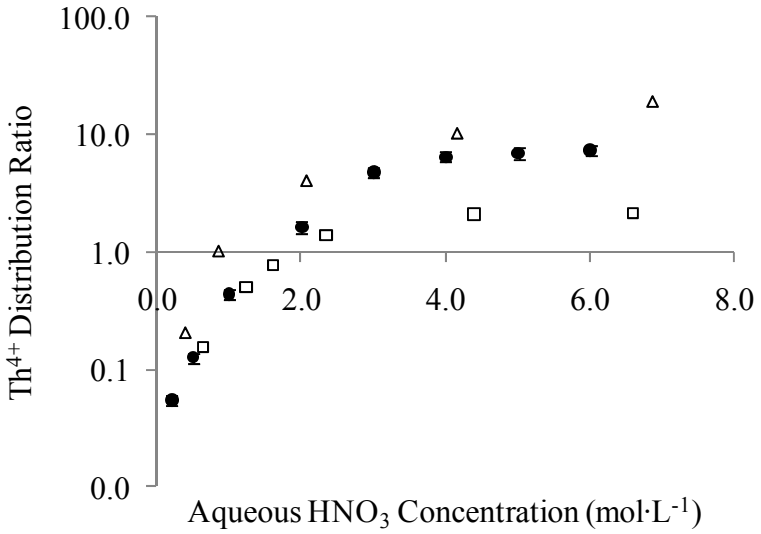

Figure 7.2: Distribution ratios of Th^{4+} as a function of the initial HNO_3 concentration.

Thorium extraction from (□) 19% v/v TBP diluted in kerosene [31], (●) 30% v/v TBP diluted in *n*-dodecane, and (△) 48% v/v TBP diluted in kerosene [31].

The neutral adducts formed with TBP and metal salts are so strong that the metals cannot be stripped from undiluted TBP back to an aqueous phase, regardless of the nitric acid concentration. Also, the density of pure TBP (0.973 g·cm^{-3} at 25°C) [39] is too similar to H_2O (0.997 g·cm^{-3} at 25°C) [171] to allow for good separation of phases. When TBP is diluted with an organic diluent, such as *n*-dodecane or kerosene, tri-and pentavalent

metals are poorly extracted while Pu^{4+}, PuO_2^{2+}, and UO_2^{2+} are still readily extracted. Therefore, TBP is diluted to increase the selectivity of uranium and plutonium in reprocessing of UNF.

Additional experiments were performed where 0.4 mol·L^{-1} AHA was added to the aqueous phase just prior to contact of the two phases. 2.2×10^{-3} mol·L^{-1} $Th(NO_3)_4$ was dissolved in nitric acid varying from 0.2-6.0 mol·L^{-1}. Results shown in Figure 7.3 indicate that AHA decreases the extraction of $Th(NO_3)_4$ to some extent. AHA did not suppress the extraction of thorium nitrate nearly as much as for tetravalent plutonium. Karraker [99] determined distribution ratios of $Pu(NO_3)_4$ in 2.0 mol·L^{-1} HNO3 as 8.1 in the absence of AHA and 0.4 in the presence of 0.3 mol·L^{-1} AHA. The greater affect of AHA on the extraction of $Pu(NO_3)_4$ is likely due to the difference in AHA complexation between the two metals. The stability constants of $Th(AHA)_n^{4-n}$ are equal to $\log\beta_n$ = 10.53 for n = 1, 19.06 for n = 2, and 25.92 for n =3 in 2 mol·L^{-1} ClO_4^- [172]. The stability constants of $Pu(AHA)_n^{4-n}$ are equal to $\log\beta_n$ = 14.2 for n = 1, 24.1 for n = 2, and 32.2 for n =3 in 2 mol·L^{-1} NO_3^- [91].

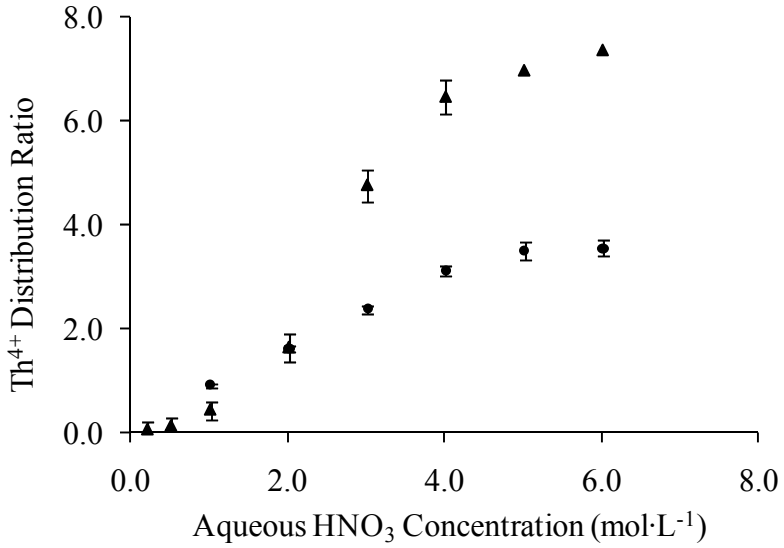

Figure 7.3: Effect of AHA on thorium nitrate extraction.

$Th(NO_3)_4$ extraction from TBP 30% v/v TBP diluted in *n*-dodecane from 0.2-6 mol·L^{-1} HNO_3 in the presence (●) and absence (▲) of AHA.

Since the stability constants of the thorium acetohydroxamate complexes are orders of magnitude less than the plutonium complexes, it can be expected that AHA will not decrease the extraction of thorium nitrate nearly as much as plutonium nitrate. However, it is important to remember that thorium does not exist in dissolved UNF in any appreciable amount so the influence of AHA on its extraction is not of concern. Thorium was used throughout these studies as a chemical analog of other tetravalent metals to observe its reactivity with AHA.

7.3.3 Zirconium

Previous studies [49, 50, 52, 173] indicate that zirconium extraction is rather complicated, as zirconium tends to form hydrolyzed and polymerized species in low acid and high zirconium concentrations. Both hydrolyzed and unhydrolyzed species are capable of being extracted by TBP, as described by Equations 2.24-2.26. Also, zirconium does not reach a maximum distribution ratio in the 5-8 $mol \cdot L^{-1}$ nitric acid concentration range that is typical of tetravalent actinoids extracted by TBP [169]. Zirconium's unusual extraction characteristics are described in detail in section 2.1.3.1.

In previous extraction experiments [50, 174], activated ^{95}Zr was used as a tracer to study the extraction of zirconium. However, the concentrations of zirconium in UNF solutions are much larger than at the tracer level. The zirconium concentration in dissolved UNF has been determined as 2.3×10^{-3} $mol \cdot L^{-1}$ [5]. A macro concentration of 2.2×10^{-3} $mol \cdot L^{-1}$ of non-radioactive zirconium was used for these studies. To determine the speciation of zirconium at this relatively high concentration in 0.1-6.0 $mol \cdot L^{-1}$ HNO_3, HySS was used to determine the relative zirconium abundance using Zr(IV) hydrolysis stability constants [47], zirconium·nitrate formation constants [136], and the pKa of HNO_3 [175] in HySS. As shown in Figure 7.4, many zirconium species were present in solution. At lower nitric acid concentrations (< 1 $mol \cdot L^{-1}$ HNO_3), zirconium hydrolyzed and polymerized species were of significant abundance, whereas several zirconium nitrate species existed at higher acidity. An additional discussion of the hydrolysis of zirconium is provided in section 3.4.3.2.

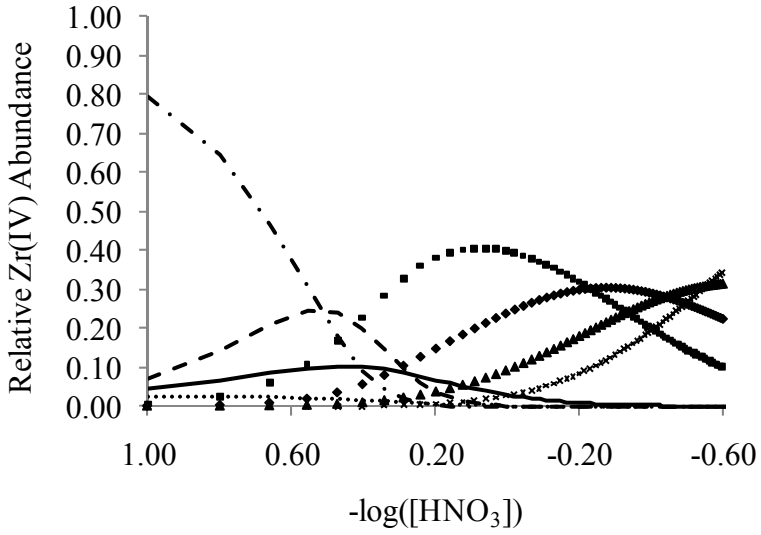

Figure 7.4: Speciation distribution diagram of Zr(IV).

0.1-6.0 mol·L^{-1} HNO_3 and 22°C. $[Zr(IV)]_{total}$ = 2.2×10^{-3} mol·L^{-1}, with hydrolyzed species represented by lines and nitrate species represented by symbols. (· – ·): $Zr_4(OH)_8^{8+}$, (– –): $Zr_3(OH)_4^{8+}$, (· · ·): $Zr(OH)_2^{2+}$, (⎯⎯): $ZrOH^{3+}$, (■): $ZrNO_3^{3+}$, (♦): $Zr(NO_3)_2^{2+}$, (▲): $Zr(NO_3)_3^{+}$, (×): $Zr(NO_3)_4$.

Extraction experiments were performed by dissolving 2.2×10^{-3} mol·L^{-1} zirconium in nitric acid varying from 0.1-6.0 mol·L^{-1} and contacting with an equal volume organic phase. At this relatively high zirconium concentration, it is likely that hydrolyzed and polymerized species formed in the aqueous phase prior to extraction, as predicted by the zirconium speciation diagram (Figure 7.4). The distribution ratios of zirconium between the aqueous and organic phases did not agree with previously published data [52, 176, 177] and are not shown in Figure 7.5. It was presumed that the analysis of the post-extraction zirconium using ICP-AES was adversely affected by the limited availability of equipment. All zirconium extraction experiments were performed at the Oregon State University Radiation Center, whereas the samples were analyzed hours to days after the extraction at a user-facility across campus. The values of distribution ratio determined would have been more accurate if the metal concentration was determined immediately following the extraction experiment.

Since zirconium is considered a problematic element in solvent extraction, additional experiments were performed to determine if AHA can prevent the extraction of zirconium. 0.4 mol·L^{-1} AHA was added to the aqueous phase just prior to contact of the two phases. Metal concentration of the aqueous measured using ICP-AES found no appreciable difference between $M_{init,aq}$ and $M_{final,aq}$. This indicates that near all zirconium was retained in the aqueous phase and that D was equal to 0.01 – 0.05 for all acid concentrations. The error associated with zirconium extraction in the presence of AHA shown in Figure 7.5 is less than the symbol used to represent the data. These findings indicate that AHA can be used to prevent zirconium extraction and allow for its separation from uranyl nitrate in UREX.

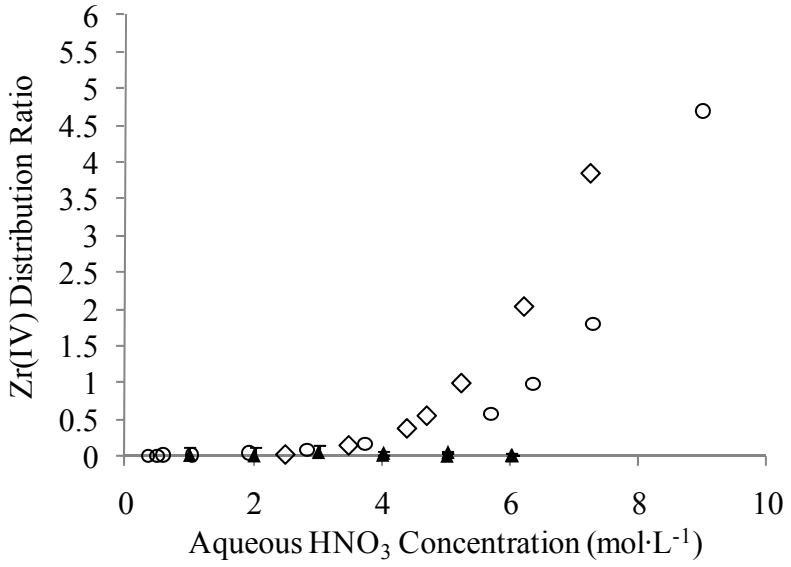

Figure 7.5: Effect of AHA on zirconium(IV) extraction by TBP.

Zr(IV) distribution ratios from 30% v/v TBP in *n*-dodecane as a function of nitric acid concentration in the presence (▲) of 0.4 mol·L^{-1} AHA. (◇): data from Suárez et. al [177], $[Zr(IV)]_i$ = 0.014 mol·L^{-1} and 30% TBP in *n*-dodecane. (○): data from Adamskii, et. al [178], $[^{95}Zr(IV)]_i = 2.2\times10^{-5} – 1.1\times10^{-4}$ mol·L^{-1} and 20% TBP in saturated hydrogcarbons.

The hydrolysis and polymerization of zirconium was not considered at the time of the experiment. With a small ionic radius and large effective cationic charge, both Zr^{4+} and

ZrO^{2+} can form hydrolyzed and polymerized species, even in highly acidic solutions [136]. ICP-AES is not able to distinguish hydrolyzed and unhydrolyzed species so the exact zirconium species was not known. It is suspected that under the relatively high zirconium concentration of 2.2×10^{-3} mol·L^{-1}, hydrolyzed and polymerized zirconium species formed in the aqueous phase prior to extraction which likely affected the distribution ratio of zirconium. A much lower concentration of ~10^{-5} mol·L^{-1} was used in the Zr·AAIII/AHA complexation experiments (section 3.4.3), so the formation of zirconium polymerized were not anticipated for the complexation studies.

7.3.4 Cerium

Tetravalent cerium is readily extracted by TBP (Equation 2.30) and can be used as an analog to study the extraction of Pu^{4+}. The extraction of tetravalent cerium in the presence and absence of AHA was performed. The aqueous phase consisted of 1-6 mol·L^{-1} HNO_3 and 2.7×10^{-2} mol·L^{-1} Ce^{4+}. A small aliquot of AHA was added immediately prior to extraction experiments so that the final AHA concentration equaled 0.4 mol·L^{-1}. The results of the extraction of Ce^{4+} in the presence and absence of AHA are shown in Figure 7.6. Without AHA, Ce^{4+} is readily extracted by TBP, with its distribution ratio values greater than 11 for all aqueous nitric acid concentrations studied. Like other tetravalent actinoids, a maximum distribution of Ce^{4+} appears near 5 mol·L^{-1} HNO_3. With the addition of AHA, the distribution ratio decreases dramatically, which indicates that AHA reduced Ce^{4+} to Ce^{3+}. Distribution ratios of cerium following the addition of AHA are ≤ 0.03 for all nitric acid concentrations studied. Like other trivalent lanthanoids, Ce^{3+} is poorly extracted by TBP [39]. This study shows the ability of AHA to control the extraction of particular metals. However, the oxidation states of the actinoids present in dissolved UNF do not have a SRP nearly as highly positive as Ce^{4+}, indicating that the reduction of cerium by AHA is more spontaneous than the actinoids. Hexavalent neptunium has a SRP of +1.24V versus SHE and its rapid reduction to NpO_2^+ has also been demonstrated (Chapter 5). Nonetheless, this study indicates that AHA can be used to prevent the extraction of Ce^{4+} that might exist in dissolved UNF during UREX reprocessing.

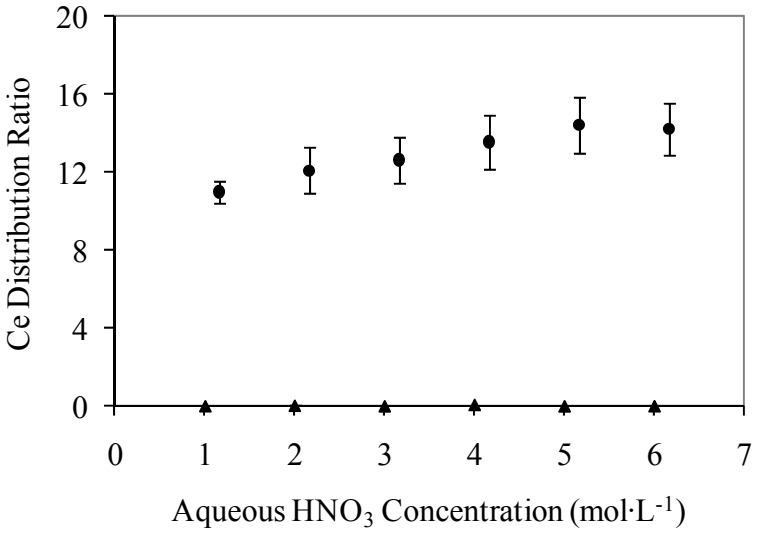

Figure 7.6: Effect of AHA on cerium extraction.

Ce(IV) distribution ratios in *n*-dodecane as a function of nitric acid concentration from 30% v/v TBP in the presence(▲) and absence (●) of 0.4 mol·L^{-1} AHA. The addition of AHA resulted in the reduction of Ce^{4+} to poorly extracted Ce^{3+}.

7.3.5 Neptunium

Prior to any experiments, the absence of ^{241}Am in the ^{237}Np was confirmed using HPGe γ spectrometry Neptunium nitrate $^{237}Np(NO_3)_4$ was completely dissolved in 1 mol·L^{-1} HNO_3 and existed primarily in the pentavalent state, which was confirmed by observing the characteristic NpO_2^+ peak at 980 nm by UV-Vis spectroscopy (Figure 7.7). In dissolved UNF, neptunium exists primarily in the pentavalent and hexavalent oxidation states, with the tetravalent oxidation state in a lesser amount. However, if a reductant/complexant such as AHA were to be used in UREX, hexavalent neptunium, which is readily extracted by TBP, would not be present in the aqueous phase. AHA rapidly reduces NpO_2^{2+} to NpO_2^+; therefore, only pentavalent neptunium and Np^{4+} complexed with AHA would exist in UREX after the addition of AHA. It is well known that NpO_2^+ is poorly extracted by TBP [179], so tetravalent neptunium was studied in these experiments, rather than NpO_2^+ or NpO_2^{2+}. The extraction of Np^{4+} by TBP is described by Equation 2.18, where the metal charge is compensated by the formation of a neutral adduct with nitrates.

7.3.5.1 Tetravalent Neptunium Speciation

Np was reduced to the tetravalent oxidation state using adding ferrous iron and hydroxylamine hydrochloride to the stock neptunium solution. Following the stripping and acidity adjustment of Np^{4+}, its characteristic peaks at 723 and 960 nm were observed without any substantial NpO_2^+ and shown in Figure 7.7. The molar extinction coefficients (ε) are approximately 55 $L \cdot mol^{-1} \cdot cm^{-1}$ for both absorption peaks in 4 $mol \cdot L^{-1}$ HNO_3 [180].

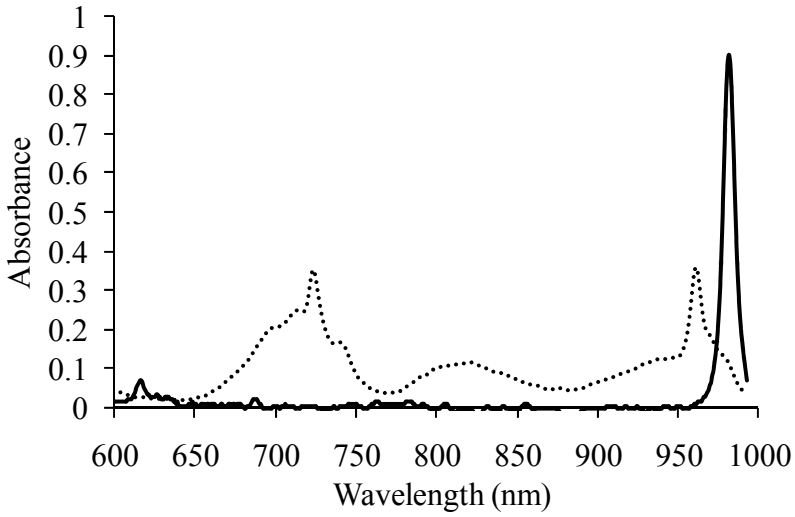

Figure 7.7: Vis-NIR spectroscopy of NpO_2^+.

1 $mol \cdot L^{-1}$ HNO_3 immediately after dissolution of $Np(NO_3)_4$ (solid line) and of Np^{4+} in 4 $mol \cdot L^{-1}$ HNO_3 after the reduction of NpO_2^+ by Fe(II) and hydroxylamine hydrochloride (dotted line).

Np^{4+} in 4 $mol \cdot L^{-1}$ HNO_3 was contacted with an equal volume of 30% TBP/n-dodecane for four minutes and then centrifuged to separation the two phases. Prior to extraction, the TBP/n-dodecane was pre-equilibrated by washing three times with a double volume of 4 $mol \cdot L^{-1}$ HNO_3 to assure that the organic phase was saturated with acid and HNO_3 was not extracted during the Np extraction. The organic and aqueous phases were then measured using UV-Vis spectroscopy. Only a minimal amount of Np remained in the aqueous phase whereas the majority of the Np was extracted to the organic phase as $Np(NO_3)_4 \cdot 2TBP$, which was confirmed by the Np^{4+} absorbance peaks in the organic phase (Figure 7.8, dashed line). It is important to point out that the decrease in neptunium absorption in the organic phase relative to the aqueous phase is due to the lower

absorption coefficient of $Np(NO_3)_4 \cdot 2TBP$ relative to $Np(IV)_{aq}$ and not because of the change in Np concentration [65]. The organic phase was then contacted with 0.1 $mol \cdot L^{-1}$ HNO_3 for 4 minutes, centrifuged, and the two phases were separated. After several hours, the aqueous phase was measured by UV-Vis spectroscopy. Only NpO_2^+ was found, indicating that tetravalent Np can oxidize over time to the pentavalent state in weakly acidic nitric acid. This re-oxidation of Np^{4+} to NpO_2^+ stresses the importance of using a complexant such as AHA in the UREX process. As shown in this experiment, any Np^{4+} present in the feed solution can oxidize to NpO_2^+ if given enough time in weakly acidic nitric acid. This would significantly alter the extraction of neptunium, as NpO_2^+ is poorly extracted by TBP, whereas Np^{4+} is readily extracted by TBP [179]. Using AHA as a reductant and complexant to stabilize the oxidation of Np^{4+} by forming $Np(AHA)_x^{(4-x)+}$ complexes will ultimately facilitate in the control of neptunium and its partitioning from uranium in advanced reprocessing.

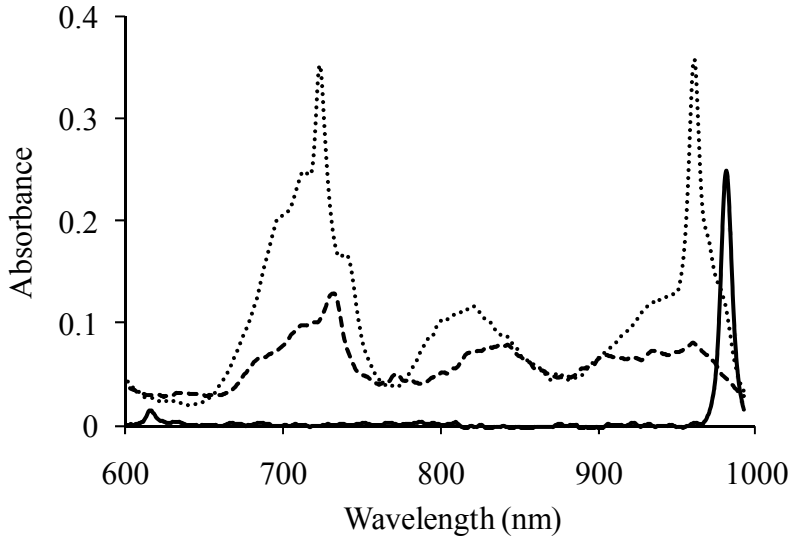

Figure 7.8: Absorbance spectra of of Np^{4+} in aqueous and organic phases.

4 $mol \cdot L^{-1}$ HNO_3 prior to extraction (dotted line) and 30% v/v TBP in *n*-dodecane (dashed line). Vis-NIR spectroscopy of neptunium after back extraction of Np^{4+} into 0.1 $mol \cdot L^{-1}$ HNO_3 and left idle for several hours (solid line).

7.3.5.2 Tetravalent Neptunium Extraction

Experiments were performed to determine the distribution ratios of Np^{4+} and study the effect of AHA on the extraction of Np. The same stock solution of neptunium reduced to Np^{4+} by $FeCl_2$ and hydroxylamine hydrochloride was used for all experiments and was checked spectrophotometrically confirming that neptunium existed exclusively in the tetravalent oxidation state and that no plutonium was present in solution. The 617 and 980nm absorbance peaks associated with NpO_2^+ were not observed. The acidity of the aqueous solution was adjusted to a final concentration of 1-6 mol·L^{-1} HNO_3. Just prior to extraction, AHA was added so that its concentration was 0.4 mol·L^{-1}, which was a 50x molar excess compared to Np^{4+}. The organic phase consisted of pre-equilibrated 30% TBP/*n*-dodecane and the two phases were contacted for four minutes, centrifuged, and separated. ^{237}Np concentrations in both phases were determined using NaI γ spectrometry using its characteristic 86 keV peak. It was assumed that the detection efficiency for both the organic and aqueous samples were equal and the distribution ratio was calculated from their count rates (*CR*) (Equation 7.2).

$$D = \frac{[M_{org}]}{[M_{aq}]} = \frac{CR_{org}}{CR_{aq}} \qquad 7.2$$

The extraction results are shown in Figure 7.9. The experimentally determined neptunium distribution ratios in the absence of AHA varied significantly from previously published literature values [53, 99, 179]. The presenting author's extraction experiments were repeated several times and the neptunium concentration was determined from 86 keV γ emissions using both HPGe and NaI γ spectrometers. Regardless of experiment repetition and measurement by either instrument, the results were unsatisfactory and scattered (Figure 7.9). Karraker used alpha spectrometry to determine the neptunium concentration in the aqueous phase LSC for the organic phase. Kolarik [53] and May [179] also determined similar neptunium distribution ratios for varying acidity using the 86 keV γ emission of ^{237}Np to determine the concentration in both phases. For future experiments, it would be prudent consider other means to measure ^{237}Np concentration in each phase, such as LSC, alpha spectrometry, or spectrophotometric titration using arsenazo(III) [181].

The addition of 0.4 mol·L^{-1} AHA showed a significant decrease in Np extraction, which results from the formation of the poorly extracted $Np(AHA)_x^{(4-x)+}$ complexes. This is encouraging if AHA were to be used as a complexant in advanced reprocessing. However, Np(IV) was partially extracted in both this study, and Karraker [99], despite a large molar excess of AHA. Therefore, it is necessary to determine why Np^{4+} is still partially extracted by TBP, despite a large molar excess of AHA.

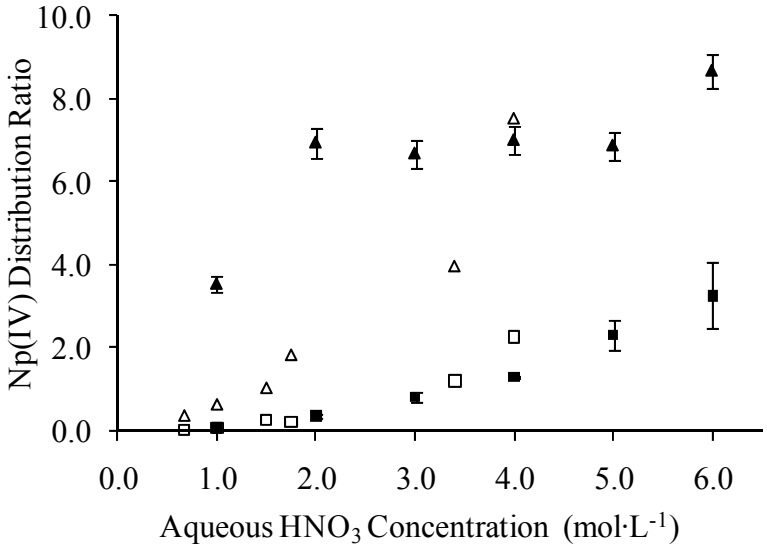

Figure 7.9: Distribution ratios of Np^{4+} extracted by TBP.

Distribution ratios of Np^{4+} as a function of nitric acid concentration in the presence (■) and absence (▲)of AHA, and from Kolarik [53] in the presence (□) and absence (△) of AHA.

It was previously reported by our research group that a mixed ternary complex $Pu(AHA)_x(NO_3)_{4-x}$ is coextracted with TBP [182]. Experiments were performed to determine whether or not the extraction of Np^{4+} in the presence of AHA was caused by the incomplete complexation of Np by AHA or if a neutral ternary complex, such as $Np{\cdot}AHA(NO_3)_3$, was extracted. For this experiment, a small quantity of AHA was dissolved in the organic solution of Np^{4+} in pre-equilibrated 30% v/v TBP in *n*-dodecane. Since AHA is a small hydrophilic organic molecule, significant mixing using a vortex mixer was needed to obtain complete dissolution of AHA. Spectra were taken before and 30 minutes after the addition of AHA, which is shown in Figure 7.10. The slight decrease of absorbance in the spectrum with AHA simply results from the increase in total volume

by the addition of a small aliquot of AHA. Compared to the Np^{4+} spectrum in the aqueous phase (Figure 7.8), the absorbance peaks of $Np{\cdot}(NO_3)_4{\cdot}2TBP$ are much less pronounced in the organic phase. This is likely caused by the complexation of nitrates and TBP molecules coordinated to Np which can affect the electronic transitions of neptunium that account for the absorbance peaks. Also, the different background matrices can account for the difference in absorbance peaks (HNO_3 in H_2O compared to TBP in *n*-dodecane). In either case, the absorbance spectra shown in the two phases are similar to the spectra reported by May, et. al [179]. The formation of ligand-metal complexes typically shows a shift in the spectrum compared to spectrum when only the metal presents in solution [90]. However, the spectra of neptunium in the presence and absence of AHA in the organic phase are essentially the same. It appears that the $Np^{4+}{\cdot}$AHA complex is sufficiently hydrophilic that the ternary complex does not exist in the organic phase during extraction and only neptunium nitrate is extracted. So it is likely that the partial extraction of neptunium (Figure 7.9) is caused by the incomplete complexation of Np^{4+} by AHA. However, nitrate/AHA ligand exchange experiments (Equation 7.3) in the organic phase should be studied to confirm these initial findings.

$$NpNO_{3(org)} + HAHA_{(aq)} \rightleftharpoons NpAHA_{(org)} + HNO_{3(aq)} \qquad 7.3$$

This finding is relevant to advanced reprocessing and it is important that no $Np(AHA)_x(NO_3)_{4-x}$ complexes exist in the organic phase. In a multistage contactor system, as proposed in UREX, repeated contact with fresh aqueous phases containing AHA will enhance the complexation of Np^{4+} and minimize its retention in the organic phase. Therefore, it can be expected that AHA will complex with any Np^{4+} present in the scrub section of UREX, and with numerous stages, the partitioning of neptunium from uranium should be achievable.

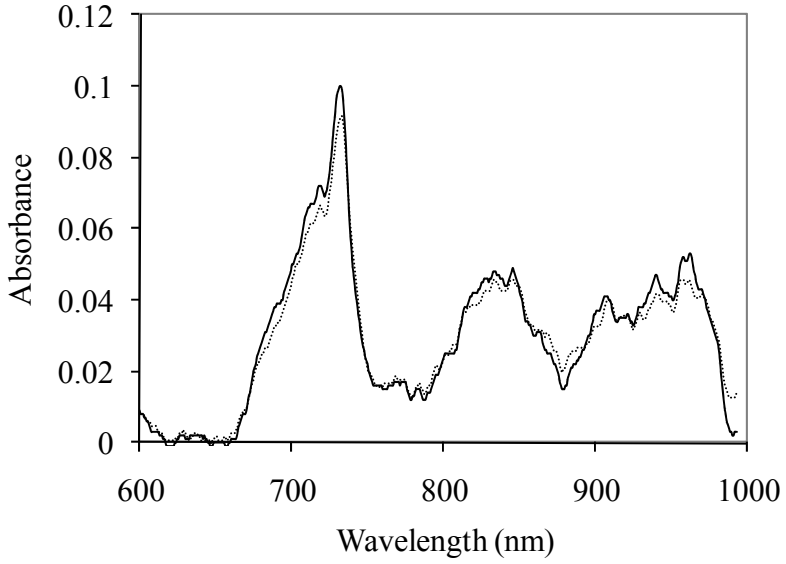

Figure 7.10: Absorbance spectra of $Np(NO_3)_4 \cdot 2TBP$.

Vis-NIR absorbance spectra as a function of wavelength in the presence (dotted line) and absence (solid line) of 0.1 $mol \cdot L^{-1}$ AHA.

8 CONCLUSIONS

8.1 Impact of Work and Summary of Results

The work presented in this dissertation contributes to the fields of radiochemistry and separation science and provides insight to the reactivity of AHA with selected metals present in UNF. Complexation, reduction, and extraction data from this work can be used in the continued development of UREX or in the flowsheet design and modeling of a new advanced reprocessing scheme. UNF rods removed from reactors contain significant amounts of ^{235}U and ^{238}U; therefore, the advanced reprocessing of UNF can provide a sustainable fuel source for the peaceful generation of electricity. The need for a geologic repository would be minimized with a reduced volume and heat generation of HLW requiring long-term storage. Also, the use of AHA in UREX prevents the isolation of Pu and minimizes proliferation concerns. Although the United States does not currently have a definitive plan for the ultimate destination of its UNF, one fact is certain: the UNF that our country has created will remain radioactive for a near infinite timescale compared to human life and must be stored or reprocessed properly.

The chemistry of AHA and its role of the thermodynamic, kinetic, and extraction features of several metals present in UNF was investigated. The distribution of selected metals resulting from their extraction by TBP from nitric acid was studied. AHA was found to prevent the extraction of zirconium and cerium by forming hydrophilic Zr·AHA complexes and reducing tetravalent cerium to its inextractable trivalent oxidation state. The extraction of tetravalent Np was significantly decreased with the addition of AHA while uranyl extraction showed no effect of the presence of AHA.

Several studies involving the complexation of AHA with zirconium(IV), uranium(VI), and iron(III) were performed. The SQUAD computational program was employed to evaluate the stability constants of the absorbance data. Conditional stability constants of the $Fe(AHA)^{2+}$, $Fe(AHA)_2^{+}$, and $Fe(AHA)_3$ complexes were determined in 0.1 $mol \cdot L^{-1}$

HNO_3 and 25°C as log β_n' = 11.00 ± 0.03, 20.93 ± 0.01, and 28.75 ± 0.01, respectively. Neither Zr(IV) nor Zr·AHA absorb in the wavelength range of the instruments used in the experiments; therefore, arsenazo III was used as a dye indicator to monitor the absorbance of Zr that was not complexed with AHA. Conditional stability constants were determined in 1 mol·L^{-1} $HClO_4$ and 25°C as log β' = 12.77 ± 0.02 and 23.13 ± 0.03 for $Zr(AHA)^{3+}$ and $Zr(AHA)_2^{2+}$, respectively and the uranyl·AHA complex was determined as log β' = 8.32 ± 0.02 for $UO_2(AHA)^+$. The conditional stability constant of the $Zr(AHA)^{3+}$ complex is more than four orders of magnitude greater than the $UO_2(AHA)^+$. This demonstrates the strength of tetravalent metal·AHA complexes compared to hexavalent UO_2^{2+}, which is due to the difference in the metal's effective cationic charge. The significant difference in calculated condition stability constants indicates that AHA is a promising complexant to separate tetravalent metals from uranium.

The reduction kinetics of NpO_2^{2+} to NpO_2^+ by AHA in perchloric and nitric acids were studied. The reaction rate was monitored using stopped-flow and standard near infrared spectroscopy. The stopped-flow apparatus was essential in these experiments to quickly mix the two solutions containing NpO_2^{2+} in acid and AHA in H_2O, as the neptunium reduction was complete within seconds. When the AHA concentration was in excess compared to the initial NpO_2^{2+} concentration, it rapidly reduces Np with a rate constant calculated as 2.57×10^3 $mol^{-1}\cdot L\cdot sec^{-1}$ in 1 mol·L^{-1} $HClO_4$ and 10°C. However, when AHA is in a concentration deficit, a slow secondary reduction of Np was observed with a rate constant of 3.7×10^{-4} sec^{-1} and 0.001 sec^{-1} in 1 mol·L^{-1} $HClO_4$ and 10°C and 22°C, respectively. Additional reduction experiments involving hyponitrous acid, a proposed oxidation products of AHA, reduced NpO_2^{2+} over the course of several hours with a rate constant of 0.001 sec^{-1} in 1 mol·L^{-1} $HClO_4$ and 22°C This secondary study indicates that additional reactions affect the reduction of NpO_2^{2+}. Nonetheless, these results showed that AHA can be used to quickly reduce hexavalent Np under proper conditions.

This work provides insight to the reactivity of AHA with several metals and confirms that AHA can be utilized for the separation of Np and other metals initially extracted by TBP from dissolved UNF. Therefore, AHA is recommended for use in advanced reprocessing

techniques as a reductant and complexant to partition Np from U containing waste streams by forming inextractable species by either reducing the metal oxidation state or forming hydrophilic complexes without affecting the extraction of uranyl.

8.2 Limitations

All neptunium experiments were limited by the amount available within an academic laboratory. Two shipments of ^{237}Np were generously donated by ANL. Both were completely used by students within the laboratory group. All neptunium used in experiments was collected, purified and regenerated. Although this was a time consuming process, I did benefit from learning several techniques to clean and manipulate the oxidation state of neptunium.

The analysis of the post-extraction concentration of metals using ICP-AES was limited by the availability of equipment hours at the W.M. Keck Collaboratory for Plasma Spectrometry at the Oregon State University College of Oceanic and Atmospheric Sciences. Many extractions samples were analyzed hours to days after the extraction experiments (performed at Radiation Center). The values of distribution ratio determined would have been more accurate if the metal concentration was determined immediately following the extraction experiment.

8.3 Future Work

Nuclear magnetic resonance and infrared spectroscopy could be employed to determine the oxidation products of AHA. These studies could determine if the hydrolysis products of AHA are the same as the oxidation products of AHA. Additional experiments need to be performed to confirm if hyponitrous acid is indeed the oxidation product of AHA that causes a slow, secondary reduction of NpO_2^{2+}.

The kinetics of reductive stripping of NpO_2^{2+} by AHA from a TBP containing organic phase would also be an experiment of interest. The rapid reduction kinetic described in Chapter 5 were only performed in the aqueous phase. In UREX reprocessing conditions,

AHA would be added to the aqueous phase just prior to contact with a NpO_2^{2+} containing organic phase. The reduction of NpO_2^{2+} could occur at the interface between the two phases or during mixing. Therefore, it is anticipated that the kinetics of reduction of hexavalent neptunium will be slower in the emulsion compared to the single phase study discussed in Chapter 5. The proposed contact time between phases in UREX is on the order of a few seconds so it will be important to know the kinetics of NpO_2^{2+} reduction and stripping to assure the partitioning of neptunium from uranium.

9 BIBLIOGRAPHY

1. Ewing, R.C., *Environmental Impact of the Nuclear Fuel Cycle*. Energy, Waste, and the Environment: A Geochemical Perspective. 2004, London, England: Geological Society.

2. http://www.ocrwm.doe.gov/.

3. Srinivasan, N., et al., *Process Chemistry of Neptunium.* Nuclear Science Abstracts, 1969. 24: p. 11646.

4. Vandegrift, G.F., et al., *Designing and Demonstration of the UREX+ Process Using Spent Nuclear Fuel.* Proceedings of Atatlante 2004, Nimes, France, 2004.

5. Bakel, A. and A.V. Gelis, *Dissolution and Analysis of Nuclear Fuels and Targets*, in *http://www.cmt.anl.gov/oldweb/Science_and_Technology/Poster_Tour/Posters/Process_Chemistry_and_Engineering/Dissolution_and_Analysis-Bakel.pdf*. 2008.

6. Stevenson, C.E., et al., *Reactor Handbook*. 2nd ed. Fuel Reprocessing, ed. W.H. Zinn, S.M. Stoller, and R.B. Richards. Vol. 2. 1961, New York: Interscience Publishers.

7. Herschel, W., *Account of a Comet.* Philosophical Transactions of the Royal Society of London, 1781. 71: p. 492-501.

8. Loveland, W.D., D.J. Morrissey, and G.T. Seaborg, *Modern Nuclear Chemistry*. 2006, New Jersey: John Wiley & Sons, Inc.

9. *Nuclides and Isotopes*. 16th ed, ed. E.M. Baum, H.D. Knox, and T.R. Miller. 2002: Lockheed Martin.

10. Field, R.W., et al., *Residential Radon Gas Exposure and Lung Cancer: The Iowa Radon Lung Cancer Study.* American Journal of Epidemiology, 2000. 151(11): p. 1091-1102.

11. Lamarsh, J.R. and A.J. Baratta, *Introduction to Nuclear Engineering*. 3rd ed. 2001, New Jersey: Prentice Hall.

12. James, M.F., *Energy Released in Fission.* Journal of Nuclear Energy, 1969. 23: p. 517-536.

13. *Standard Potentials in Aqueous Solution*, ed. A.J. Bard, R. Parsons, and J. Jordan. 1985, New York and Basel: Marcel Dekker, Inc.

14. Sullivan, J.C., A.J. Zielen, and J. Hindman, *Kinetics of the Reduction of Neptunium(VI) by Uranium(IV)*. Journal of the American Chemical Society, 1960. 82: p. 5288-5292.

15. Wilson, A.S., *Organic Phase Reduction of Plutonium in a PUREX-Type Process*. United States Patent, 1971.

16. Baes, C.F. and R.E. Mesmer, *The Hydrolysis of Cations*. 2nd ed. 1986, New York: Kreiger.

17. *Science and Technology of Tributyl Phosphate, Volume I: Synthesis, Properties, Reactions, and Analysis*, ed. J.D. Navratil, W.W. Schulz, and A.E. Talbot. 1984: CRC Press, Boca Raton, Florida.

18. Seaborg, G.T., et al., *Radioactive Element 94 from Deuterons on Uranium.* Physical Review, 1946. 69(7-8): p. 366-367.

19. Tombaugh, C.W., *The Search of the Ninth Planet, Pluto.* Astronomical Society of the Pacific Leaflets, 1946. 5: p. 73-80.

20. Choppin, G., J. Rydberg, and J.O. Liljenzin, *Radiochemistry and Nuclear Chemistry*. 2nd ed. 1995: Butterworth-Heinemann, Ltd.

21. Mallela, V.S., V. Ilankumaran, and N.S. Rao, *Trends in Cardiac Pacemaker Batteries.* Indian Pacing and Electrophysiol Journal, 2004. 4(4): p. 201-212.

22. Hecker, S.S., *Plutonium and Its Alloys: From Atoms to Microstructure.* Los Alamos Science, 2000. 26: p. 290-335.

23. Seaborg, G.T. and W.D. Loveland, *The Elements Beyond Uranium*. 1990, New York: Wiley.

24. Coleman, G.H., *The Radiochemistry of Plutonium*. 1965, Atomic Energy Commission: Livermore, California.

25. Cleveland, J.M., *The Chemistry of Plutonium*. 1970, New York: Gordon & Breach.

26. *The Chemistry of the Actinides Elements*. 2nd ed, ed. J.J. Katz, G.T. Seaborg, and L.R. Morss. 1986, New York: Chapman and Hall.

27. Ekberg, C., et al., *Studies on the Complexation Behavior of Thorium(IV). 1. Hydrolysis Equilibria.* Journal of Solution Chemistry, 2000. 29(1): p. 63-86.

28. Guillaumont, R., et al., *Chemical Thermodynamics 5*. Update on the Chemical Thermodynamics of Uranium, Neptunium, Plutonium, Americium and Technetium, ed. F.J. Mompean, et al. 2003, Amsterdam, The Netherlands: Elsevier.

29. *Thorium Based Fuel Options for the Generation of Electricity: Developments in the 1990s*. 2000: IAEA-TECDOC-1155. Vienna, Austria.

30. Ekberg, C., et al., *Studies on the Complexation Behavior of Thorium(IV). 1. Hydrolysis Equilbria.* Journal of Solution Chemistry, 2000. 29(1): p. 63-86.

31. Hesford, E., H.A.C. McKay, and D. Scargill, *Tri-n-Butyl Phosphate as an Extracting Solvent for Inorganic Nitrates-IV: Thorium Nitrate.* Journal of Inorganic and Nuclear Chemistry, 1957. 4: p. 321-325.

32. McMillan, E., *Radioactive Recoils from Uranium Activated by Neutrons.* Physical Review, 1939. 39: p. 510.

33. McMillan, E. and P.H. Abelson, *Radioactive Element 93.* Physical Review, 1940. 57: p. 1185-1186.

34. Katz, J.J. and G.T. Seaborg, *The Chemistry of the Actinide Elements*. 1957, London: Methuen.

35. Thompson, R.C., *Neptunium - The Neglected Actinide: A Review of the Biological and Environmental Literature.* Radation Research, 1982. 90: p. 1-32.

36. Burney, G.A. and R.M. Harbour, *Radiochemistry of Neptunium.* United States Atomic Energy Commission, 1974.

37. Schulz, W.W. and E.P. Horwitz, *The TRUEX Process and the Management of Liquid TRU Waste.* Separation Science and Technology, 1988. 23(12&13): p. 1191-1210.

38. Keller, O.L., *The Chemistry of Protactinium, Neptunium, Americium, and Curium in the Nuclear Fuel Cycle.* Radiochimica Acta, 1978. 25: p. 211-233.

39. *Science and Technology of Tributyl Phosphate, Volume III: Applications of Tributyl Phosphate in Nuclear Fuel Processing*, ed. W.W. Schulz, et al. 1990: CRC Press, Boca Raton, Florida.

40. Korkisch, J., *Modern Methods for the Separation of Rarer Metals*. 1969, New York: Pergamon Press.

41. Cassol, A., et al., *Soluble Intermediates in the Hydrolysis of Neptunium(VI) and Comparison with Other Actinides(VI).* Inorganic Chemistry, 1972. 11(3): p. 515-519.

42. Seaborg, G.T., *The Transuranium Elements.* Science, 1946. 104(2704): p. 379-386.

43. Guillaume, B., *Problems Raised by the Presence of Transuranic Elements in Nuclear Fuel Reprocessing Wastes.* Bulletin d'Informations Scientifiques et Techniques, 1976. 217: p. 31-46.

44. *Light Water Reactor Nuclear Fuel Cycle*, ed. R.G. Wymer and B.L. Vondra. 1981, Boca Raton, FL: CRC Press.

45. Holder, J.V., *A Review of the Solvent Extraction Process Chemistry of Fission Products.* Radiochimica Acta, 1978. 25: p. 171-180.

46. Zielen, A.J. and R.E. Connick, *The Hydrolytic Polymerization of Zirconium in Perchloric Acid Solutions.* Journal of the American Chemical Society, 1956. 78(22): p. 5785-5792.

47. Ekberg, C., et al., *Studies of the Hydrolytic Behavior of Zirconium(IV).* Journal of Solution Chemistry, 2004. 33(1): p. 47-79.

48. Hesford, E. and H.A.C. McKay, *The Extraction of Nitrates by Tri-n-butyl Phosphate (TBP) - Part 3. Extraction at Trace Concentrations.* Transactions of the Faraday Society, 1958. 54: p. 573-586.

49. Solovkin, A.S., *Thermodynamics of the Extraction of Zirconium, Present in the Monomeric State, from Nitric Acid Solutions by Tri-n-butyl Phosphate (TBP).* Russian Journal of Inorganic Chemistry, 1970. 15(7): p. 983-984.

50. Solovkin, A.S., *Thermodynamics of Extraction of Tetravalent Plutonium, Uranium, Thorium and Zirconium.* Journal of Radioanalytical Chemistry, 1974. 21: p. 15-29.

51. Maya, L., *Zirconium Behavior in the System HNO3-30% Tributyl Phosphate-Dodecane in the Presence of Monobutyl Phosphoric Acid.* Journal of Inorganic and Nuclear Chemistry, 1981. 43: p. 379-384.

52. Mailen, J.C., et al., *Solvent Extraction Chemistry and Kinetics of Zirconium.* Separation Science and Technology, 1980. 15(4): p. 959-973.

53. Kolarik, Z. and P. Dressler, *Extraction and Coextraction of Tc(VII), Zr(IV), Np(IV,VI), Pa(V) and Nb(V) with Tributyl Phosphate from Nitric Acid Solutions.* Solvent Extraction and Ion Exchange, 1989. 7(4): p. 625-644.

54. Garraway, J. and P.D. Wilson, *Coextraction of Pertechnetate and Zirconium by Tri-n-Butyl Phosphate.* Journal of the Less-Common Metals, 1985. 106: p. 183-192.

55. Chen, C.C. and G. Ting, *Temperature Effect on the Extraction of 233Pa, 95Zr, 95Nb, and 106Ru by Tributylphosphate in Kerosene.* Nuclear Science Journal, 1976. 13: p. 1-8.

56. Anderegg, G., F. L'Eplattenier, and G. Schwarzenbach, *Hydroxamatkomplexe II. Die Anwendung der pH-Methode.* Helvetica Chimica Acta, 1963. 46(1400-1408).

57. Coleman, C.F. and R.E. Leuze, *Some Milestone Solvent Extraction Processes at the Oak Ridge National Laboratory.* Journal of the Tennessee Academy of Science, 1978. 53: p. 102.

58. Warf, J.C., *Extraction of Cerium(IV) Nitrate by Butyl Phosphate.* Journal of the American Chemical Society, 1949. 71: p. 3257-3258.

59. Navratil, J.D., W.W. Schulz, and A.E. Talbot, *Science and Technology of Tributyl Phosphate*. Vol. I. 1984: CRC Press, Boca Raton, Florida.

60. Paiva, A.P. and P. Malik, *Recent Advances on the Chemistry of Solvent Extraction Applied to the Reprocessing of Spent Nuclear Fuels and Radioactive Wastes.* Journal of Radioanalytical and Nuclear Chemistry, 2004. 261(2): p. 485-496.

61. Gelis, A.V., et al. *Chemistry of Actinides and Lanthanides in the Solvent Extraction Processes of UREX+*. in *32nd Actinide Separation Conference*. 2008. Park City, Utah.

62. Pereira, C., et al., *Lab-Scale Demonstrations of the UREX+1a Process Using Spent Fuel.* Proceedings of WM-07, Tucson, AZ, 2007.

63. Taylor, R.J., et al., *The Applications of Formo- and Aceto-hydroxamic Acids in Nuclear Fuel Reprocessing.* Journal of Alloys and Compounds, 1998. 271-273: p. 534-537.

64. Tkac, P. and A. Paulenova, *The Effect of Acetohydroxamic Acid on Extraction and Speciation of Plutonium.* Separation Science and Technology, 2008. 43(9): p. 2670-2683.

65. May, I., R.J. Taylor, and G. Brown, *The Formation of Hydrophilic Np(IV) complexes and Their Potential Application in Nuclear Fuel Reprocessing.* Journal of Alloys and Compounds, 1998. 271-273: p. 650-653.

66. Tkac, P., et al., *Complexation of Uranium(VI) with Acetohydroxamic Acid.* Journal of Radioanalytical and Nuclear Chemistry, 2008. 277(1): p. 31-36.

67. Tkac, P., A. Paulenova, and G.K. P., *Spectroscopic Study of the Uranyl-Acetohydroxamate Adduct with Tributyl Phosphate.* Applied Spectroscopy, 2007. 61(7): p. 772-776.

68. Paulenova, A., P. Tkac, and B. Matteson. *Speciation of Plutonium and Other Metals Under UREX Process Conditions*. in *Global 2007, Advanced Nuclear Fuel Cycles and Systems, September 9-13*. 2007. Boise, ID, USA: 723-727.

69. Karracker, D.G., T.S. Rudisill, and M.C. Thompson, *Studies of the Effect of Acetohydroxamic Acid on Distribution of Plutonium and Neptunium by 30 Vol% Tributyl Phosphate*. 2001, Westinghouse Savannah River Company.

70. May, I., et al., *Actinide Complexation in the PUREX Process.* Czechoslovak Journal of Physics, 1999. 49: p. 597-601.

71. Taylor, R.J., et al., *The Application of Formo- and Aceto-Hydroxamic Acids in Nuclear Fuel Reprocessing.* Journal of Alloys and Compounds, 1998. 271-273: p. 534-537.

72. Poineau, F., et al., *Uranium/Technetium Separation for the UREX Process-Synthesis and Characterization of Solid Reprocessing Forms.* Radiochimica Acta, 2008. 96: p. 527-533.

73. Law, J.D., et al., *Development of a Colbalt Dicarbollide/Polyethylene Glycol Solvent Extraction Process for Separation of Cesium and Strontium to Support Advanced Aqueous Reprocessing*, in *Global 2003*: New Orleans, LA. p. 2245-2250.

74. Law, J.D., et al. *Development of Technologies for the Simultaneous Separation of Cesium and Strontium from Spent Nuclear Fuel as Part of an Advanced Fuel Cycle*. in *American Institute of Chemical Engineers Spring National Meeting*. 2005. Atlanta, Georgia.

75. Koltunov, V.S., K.M. Frolov, and V.I. Marchenko, *Interaction of Actinides with Vanadium Ions. IV. Kinetics of Oxidation of Np(V) with Vanadium(V) in HClO4 Solution.* Radiochemistry, 1981. 23(1): p. 70-76.

76. Horwitz, E.P., H. Diamond, and K.A. Martin, *The Extraction of Selected Actinides in the (III) (IV) and (VI) Oxidation States from Hydrochloric Acid by OoD(iB)CMPO: The TRUEX-Chloride Process.* Solvent Extraction and Ion Exchange, 1987. 5(3): p. 447-470.

77. Horwitz, E.P. and R. Chiarizia, *Separation Techniques in Nuclear Waste Management*, ed. T.E. Carleson, N.A. Chipman, and C.M. Wai. 1995, New York: CRC Press.

78. Schulz, W.W. and E.P. Horwitz, *The TRUEX Process and the Management of Liquid TRU Waste.* Separation Science and Technology, 1988. 23: p. 1191.

79. Kolarik, Z., *The Formation of a Third Phase in the Extraction of Pu(IV), U(IV), and Th(IV) with Nitrates with Tributyl Phosphate in Alkane Diluents*, in *International Solvent Extraction Conference*. 1979: Toronto, Canada. p. 178-182.

80. Kolarik, Z.J. and E.P. Horwitz, *Extraction of Metal Nitrates with Octyl(phenyl)-n,n-diisobutylcarbamoylmethyl Phosphine Oxides in Alkane Diluents at High Solvent Loading.* Solvent Extraction and Ion Exchange, 1988. 6(1): p. 61-91.

81. Weaver, B. and F.A. Kappelmann, *Talspeak: A New Method of Separating Americium and Curium from Lanthanides by Extraction from an Aqueous Solution of Aminopolyacetic Acid Complex with a Monoacidic Phosphate or Phosphorate.* U. S. DOE, ORNL-3559, 1964.

82. Jensen, M.P. and K.L. Nash, *Solvent Extraction Separations of Trivalent Lanthanide and Actinide Ions using an Aqueous Aminomethanediposphonic Acid.* U. S. DOE, ANL/CHM/CP95678, 1999.

83. Shannon, R.D., *Revised Effective Ionic Radii and Systematic Studies of Interatomic Distances in Halides and Chalcogenides.* Acta Crystallographica Section A, 1976. 32: p. 751-767.

84. Nilsson, M. and K.L. Nash, *Review Article: A Review of the Development and Operational Characteristics of the TALSPEAK Process.* Solvent Extraction and Ion Exchange, 2007. 25: p. 665-701.

85. Jensen, W.B., *The Lewis Acid-Base Concepts: An Overview*. 1980, New York: Wiley.

86. Martell, A.E. and R.M. Smith, *NIST Critically Selected Stability Constants of Metal Complexes*, in *NIST Standard Reference Database 46 Version 2.0*. 1995.

87. Taylor, R.J., I.S. Denniss, and A.L. Wallwork, *Neptunium Control in an Advanced Purex Process.* Nuclear Energy, 1997. 36(1): p. 39-46.

88. Sinkov, S.I. and G.R. Choppin, *Acetohydroxamic Acid Complexes with Trivalent f-Block Metal Cations.* Journal of Nuclear Science and Technology, 2002. Supp. 3: p. 359-362.

89. Matteson, B.S., P. Tkac, and A. Paulenova, *Complexation Chemistry of Zirconium(IV), Uranium(VI), and Iron(III) with Acetohydroxamic Acid.* Separation Science and Technology, Accepted for Publication, 2010.

90. Andrieux, F.P.L., et al., *The Hydrolysis of Hydroxamic Acid Complexants in the Presence of Non-Oxidizing Metal Ions 2: Neptunium (IV) Ions.* Journal of Solution Chemistry, 2008. 37: p. 215-232.

91. Carrott, M.J., et al., *Solvent Extraction Behavior of Plutonium(IV) Ions in the Presence of Simple Hydroxamic Acids.* Solvent Extraction and Ion Exchange, 2007. 25: p. 723-745.

92. Koide, Y., et al., *Studies of Collectors. X. Complexing Ability of Amino Hydroxamic Acid Ligands with Dioxouranium(VI) in Aqueous Solution.* Bulletin of the Chemical Society of Japan, 1989. 62(11): p. 3714-3715.

93. Glennon, J.D., et al., *Analysis of Siderophores and Synthetic Hydroxamic Acids by High-Performance Liquid Chromatography with Amperometric Detection.* Analytical Chemistry, 1989. 61: p. 1474-1478.

94. Ramsbottom, J.V. and W.A. Waters, *The Electron Spin Resonance Spectra of Some Hydroxamine Free Radicals. Part III. Radicals Formed by Oxidations in Alkaline Solution.* Journal of the Chemical Society (B), 1967: p. 180-184.

95. Carrott, M.J., et al., *Oxidation-Reduction Reactions of Simple Hydroxamic Acids and Plutonium(IV) Ions in Nitric Acid.* Radiochimica Acta, 2008. 96: p. 333-343.

96. Matteson, B.S., M. Precek, and A. Paulenova, *A Study of the Kinetics of the Reduction of Neptunium(VI) by Acetohydroxamic Acid in Perchloric Acid.* Materials Science and Engineering, accepted 2009.

97. Tkac, P., M. Precek, and A. Paulenova. *Reduction of Tetravalent Plutonium in the Presence of Acetohydroxamic Acid*. in *Global*. 2009. Paris, France.

98. Tkac, P., M. Precek, and A. Paulenova, *Redox Reactions of Pu(IV) and Pu(III) in the Presence of Acetohydroxamic and HNO3 Solutions.* Inorganic Chemistry, 2009. 48(24): p. 12431-12440.

99. Karraker, D.G., T.S. Rudisill, and M.C. Thompson, *Studies of the Effect of Acetohydroxamic Acid on Distribution of Plutonium and Neptunium by 30 Vol% Tributyl Phosphate.* 2001(WSRC-TR-2001-00509).

100. Colston, B.J., G.R. Choppin, and R.J. Taylor, *A Preliminary Study of the Reduction of Np(VI) by Formohydroxamic Acid using Stopped-Flow Near-Infrared Spectrophotometry.* Radiochimica Acta, 2000. 88: p. 329-334.

101. Koltunov, V.S. and S.M. Baranov, *Organic Derivatives of Hydrazine and Hydroxylame in Future Technology of Spent Nuclear Fuel Reprocessing.* Radiochemistry, 1993. 35(6).

102. Koltunov, V.S., R.J. Taylor, and S.M. Baranov, *The Reduction of Plutonium and Neptunium Ions by Acetaldoxime in Nitric Acid.* Radiochimica Acta, 2000. 88: p. 65-70.

103. Uchiyama, G., et al., *New Separation Process for Neptunium, Plutonium, and Uranium using Butyraldehydes as Reductants in Reprocessing.* Nuclear Technology, 1993. 102: p. 341-352.

104. Ghosh, K.K., *Kinetic and Mechanistic Aspects of Acid-Catalysed Hydrolysis of Hydroxamic Acids.* Indian Journal of Chemistry. Section B, 1997. 36: p. 1089.

105. Taylor, R.J. and I. May, *The Reduction of Actinide Ions by Hydroxamic Acids.* Czechoslovak Journal of Physics, 1999. 49(Suppl. S1): p. 617-621.

106. Alyapyshev, M., et al., *Hydrolysis of Acetohydroxamic Acid under UREX+ Conditions*, in *Global 2007*. 2007: Boise, Idaho. p. 1861-1864.

107. Chung, D.Y. and E.H. Lee, *Kinetics of the Hydrolysis of Acetohydroxamic Acid in a Nitric Acid Solution.* Journal of Industrial and Engineering Chemistry, 2006. 12(6): p. 962-966.

108. Andrieux, F.P.L., C. Boxall, and R.J. Taylor, *The Hydrolysis of Hydroxamic Acid Complexants in the Presence of Non-oxidizing Metal Ions 1: Ferric Ions*. Journal of Solution Chemistry, 2007. 36: p. 1201-1217.

109. *Computational Methods for the Determination of Formation Constants*, ed. D.J. Leggett. 1985, New York: Plenum Press.

110. Gans, P., A. Sabatini, and A. Vacca, *Hyperquad2006: Equilibrium Constants from Potentiometric and/or Absorbance Data*, in *http://www.hyperquad.co.uk/hq2000.htm*. 2006.

111. Gans, P., A. Sabatini, and A. Vacca, *Investigation of Equilibria in Solution. Determination of Equilibrium Constants with the HYPERQUAD Suite of Programs.* Talanta, 1997. 43: p. 1739-1753.

112. Pettit, D., *Ionic Strength Corrections Using Specific Interaction Theory, Version 1.2*. 2002, Ionic Strength Corrections Using Specific Interaction Theory, Version 1.2, IUPAC, Academic Software: Otley Yorks, U.K.

113. Guggenheim, E.A. and J.C. Turgeon, *Specific Interactions of Ions.* Transactions of the Faraday Society, 1955. 51: p. 747-761.

114. Rydberg, J., et al., *Solvent Extraction Principles and Practice*. 2nd ed. 2004, New York: Marcel Dekker, Inc.

115. Freiser, H. and G.H. Nancollas, *Compendium of Analytical Nomenclature. Definitive Rules 1997*. 3rd ed. IUPAC. 1997, Oxford: Blackwell Scientific Publications.

116. Delmau, L.H., et al., *Caustic-Side Solvent Extraction Chemical and Physical Properties: Equilibrium Modeling of Distribution Behavior.* U.S. DOE, ORNL/TM-2001-267, 2001.

117. Lumetta, G.J., B.K. McNamara, and B.M. Rapko, *The SX Solver: A New Computer Program for Analyzing Solvent-Extraction Equilibria.* U.S. DOE, PNNL-12085, 1999.

118. Lumetta, G.J., et al., *Complexation of Uranyl Ion by Tetrahexylmalonamides: An Equilibrium Modeling and Infrared Spectroscopic Study*. Inorganic Chimica Acta, 1999. 293(2): p. 195-205.

119. Regalbuto, M.C., et al., *Development of the AMUSE Code*, in *Advanced Nuclear Fuel Cycle Initiative Quarterly Review*. January 21-24, 2003: Albuquerque, NM.

120. Regalbuto, M.C., J.M. Copple, and G.F. Vandegrift. *AMUSE Code Update*. in *Advanced Fuel Cycle Initiative Semi-Annual Meeting*. August 26-28, 2003. Santa Fe, NM.

121. Laidler, K.J., *Chemical Kinetics*. 2nd ed. 1965, New York: McGraw-Hill Book Company.

122. Chung, D.Y. and E.H. Lee, *The Reduction of Np(VI) by Acetohydroxamic Acid in Nitric Acid Solution.* Bulletin of the Korean Chemical Society, 2005. 26(11): p. 1692-1694.

123. Kaw, A.K., *Runge-Kutta 4th Order Method for Ordinary Differential Equations. Available at: http://numericalmethods.eng.usf.edu/topics/runge_kutta_4th_method.html*. 2009, University of South Florida: Tampa, FL.

124. Kelly, J. and C. Savage, *Advanced Fuel Cycle Initiative Program Plan*. May 1, 2005.

125. Chatterjee, B., *Donor Properties of Hydroxamic Acids.* Coordination Chemistry Review, 1978. 26: p. 281-303.

126. Bass, V.C. and J.H. Voe, *Hydroxamic Acids as Colorimetric Reagents.* Talanta, 1966. 13(5): p. 735-744.

127. Pokhitonov, Y., et al., *Composition of Insoluble Residues Generated during Spent Fuel Dissolution*, in *Waste Management 2002*. 2002: Tucson, AZ.

128. Brewer, K.N., et al., *Zirconium Extraction into Octyl(phenyl)-N,N-Diisobutylcarbamoylmethyl Phosphine Oxide and Tributyl Phosphate.* Solvent Extraction and Ion Exchange, 1998. 16(4): p. 1047-1066.

129. Leggett, D.J., *Computational Methods for the Determination of Formation Constants*, ed. L.D. J. 1985, New York: Plenum.

130. Tkac, P., et al., *Complexation of Uranium (VI) with Acetohydroxamic Acid.* Journal of Radioanalytical and Nuclear Chemistry, 2008. 277(1): p. 31-36.

131. Taylor, R.J., et al., *The Applications of Formo- and Aceto-hydroxamic Acid in Nuclear Fuel Reprocessing.* Journal of Alloys and Compounds, 1998. 271-273: p. 534-537.

132. Govindan, P., S. Sukumar, and R.V. Subba Rao, *Partitioning of Uranium and Plutonium by Acetohydroxamic Acid.* Desalination, 2008. 232(1-3): p. 166-171.

133. Sekhon, B.S. and N. Kaur, *Complex Formation Equilibria of Acetohydroxamic Acid with H+ and UO22+ Ion in Aqueous Organic Mixtures.* Journal of the Indian Chemical Society, 1995. 72: p. 545-546.

134. Birus, M., et al., *Stopped-Flow and Rapid-Scan Spectral Examination of the Iron(III)-Acetohydroxamic Acid System.* Inorganic Chemistry, 1985. 24: p. 3980-3983.

135. Andrieux, F.P.L., C. Boxall, and R.J. Taylor, *Acetohydroxamatoiron(III) Complexes: Thermodynamics of Formation and Temperature Dependent Speciation.* Journal of Solution Chemistry, 2008. 37: p. 1511-1527.

136. Connick, R.E. and W.H. McVey, *The Aqueous Chemistry of Zirconium.* Journal of the American Chemical Society, 1949. 71: p. 3182-3191.

137. Schultz, B.G. and E.M. Larsen, *The Fractional Separation of Zirconium and Halfnium by Extraction with Trifluoroacetylacetone.* Journal of the American Chemical Society, 1950. 72: p. 3610-3614.

138. Cornell, R.M. and U. Schwertmann, *The Iron Oxides*. 1996, New York: VCH.

139. Renshaw, J.C., et al., *Fungal Siderophores: Structures, Functions and Applications.* Mycological Research, 2002. 106(10): p. 1123-1142.

140. Fuger, J., et al., *Chemical Thermodynamics of Uranium*, ed. H. Wanner and I. Forest. 2004, Paris, France: Nuclear Energy Agency, OECD.

141. Baroncelli, F. and G. Grossi, *The Complexing Power of Hydroxamic Acids and its Effect on the Behaviour of Organic Extractants in the Reprocessing of Irradiated Fuels.* Journal of Inorganic and Nuclear Chemistry, 1965. 27(5): p. 1085-1092.

142. Buděšínský, B., *Spektralphotometrische Studie der Reaktion von Zirkonium(IV) mit Arsenazo III: Über die Unterscheidung der Mehrkernigkeit der Komplexe 1:1* Zeitschrift fur Analytische Chemie, 1964. 206(6): p. 401-409.

143. Savvin, S.B., *Analytical Use of Arsenazo III: Determination of Thorium, Zirconium, Uranium and Rare Earth Elements.* Talanta, 1961. 8: p. 673-685.

144. Davydov, Y.P., D.Y. Davydov, and L.M. Zemskova, *Speciation of Zr(IV) Radionuclides in Solutions.* Radiochemistry, 2006. 48(4): p. 358-364.

145. Buděšínský, B., *Spektralphotometrische Studie der Reaktion von Zirkonium(IV) mit Arsenazo III: Über die Unterscheidung der Mehrkernigkeit der Komplexe 1:1.* Zeitschrift fur Analytische Chemie, 1964. 206(6): p. 401-409.

146. Mel'chakova, N.V., M.N. Stanislavskaya, and V.M. Peshkova, *Spectrophotometric Titration of Zirconium with a Solution of Arsenazo III.*

Journal of Analytical Chemistry of the USSR, 1964. 19: p. 650-653. Translated from Zhurnal Analiticheskoi Khimii, Vol. 19, No. 6, pp. 701-704, June, 1964.

147. Kus, S., N. Obarski, and Z. Marczenko, *Determination of Thorium, Uranium and Zirconium with Arsenazo III Using Third-Order Derivative Spectrophotometry.* Analytical Sciences, 1992. 8(2): p. 213-218.

148. Grigor'eva, M.G., et al., *Precision Spectrometric Determination of Th and Pu in Solutions with Arsenazo III Using Internal Standardization.* Radiochemistry, 2003. 45(4): p. 388-393.

149. Surin, I.G., P.K. Spitsyn, and V.F. Barkovskii, *Study of Reactions Between Rare Earth Elements and Arsenazo III over a pH Range of 0.5 - 4.0.* Zhurnal Analiticheskoi Khimii, 1979. 34(6): p. 1103-1109.

150. Muk, A.A. and S.B. Savvin, *Complex Formation of Zirconium and Thorium Ions with Arsenazo III in Perchloric Acid Solutions.* Journal of Analytical Chemistry of the USSR, 1971. 26(1): p. 98-109.

151. Muk, A.A. and R. Radosavljevic, *Formation of Metal Complexes with the Arsenazo I and Arsenazo III Reagents as Functions of the Medium Acidity.* Croatica Chemica Acta, 1967. 39: p. 1-9.

152. Tkac, P., et al., *Distribution and Identification of Plutonium(IV) Species in Tri-n-Butyl Phosphate/HNO3 Extraction System Containing Acetohydroxamic Acid.* Journal of Radioanalytical and Nuclear Chemistry, 2009. 280(2): p. 339-342.

153. Tkac, P., et al. *Extraction of Tetravalent Metals by TBP: Effect of Nitrate and Acetohydroxamic Acid*. in *MARC VII*. 2006. Hawaii.

154. Ryabchikov, D.I., et al., *Stability of some inorganic and organic complex compounds of Zr and Hf* Journal of Inorganic and Nuclear Chemistry, 1964. 26(6): p. 965-980.

155. *Ionisation Constants of Organic Acids in Aqueous Solution: International Union of Pure and Applied Chemistry. Commission on Equilibrium Data*, ed. E.P. Serjeant and B. Dempsey. 1979, Oxford, UK: Pergamon Press.

156. Advanced Fuel Cycle Initiative Program Plan., 2005. Available at: http://afci.sandia.gov/downloads/2005_AFCI_Program_Plan.pdf.

157. Vandegrift, G.F., et al., *Lab-Scale Demonstration of the UREX+ Process*, in *Waste Management Conference*. 2004: Tucson, AZ.

158. May, I., et al., *Neptunium(IV) and Uranium(VI) Complexation by Hydroxamic Acids.* Journal of Alloys and Compounds, 1998. 275-277: p. 769-772.

159. Carrott, M.J., et al., *Solvent Extraction Behavior of Plutonium (IV) Ions in the Presence of Simple Hydroxamic Acids.* Solvent Extraction and Ion Exchange, 2007. 25: p. 723-745.

160. Olis Rapid Scanning Monochromator. . Please refer to: http://olisweb.com/products/rsm/.

161. Tkac, P., M. Precek, and A. Paulenova, *Redox Reactions of Pu(IV) and Pu(III) in the Presence of Acetohydroxamic and Nitric Acid.* Inorganic Chemistry, 2009(submitted).

162. Grossi, G., *Solvent Extraction with Hydroxamic Acids I.* Lab. Chim. Ind., Com. Naz. Energ. Nucl., Italy, 1970(RT/CHI(70)15).

163. Patil, S.K., R. Swarup, and V. Bhandiwad, *Some Studies on the Extraction of Hexavalent Actinide Ions from Aqueous Carboxylic Acid Media by Long-Chain Amines.* Journal of Radioanalytical Chemistry, 1979. 53(1-2): p. 115-129.

164. Choppin, G.R., P.A. Bertrand, and L.F. Rao, *Reduction Reactions of Tracer-Level Neptunium(VI) with Aromatic Compounds.* Revue de Chimie Minerale, 1983. 20(4-5): p. 745-752.

165. Kolarik, Z. and R. Schuler, *Separation of Neptunium from Uranium and Plutonium in the PUREX Process*, in *Extraction '84: Symposium on Liquid-Liquid Extraction Science*. 1984: Dounreay, Scotland. p. 83-90.

166. Koltunov, V.S. and S.M. Baranov, *Organic Derivatives of Hydrazine and Hydroxylame in Future Technology of Spent Nuclear Fuel Reprocessing*, in *GLOBAL '95*. 1995: Versailles, France.

167. Boyland, E. and R. Nery, *The Oxidation of Hydroxamic Acids.* Journal of the Chemical Society (C), 1966: p. 354-358.

168. Koltunov, V.S. and Tikhonov, *Kinetics of the Reduction of Actinides by Hydroxylamine. I. Reduction of Neptunium(VI) in Nitric Acid Solution.* Radiokhimiya, 1977. 19(5): p. 611-619.

169. Alcock, K., et al., *TBP as an Extracting Solvent for Inorganic Nitrates-V: Further Results for the IV and VI Actinide Nitrates.* Journal of Inorganic and Nuclear Chemistry, 1958. 6: p. 328-333.

170. Ishimori, T. and K. Watanabe, *Inorganic Extraction Studies on the System of Tri-n-Butyl Phosphate-Nitric Acid.* Bulletin of the Chemical Society of Japan, 1960. 33(10): p. 1443-1448.

171. *Chemical Rubber Company Handbook of Chemistry and Physics*. 70th ed, ed. D.R. Lide. 1990, Boca Raton, FL.

172. Taylor, R.J., S.I. Sinkov, and G.R. Choppin. *Complexation of Lanthanides and Actinides by Acetohydroxamic Acid*. in *International Solvent Extraction Conference*. 2008. Quebec, Canada.

173. Sarsenov, A., et al., *The Extractability of Zirconium Nitrate as a Function of the Initial Compound used to Prepare the Solutions.* Russian Journal of Inorganic Chemistry, 1974. 19: p. 1375.

174. Shevchenko, V.B., et al., *The Influence of Hydrocarbons of the Fatty and the Aromatic Series on the Extraction U(VI), Pu(IV), Zr(IV) and Ce(III) with Tri-n-Butyl Phosphate from Nitric Acid Solutions.* Radiochemistry, USSR, 1960. 2(3): p. 18-27.

175. Hood, G.C. and C.A. Reilly, *1960_Hood-Ionization of Strong Electrolytes. VIII. Temperature Coefficients of Dissociation of Strong Acids by Proton Magnetic Resonance.* Journal of Chemical Physics, 1960. 32(1): p. 127-130.

176. Alcock, K., et al., *Tri-n-butyl Phosphate as an Extracting Solvent for Inorganic Nitrates. I. Zirconium Nitrate.* Journal of Inorganic and Nuclear Chemistry, 1957. 4: p. 100.

177. Suarez, J.A., et al. *Studies on Behaviour of Selenium and Zirconium in PUREX Process*. in *Atalante*. 2000. Madrid, Spain.

178. Adamskii, N.M., et al., *The Distribution of Zirconium on Extraction with n-Tributyl Phosphate.* Radiochemistry, USSR, 1960. 2(4): p. 142-153.

179. May, I., et al., *Np(IV) Distribution between 30% Tributylphosphate in Odourless Kerosene and NItric Acid.* Radiochimica Acta, 1998. 83: p. 135-138.

180. Friedman, H.A. and L.M. Toth, *Absorption Spectra of Np(III), (IV), (V) and (VI) in Nitric Acid Solution.* Journal of Inorganic and Nuclear Chemistry, 1980. 42: p. 1347-1349.

181. Vasudeva Rao, P.R. and S.K. Patil, *A spectrophotometric method for the determination of neptunium and plutonium in process solutions* Journal of Radioanalytical and Nuclear Chemistry, 1978. 42(2): p. 399-410.

182. Paulenova, A. and P. Tkac, *Effect of Acetohydroxamic Acid on Distribution of Pu(IV) in 30% TBP.* Abstracts, 62nd Northwest Regional Meeting of the American Chemical Society, Boise, ID, 2007.

183. http://zeiss-campus.magnet.fsu.edu/.

184. www.aicl.com.

10 APPENDIX A: SUPPLIMENTAL INFORMATION FOR COMPLEXATION STUDIES

10.1 Experimental Information for Chapter 3

10.1.1 Ferric Iron·AHA Complexation in HNO_3

Table 10.1: Fe/AHA experimental concentrations.

Experiments: 0.1 mol·L^{-1} HNO_3, I = 0.1 mol·L^{-1} NO_3^-, and 25°C.

[Fe(III)] (mol·L^{-1})	**[AHA]$_{init}$ (mol·L^{-1})**	**[Fe(III)] (mol·L^{-1})**	**[AHA]$_{init}$ (mol·L^{-1})**	**[Fe(III)] (mol·L^{-1})**	**[AHA]$_{init}$ (mol·L^{-1})**
1.00×10^{-2}	-	5.00×10^{-4}	-	5.00×10^{-4}	8.00×10^{-2}
1.00×10^{-2}	1.00×10^{-5}	5.00×10^{-4}	1.00×10^{-3}	5.00×10^{-4}	9.00×10^{-2}
1.00×10^{-2}	5.00×10^{-5}	5.00×10^{-4}	2.00×10^{-3}	5.00×10^{-4}	9.50×10^{-2}
1.00×10^{-2}	1.00×10^{-4}	5.00×10^{-4}	4.00×10^{-3}	5.00×10^{-4}	1.00×10^{-1}
1.00×10^{-2}	2.00×10^{-4}	5.00×10^{-4}	6.00×10^{-3}	5.00×10^{-4}	1.05×10^{-1}
1.00×10^{-2}	4.00×10^{-4}	5.00×10^{-4}	8.00×10^{-3}	5.00×10^{-4}	1.12×10^{-1}
1.00×10^{-2}	6.00×10^{-4}	5.00×10^{-4}	9.00×10^{-3}	5.00×10^{-4}	2.52×10^{-1}
1.00×10^{-2}	8.00×10^{-4}	5.00×10^{-4}	1.25×10^{-2}	5.00×10^{-4}	5.00×10^{-1}
1.00×10^{-2}	1.00×10^{-3}	5.00×10^{-4}	1.60×10^{-2}	5.00×10^{-4}	7.76×10^{-1}
5.00×10^{-2}	1.00×10^{-3}	5.00×10^{-4}	1.75×10^{-2}	1.5×10^{-4}	7.74×10^{-1}
-	-	5.00×10^{-4}	2.00×10^{-1}	7.5×10^{-5}	7.73×10^{-1}
-	-	-	-	4.0×10^{-4}	6.3×10^{0}

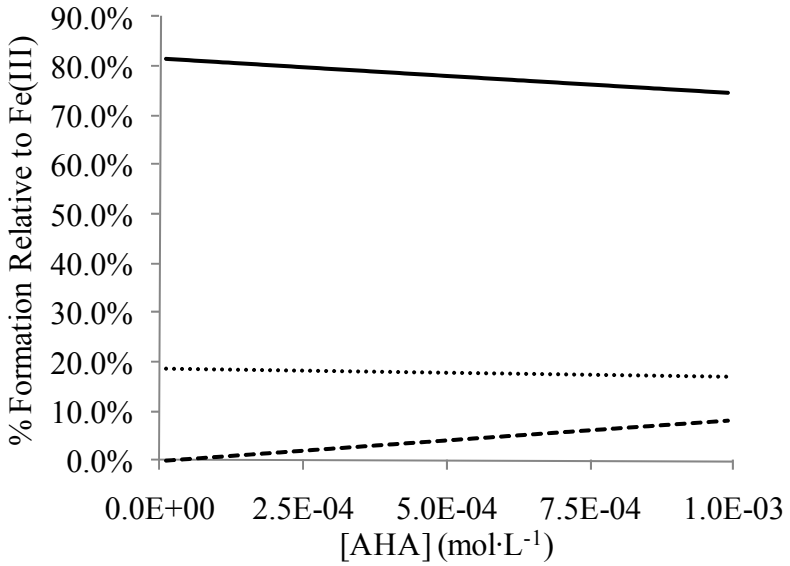

Figure 10.1: Speciation distribution diagram of Fe^{3+} in HNO_3 (low [AHA]).

System: 0.1 mol·L^{-1} HNO_3, 25 °C, $[Fe^{3+}]_{total}$ = 1.0×10^{-2} mol·L^{-1}, [AHA] = 1.0×10^{-5} - 1.0×10^{-3} mol·L^{-1}. Fe^{3+} (solid line), $Fe(NO_3)^{2+}$ (dotted line), $Fe(AHA)^{2+}$ (dashed line).

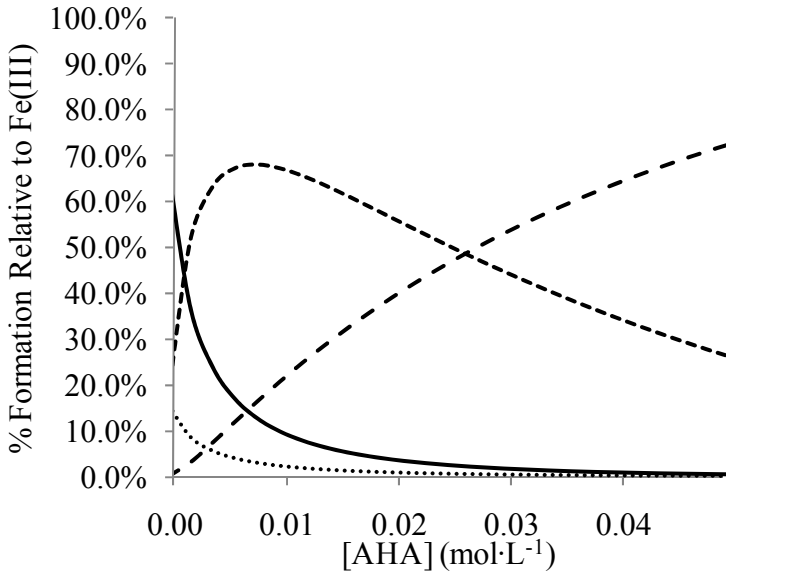

Figure 10.2: Speciation distribution diagram of Fe^{3+} in HNO_3 (medium [AHA]).

System: 0.1 mol·L^{-1} HNO_3, 25 °C, $[Fe^{3+}]_{total}$ = 5.0×10^{-4} mol·L^{-1}, [AHA] = 1.0×10^{-3} - 5.0×10^{-2} mol·L^{-1}. Fe^{3+} (solid line), $Fe(NO_3)^{2+}$ (dotted line), $Fe(AHA)^{2+}$ (narrow dashed line), $Fe(AHA)_2^{2+}$ (medium dashed line).

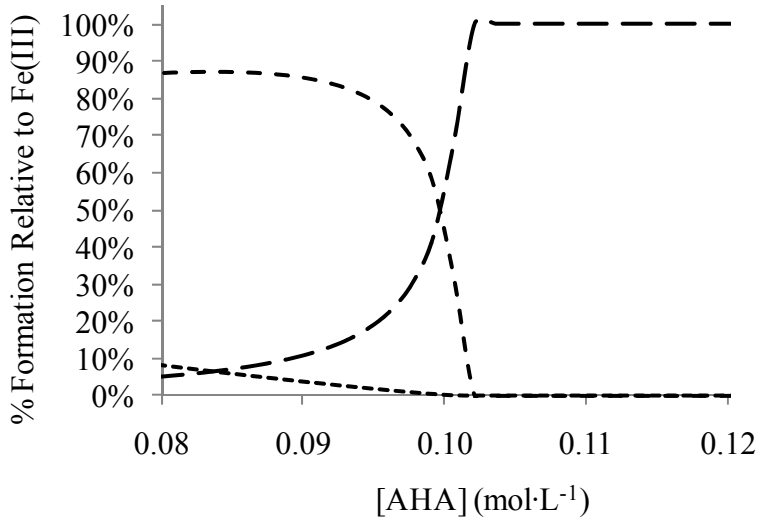

Figure 10.3: Speciation distribution diagram of Fe^{3+} in HNO_3 (high [AHA]).

System: 0.1 mol·L^{-1} HNO_3, 25 °C, $[Fe^{3+}]_{total}$ = 5.0×10^{-4} mol·L^{-1}, [AHA] = 8.0×10^{-3} - 1.2×10^{-1} mol·L^{-1}. Fe^{3+} (solid line), $Fe(NO_3)^{2+}$ (dotted line), $Fe(AHA)^{2+}$ (narrow dashed line), $Fe(AHA)_2^{2+}$ (medium dashed line), $Fe(AHA)_3$ (wide dashed lines).

10.1.2 Uranyl·AHA Complexation in HNO_3 and $HClO_4$

Table 10.2: Uranyl/AHA experimental concentrations ($\Delta[UO_2^{2+}]$).

Experiments:
0.1 mol·L^{-1} HNO_3, I = 0.1 mol·L^{-1} NO_3^-, 25°C.
0.1 mol·L^{-1} HNO_3, I = 1.0 mol·L^{-1} NO_3^-, 25°C.
0.1 mol·L^{-1} $HClO_4$, I = 0.1 mol·L^{-1} ClO_4^-, 25°C.
0.1 mol·L^{-1} $HClO_4$, I = 1.0 mol·L^{-1} $ClO4_4^-$, 25°C.

$[UO_2^{2+}]$ (mol·L^{-1})	**$[AHA]_{init}$ (mol·L^{-1})**	**$UO_2^{2+}]$ (mol·L^{-1})**	**$[AHA]_{init}$ (mol·L^{-1})**
2.00×10^{-2}	6.25×10^{-2}	6.00×10^{-2}	6.25×10^{-2}
2.50×10^{-2}	6.25×10^{-2}	6.50×10^{-2}	6.25×10^{-2}
3.00×10^{-2}	6.25×10^{-2}	7.00×10^{-2}	6.25×10^{-2}
3.50×10^{-2}	6.25×10^{-2}	7.50×10^{-2}	6.25×10^{-2}
4.00×10^{-2}	6.25×10^{-2}	8.00×10^{-2}	6.25×10^{-2}
4.50×10^{-2}	6.25×10^{-2}	8.50×10^{-2}	6.25×10^{-2}
5.00×10^{-2}	6.25×10^{-2}	9.00×10^{-2}	6.25×10^{-2}
5.50×10^{-2}	6.25×10^{-2}	5.00×10^{-2}	-

Table 10.3: Uranyl/AHA experimental concentrations (Δ[AHA]).

Experiments:
0.1 mol·L^{-1} HNO_3, I = 0.1 mol·L^{-1} NO_3^-, 25°C.
0.1 mol·L^{-1} HNO_3, I = 1.0 mol·L^{-1} NO_3^-, 25°C.
0.1 mol·L^{-1} $HClO_4$, I = 0.1 mol·L^{-1} ClO_4^-, 25°C.
0.1 mol·L^{-1} $HClO_4$, I = 1.0 mol·L^{-1} $ClO4_4^-$, 25°C.

$[UO_2^{2+}]$ (mol·L^{-1})	$[AHA]_{init}$ (mol·L^{-1})	$UO_2^{2+}]$ (mol·L^{-1})	$[AHA]_{init}$ (mol·L^{-1})
5.00×10^{-2}	-	5.00×10^{-2}	4.00×10^{-2}
5.00×10^{-2}	5.00×10^{-3}	5.00×10^{-2}	4.50×10^{-2}
5.00×10^{-2}	1.00×10^{-2}	5.00×10^{-2}	5.00×10^{-2}
5.00×10^{-2}	1.50×10^{-2}	5.00×10^{-2}	6.25×10^{-2}
5.00×10^{-2}	2.00×10^{-2}	5.00×10^{-2}	7.50×10^{-2}
5.00×10^{-2}	2.50×10^{-2}	5.00×10^{-2}	8.75×10^{-2}
5.00×10^{-2}	3.00×10^{-2}	5.00×10^{-2}	1.00×10^{-1}
5.00×10^{-2}	3.50×10^{-2}	5.00×10^{-2}	2.00×10^{-1}

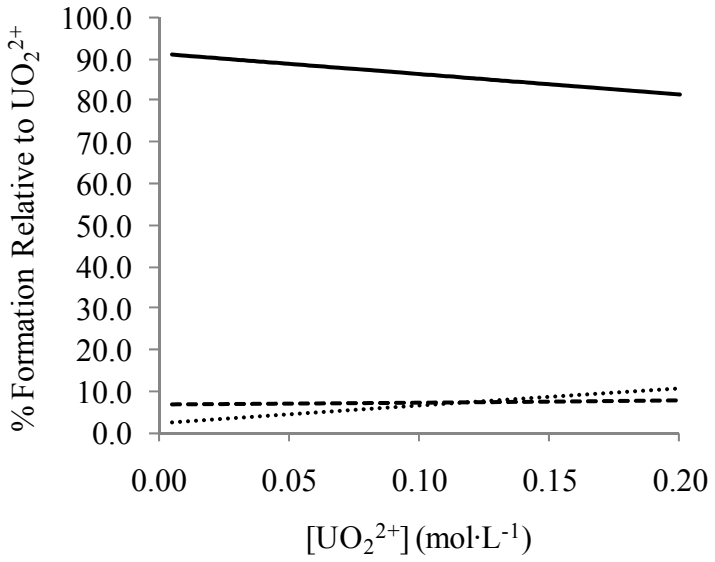

Figure 10.4: Speciation distribution diagram of UO_2^{2+} in HNO_3 (Δ[UO_2^{2+}]).

System: 1 mol·L^{-1} HNO_3, 1 mol·L^{-1} total NO_3^-, 25 °C, $[UO_2^{2+}]_{total}$ = 2.0×10^{-2} - 2.0×10^{-1} mol·L^{-1}, [AHA] = 6.25×10^{-2} mol·L^{-1}. UO_2^{2+} (solid line), $UO2(NO_3)^+$, (dotted line), $UO_2(AHA)^+$ (narrow dashed line).

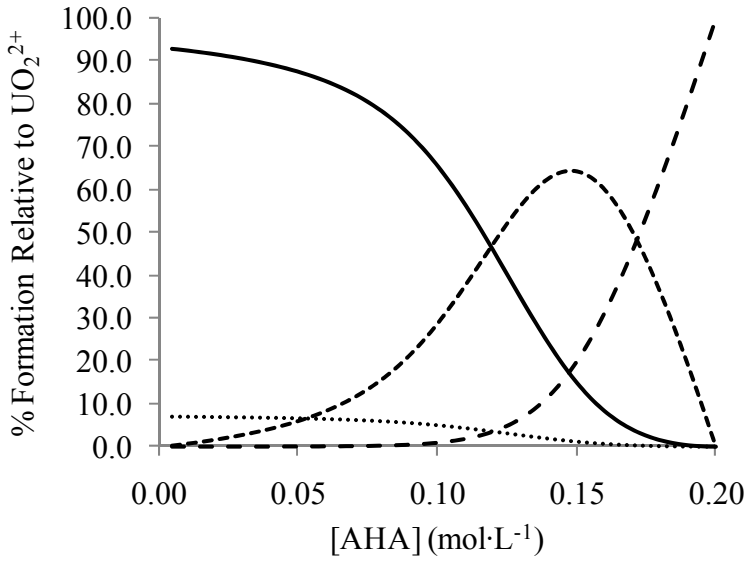

Figure 10.5: Speciation distribution diagram of UO_2^{2+} in HNO_3 (Δ[AHA]).

System: 1 mol·L^{-1} HNO_3, 1 mol·L^{-1} total NO_3^-, 25 °C, $[UO_2^{2+}]_{total}$ = 5.0×10^{-2} mol·L^{-1}, [AHA] = 5.0×10^{-3} – 2.0×10^{-1} mol·L^{-1}. Note: 1.0×10^{-1} and 2.0×10^{-1} AHA spectra were not used in SQUAD for determining logβ $UO_2(AHA)^+$. UO_2^{2+} (solid line), $UO2(NO_3)^+$, (dotted line), $UO_2(AHA)^+$ (narrow dashed line), $UO_2(AHA)_2$ (medium dashed line).

10.1.3 Zirconium·Arsenazo III Complexation in $HClO_4$.

Table 10.4: Zr/AAIII in $HClO_4$ experimental concentrations.

1.0 mol·L^{-1} $HClO_4$ and 25°C for I = 1.0 mol·L^{-1} ClO_4^- experiments.
1.0 mol·L^{-1} $HClO_4$, 1.0 mol·L^{-1} $NaClO_4$ and 25°C for I = 2.0 mol·L^{-1} ClO_4^- experiments.

[Zr^{4+}] (mol·L^{-1})	**[AAIII] (mol·L^{-1})**	**[Zr^{4+}] (mol·L^{-1})**	**[AAIII] (mol·L^{-1})**
2.5×10^{-6}	1.25×10^{-4}	4.0×10^{-5}	1.0×10^{-5}
5.0×10^{-6}	1.25×10^{-4}	4.0×10^{-5}	2.5×10^{-5}
1.0×10^{-5}	1.25×10^{-4}	4.0×10^{-5}	4.0×10^{-5}
1.5×10^{-5}	1.25×10^{-4}	4.0×10^{-5}	5.0×10^{-5}
2.0×10^{-5}	1.25×10^{-4}	4.0×10^{-5}	6.0×10^{-5}
2.5×10^{-5}	1.25×10^{-4}	4.0×10^{-5}	7.0×10^{-5}
3.0×10^{-5}	1.25×10^{-4}	4.0×10^{-5}	8.0×10^{-5}
3.5×10^{-5}	1.25×10^{-4}	4.0×10^{-5}	9.0×10^{-5}
4.0×10^{-5}	1.25×10^{-4}	4.0×10^{-5}	1.00×10^{-4}
4.5×10^{-5}	1.25×10^{-4}	4.0×10^{-5}	1.10×10^{-4}
5.0×10^{-5}	1.25×10^{-4}	-	1.25×10^{-4}

Table 10.5: AAIII in $HClO_4$ experimental concentrations.

1.0 mol·L^{-1} $HClO_4$ and 25°C for I = 1.0 mol·L^{-1} ClO_4^- experiments.
1.0 mol·L^{-1} $HClO_4$, 1.0 mol·L^{-1} $NaClO_4$ and 25°C for I = 2.0 mol·L^{-1} ClO_4^- experiments.

[Zr^{4+}] (mol·L^{-1})	**[AAIII] (mol·L^{-1})**
-	1.0×10^{-5}
-	2.5×10^{-5}
-	4.0×10^{-5}
-	5.0×10^{-5}
-	6.0×10^{-5}
-	7.0×10^{-5}
-	8.0×10^{-5}
-	9.0×10^{-5}
-	1.00×10^{-4}
-	1.10×10^{-4}
-	1.25×10^{-4}

10.1.4 Zirconium·AHA Complexation in $HClO_4$.

Table 10.6: Zr/AAIII/AHA in $HClO_4$ experimental concentrations.

1.0 mol·L^{-1} $HClO_4$ and 25°C for I = 1.0 mol·L^{-1} ClO_4^- experiments.
1.0 mol·L^{-1} $HClO_4$, 1.0 mol·L^{-1} $NaClO_4$ and 25°C for I = 2.0 mol·L^{-1} ClO_4^- experiments.

[Zr^{4+}] (mol·L^{-1})	**[AAIII] (mol·L^{-1})**	**[AHA] (mol·L^{-1})**	**[Zr^{4+}] (mol·L^{-1})**	**[AAIII] (mol·L^{-1})**	**[AHA] (mol·L^{-1})**
4.5×10^{-5}	1.25×10^{-4}	-	1.0×10^{-5}	1.25×10^{-4}	4.0×10^{-2}
4.5×10^{-5}	1.25×10^{-4}	5.0×10^{-3}	1.5×10^{-5}	1.25×10^{-4}	4.0×10^{-2}
4.5×10^{-5}	1.25×10^{-4}	1.0×10^{-2}	2.0×10^{-5}	1.25×10^{-4}	4.0×10^{-2}
4.5×10^{-5}	1.25×10^{-4}	1.5×10^{-2}	2.5×10^{-5}	1.25×10^{-4}	4.0×10^{-2}
4.5×10^{-5}	1.25×10^{-4}	2.0×10^{-2}	3.0×10^{-5}	1.25×10^{-4}	4.0×10^{-2}
4.5×10^{-5}	1.25×10^{-4}	3.0×10^{-2}	4.0×10^{-5}	1.25×10^{-4}	4.0×10^{-2}
4.5×10^{-5}	1.25×10^{-4}	3.5×10^{-2}	5.0×10^{-5}	1.25×10^{-4}	4.0×10^{-2}
4.5×10^{-5}	1.25×10^{-4}	4.0×10^{-2}	6.0×10^{-5}	1.25×10^{-4}	4.0×10^{-2}
4.5×10^{-5}	1.25×10^{-4}	4.0×10^{-2}	7.0×10^{-5}	1.25×10^{-4}	4.0×10^{-2}
4.5×10^{-5}	1.25×10^{-4}	5.0×10^{-2}	-	-	-
4.5×10^{-5}	1.25×10^{-4}	6.25×10^{-2}	-	-	-
4.5×10^{-5}	1.25×10^{-4}	7.5×10^{-2}	-	-	-
4.5×10^{-5}	1.25×10^{-4}	8.75×10^{-2}	-	-	-
4.5×10^{-5}	1.25×10^{-4}	1.0×10^{-1}	-	-	-
4.5×10^{-5}	1.25×10^{-4}	1.13×10^{-1}	-	-	-

10.2 Experimental Information for Chapter 4

10.2.1 Zirconium Complexation in HNO_3

Table 10.7: Zr/AAIII in HNO_3 experimental concentrations.

1 mol·L^{-1} HNO_3 and 25°C for all experiments.

[Zr^{4+}] (mol·L^{-1})	**[AAIII] (mol·L^{-1})**	**[Zr^{4+}] (mol·L^{-1})**	**[AAIII] (mol·L^{-1})**
5.0×10^{-6}	3.0×10^{-5}	3.0×10^{-5}	6.7×10^{-6}
6.7×10^{-6}	3.0×10^{-5}	3.0×10^{-5}	1.5×10^{-5}
1.0×10^{-5}	3.0×10^{-5}	3.0×10^{-5}	3.0×10^{-5}
2.0×10^{-5}	3.0×10^{-5}	3.0×10^{-5}	4.0×10^{-5}
2.5×10^{-5}	3.0×10^{-5}	3.0×10^{-5}	5.0×10^{-5}
4.2×10^{-5}	3.0×10^{-5}	3.0×10^{-5}	6.0×10^{-5}
5.0×10^{-5}	3.0×10^{-5}	3.0×10^{-5}	9.0×10^{-5}
-	3.0×10^{-5}	3.0×10^{-5}	1.2×10^{-4}

Table 10.8: Zr/AAIII/AHA in HNO_3 experimental concentrations.

1 mol·L^{-1} HNO_3 and 25°C for all experiments.

[Zr^{4+}] (mol·L^{-1})	**[AAIII] (mol·L^{-1})**	**[AHA] (mol·L^{-1})**	**[Zr^{4+}] (mol·L^{-1})**	**[AAIII] (mol·L^{-1})**	**[AHA] (mol·L^{-1})**
3.0×10^{-5}	3.0×10^{-5}	7.0×10^{-2}	5.0×10^{-6}	3.0×10^{-5}	1.0×10^{-2}
3.0×10^{-5}	3.0×10^{-5}	4.0×10^{-2}	1.0×10^{-5}	3.0×10^{-5}	1.0×10^{-2}
3.0×10^{-5}	3.0×10^{-5}	2.0×10^{-2}	1.5×10^{-5}	3.0×10^{-5}	1.0×10^{-2}
3.0×10^{-5}	3.0×10^{-5}	1.5×10^{-2}	2.0×10^{-5}	3.0×10^{-5}	1.0×10^{-2}
3.0×10^{-5}	3.0×10^{-5}	1.0×10^{-2}	2.5×10^{-5}	3.0×10^{-5}	1.0×10^{-2}
3.0×10^{-5}	3.0×10^{-5}	7.5×10^{-3}	3.0×10^{-5}	3.0×10^{-5}	1.0×10^{-2}
3.0×10^{-5}	3.0×10^{-5}	4.0×10^{-3}	4.0×10^{-5}	3.0×10^{-5}	1.0×10^{-2}
3.0×10^{-5}	3.0×10^{-5}	2.0×10^{-3}	6.0×10^{-5}	3.0×10^{-5}	1.0×10^{-2}
3.0×10^{-5}	3.0×10^{-5}	1.0×10^{-3}	-	-	-
3.0×10^{-5}	3.0×10^{-5}	6.7×10^{-4}	-	-	-

11 APPENDIX B: SUPPLIMENTAL INFORMATION FOR NEPTUNIUM REDUCTION STUDIES

11.1 Experimental Information for Chapter 5

Table 11.1: NpO_2^{2+} reduction in $HClO_4$ experimental conditions.

Syringe 1		*Syringe 2*		*Reaction Conditions*			
$[NpO_2^{2+}]_o$ (mmol·L^{-1})	Solvent ($HClO_4$)	$[AHA]_o$ (mmol·L^{-1})	Solvent	$[NpO_2^{2+}]_o$ (mmol·L^{-1})	$[AHA]_o$ (mmol·L^{-1})	$[HClO_4]$ (mmol·L$^{-1)}$	NpO_2^{2+}: AHA
1.05	2 mol·L^{-1}	1.05	H_2O	0.53	0.53	2.00	1:1
1.05	2 mol·L^{-1}	2.10	H_2O	0.53	1.05	2.00	1:2
1.05	2 mol·L^{-1}	4.20	H_2O	0.53	2.10	2.00	1:4
1.05	2 mol·L^{-1}	8.40	H_2O	0.53	4.20	2.00	1:8
0.45	2 mol·L^{-1}	3.60	H_2O	0.23	1.80	2.00	1:8
1.80	2 mol·L^{-1}	3.60	H_2O	0.90	1.80	2.00	1:2
3.60	2 mol·L^{-1}	3.60	H_2O	1.80	1.80	2.00	1:1

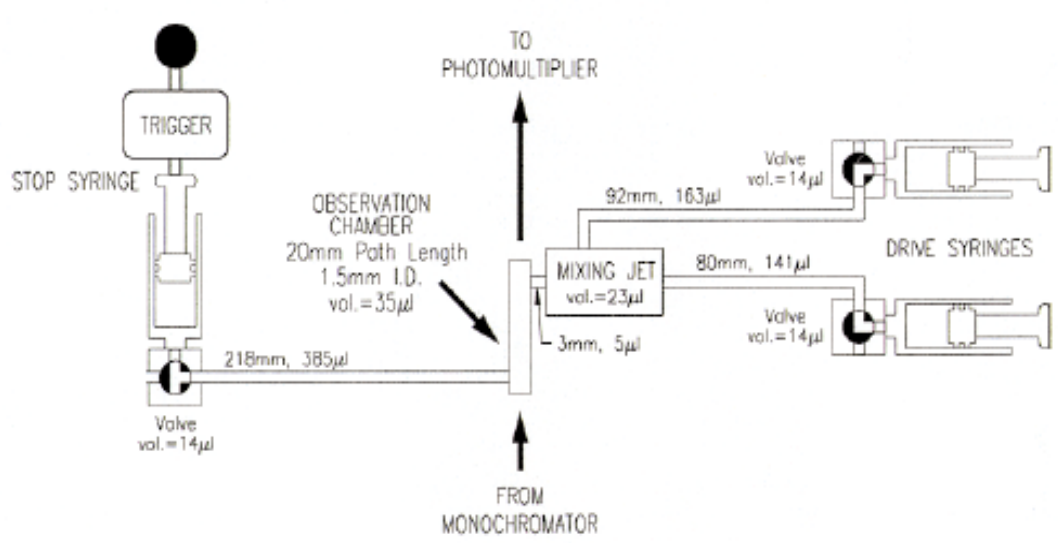

Figure 11.1: Schematic of stopped-flow apparatus.

Reprinted from On-Line Instrument Systems, Inc., with permission.

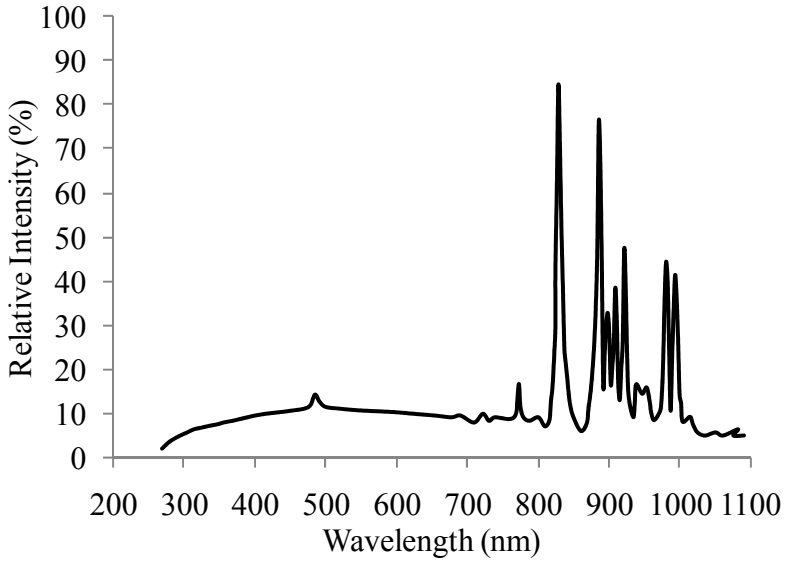

Figure 11.2: Light intensity from xenon arc lamp.

Used for all experiments in chapter 5. Adapted from [183].

11.2 Experimental Information for Chapter 6

Table 11.2: NpO_2^{2+} reduction in HNO_3 experimental conditions.

	Syringe 1		***Syringe 2***		***Reaction Conditions***		
Expt. Number	**$[NpO_2^{2+}]_o$ (mmol·L^{-1})**	**$[HNO_3]$ (mol·L^{-1})**	**$[AHA]_o$ (mmol·L^{-1})**	**Solvent**	**$[NpO_2^{2+}]_o$ (mmol·L^{-1})**	**$[AHA]_o$ (mmol·L^{-1})**	**$[HNO_3]$ (mmol·L$^{-1)}$**
1	1.05	2.00	1.05	H_2O	0.53	0.53	2.00
2	1.05	2.00	2.10	H_2O	0.53	1.05	2.00
3	1.05	2.00	4.20	H_2O	0.53	2.10	2.00
4	1.05	2.00	8.40	H_2O	0.53	4.20	2.00
5	0.45	2.00	3.60	H_2O	0.23	1.80	2.00
6	1.80	2.00	3.60	H_2O	0.90	1.80	2.00
7	3.60	2.00	3.60	H_2O	1.80	1.80	2.00

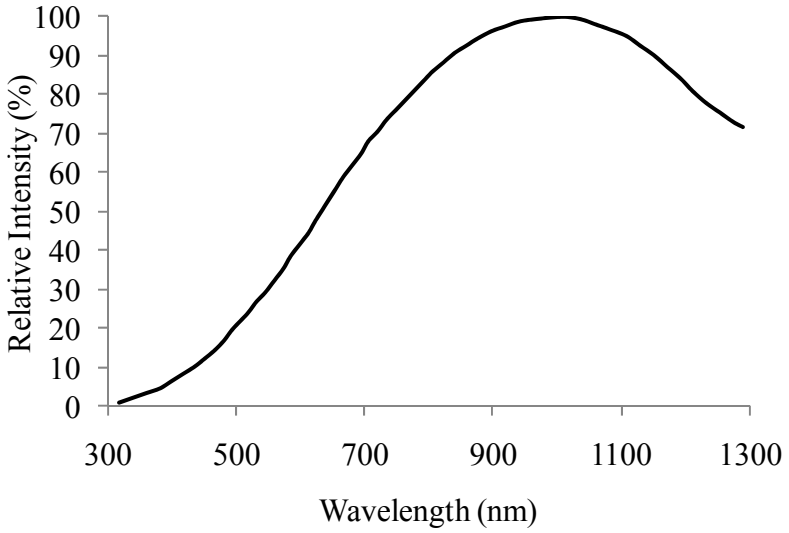

Figure 11.3: Light intensity from tungsten lamp.

Used for all experiments in chapter 6. Adapted from [184].

12 APPENDIX C: SUPPLIMENTAL INFORMATION FOR EXTRACTION STUDIES

12.1 Experimental Information for Chapter 7

12.1.1 ICP-AES calibration curves

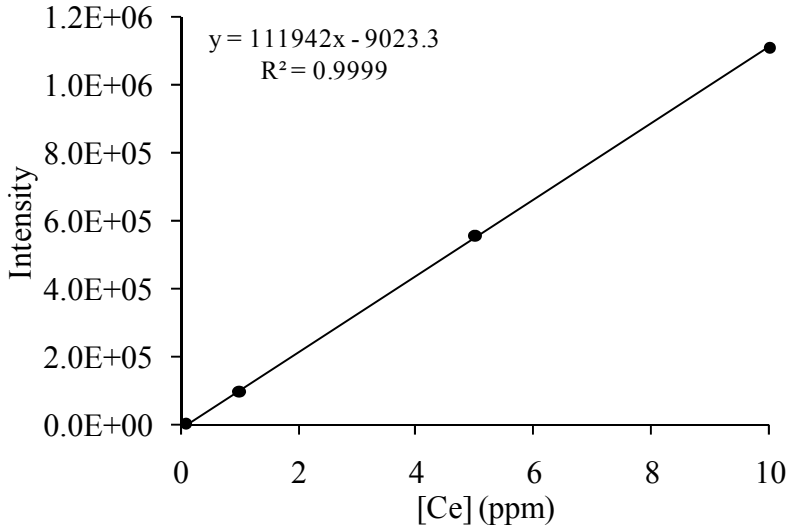

Figure 12.1: Cerium ICP-AES calibration curve.

404.1nm emission line. Cerium ICP-MS standard (1000ppm in 2% HNO_3, Spex CertiPrep, Inc.) diluted to 0.0, 0.1, 1.0, 5.0, and 10.0 ppm Ce.

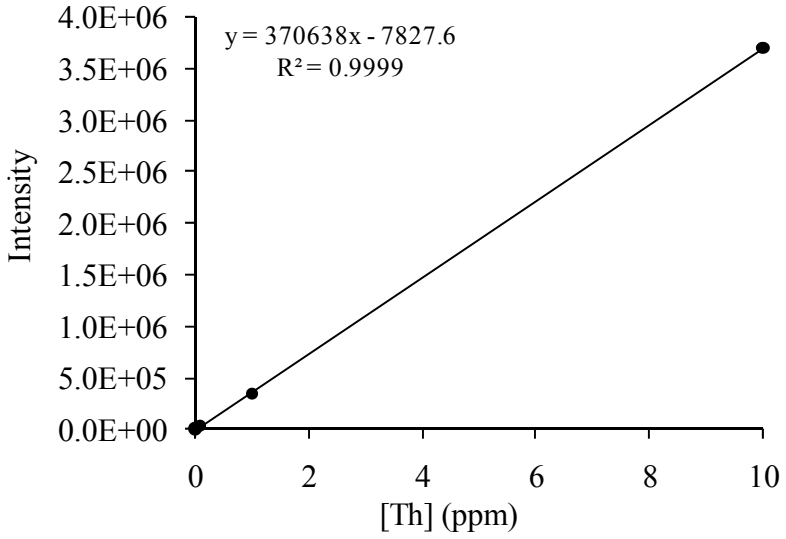

Figure 12.2: Thorium ICP-AES calibration curve.

283.7nm emission line. Thorium ICP-MS standard (1000ppm in 2% HNO_3, Spex CertiPrep, Inc.) diluted to 0.0, 0.1, 1.0, and 10.0 ppm Th.

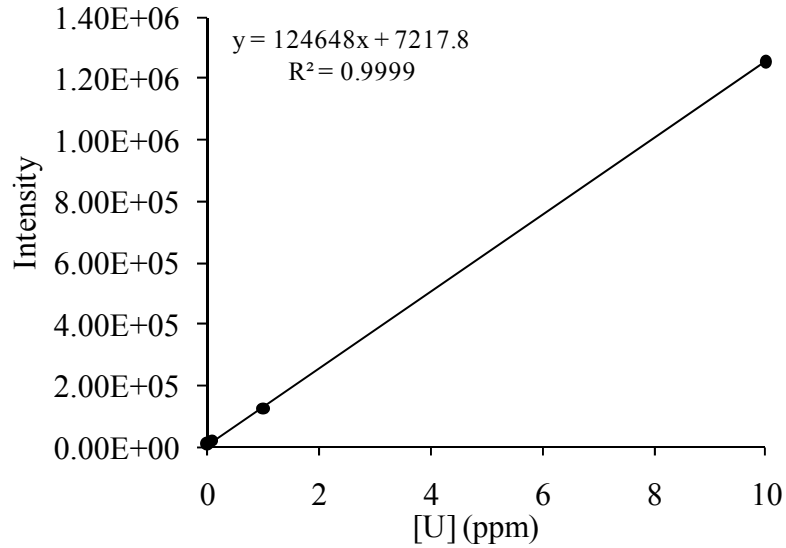

Figure 12.3: Uranium ICP-AES calibration curve.

367.0nm emission line. Uranium ICP-MS standard (1007ppm in 2% HNO_3, Inorganic Ventures, Inc.) diluted to 0.0, 0.1, 1.0, and 10.0 ppm U.

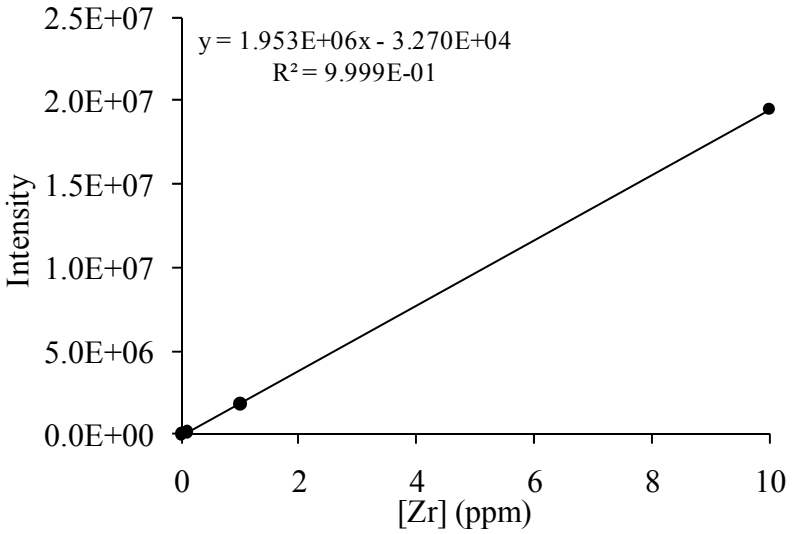

Figure 12.4: Zirconium ICP-AES calibration curve.

343.8nm emission line. Zirconium ICP-MS standard (1000ppm in 3% HNO_3, Ricca Chemical Company) diluted to 0.0, 0.1, 1.0, and 10.0 ppm Zr.

12.1.2 Extraction Data

12.1.2.1 Uranium

Table 12.1: Uranium extraction experimental conditions.

30% v/v TBP in n-dodecane. [AHA] = 0.4 mol·L^{-1}.

$[HNO_3]$ (mol·L^{-1})	**$[UO_2^{2+}]$ (mol·L^{-1})**	**$D_{(U)}$ no AHA**	**Error**	**$D_{(U)}$ with AHA**	**Error**
1.00	0.27	5.47	0.55	4.01	0.58
2.00	0.27	9.35	0.91	8.97	1.53
3.01	0.27	21.50	1.39	22.42	1.98
3.99	0.27	36.60	2.48	35.35	2.70
4.99	0.27	52.99	4.67	49.78	4.42
6.00	0.27	51.52	5.22	46.18	4.41

12.1.2.2 Thorium

Table 12.2: Thorium extraction experimental conditions.

30% v/v TBP in n-dodecane. [AHA] = 0.4 mol·L^{-1}.

$[HNO_3]$ (mol·L^{-1})	$[Th^{4+}]$ (mol·L^{-1})	$D_{(Th)}$ no AHA	Error	$D_{(Th)}$ with AHA	Error
0.21	0.0022	0.055	0.09	-	-
0.51	0.0022	0.13	0.12	-	-
1.01	0.0022	0.44	0.15	0.93	0.038
2.01	0.0022	1.63	0.16	1.61	0.052
3.01	0.0022	4.76	0.17	2.38	0.075
4.01	0.0022	6.46	0.26	3.12	0.11
5.01	0.0022	6.96	0.31	3.50	0.16
6.01	0.0022	7.36	0.34	3.55	0.16

12.1.2.3 Zirconium

Table 12.3: Zirconium extraction experimental conditions.

30% v/v TBP in n-dodecane. [AHA] = 0.4 mol·L^{-1}.

$[HNO_3]$ (mol·L^{-1})	$[Zr^{4+}]$ (mol·L^{-1})	$D_{(Zr)}$ with AHA	Error
1.01	0.0022	0.018	0.096
2.01	0.0022	0.011	0.11
3.01	0.0022	0.053	0.11
4.01	0.0022	0.020	0.01
4.03	0.0022	0.044	0.016
5.03	0.0022	0.054	0.014
6.02	0.0022	0.015	0.025

12.1.2.4 Cerium

Table 12.4: Cerium extraction experimental conditions.

30% v/v TBP in n-dodecane. [AHA] = 0.4 mol·L^{-1}. ND = not detectable.

$[HNO_3]$ (mol·L^{-1})	$[Ce^{4+}]$ (mol·L^{-1})	$D_{(Ce)}$ no AHA	Error	$D_{(Ce)}$ with AHA	Error
1.00	0.027	11.02	0.57	0.007	0.014
1.99	0.027	11.66	1.15	0.008	0.016
2.99	0.027	12.12	1.16	0.034	0.016
4.00	0.027	11.67	1.12	ND	0.29
5.00	0.027	12.64	1.17	0.007	0.013
6.00	0.027	9.48	0.90	0.129	0.018

12.1.2.5 Neptunium

Table 12.5: Neptunium extraction experimental conditions.

30% v/v TBP in n-dodecane. [AHA] = 0.4 mol·L^{-1}. *Data from Karraker [99]. †Not determined experimentally.

[HNO_3] (mol·L^{-1})	**[Np^{4+}] (mmol·L^{-1})**	**Eqm [HNO_3] (mol·L^{-1})**	**$D_{(Np)}$ no AHA**	**Error**	**$D_{(Np)}$ with AHA**	**Error**
1.00	0.138	0.91*	0.62*	-	0.076	0.001
2.01	0.138	1.66*	1.82*	-	0.36	0.033
2.96	0.138	3.17*	3.97*	-	0.81	0.13
4.00	0.138	3.68*	7.55*	-	1.30	0.016
5.02	0.138	5.02†	6.88	0.68	2.31	0.35
5.97	0.138	5.97†	8.67	1.30	3.26	0.80